Norwegian University
of Life Sciences

Master's Thesis 2023 30 ECTS
Faculty of Science and Technology

Validation of the AROME MetCoOp Model Wind Predictions using Radiosonde Observations

Investigating the Impact of wind prediction errors on the modelled transportation of radioactivity after the Chernobyl Accident

Nora Helgeland
Environmental Physics and Renewable Energy

Acknowledgements

First I would like to thank my supervisors, Associate Professor Mareile Astrid Wolff and Senior Scientist Erik Berge for invaluable help and support through the last five months. This thesis would not have been possible without their encouragements, patience and good advice.

I would also like to thank the department of climate and air quality at the Norwegian Meteorological Institute for for sharing their knowledge and their good company. I would especially like to thank M.Sc Magnus Ulimoen for sharing his office and knowledge in abundance.

Lastly I would like to thank my friends and family for supporting me throughout my whole education.

Abstract

The main objective of this thesis was to investigate the error in the wind speed and wind direction predicted by the AROME MetCoOp model for the time period after the Chernobyl accident, using radiosonde data with and without adjusting for horizontal displacement. The second objective was to examine specific radiosonde soundings to investigate the error in wind direction along the movement of the plume over the first four days, using radiosonde observations with horizontal drift and discussing the significance of these errors for the transportation of the radioactivity.

To do this, the radiosonde observations were adjusted for horizontal drift by using methods explained in Laroche and Sarrazin (2013), and it was applied to the analysis of the model wind predictions, so that it could be compared to the analysis without adjustment. Then the model data was interpolated for the data to have the same position in space and time as the radiosonde observations. Then the mean absolute error and mean error were found for each timestep and for different height bins. Before this there was a scatter plot analysis of the mean absolute error and removal of outliers. To investigate the error in selected radiosonde stations, polar plots were presented to visualize the difference in predicted and observed wind direction, giving a picture of the difference in the observed and predicted path of the plume.

Among other findings, this thesis concluded that the horizontal displacement of radiosondes, when comparing radiosonde observations with the AROME model, was not necessary to include in the analysis seeing that there were very little difference between the analysis with adjustment for horizontal displacement of the radiosonde observations and the analysis without. It was further observed that there was a larger error below 1000 meters than above, and an under prediction of the rotation of the wind direction from the surface of the earth to the free atmosphere. Therefore this thesis also concluded that depending on the vertical position of the radioactivity there could be more or less deviations between the model predictions and the actual transportation. Further, this thesis also came to the conclusion, based on the errors in wind direction, that radioactivity above 1000 meters during the first few days could be transported more north than predicted, and the radioactivity below 1000 meters could be transported more towards the west than predicted.

Table of Contents

Chapter 1

Introduction

1.1 Background

Around 01:30 local time on the 26^{th} of April 1986, there was an explosion at Chernobyl 4, one of the nuclear reactors at the Chernobyl power plant (Persson et al., 1987). The explosion lifted the roof of the reactor and a cloud containing radioactive particles and gases was thrown into the sky. The radioactivity was later detected at 1200 meters height, before traveling to different places in Europe (Persson et al., 1987).

From the turn of the 20^{th} century when it was first proposed that the laws of physics describing the state of the atmosphere could be moved forward in time through partial differential equations to predict future weather, amazing things have happened in the field of weather prediction. The models being able to predict weather in impressive detail is significant for many industries and purposes, and a computer's ability to handle more calculations allows for finer resolution in space and time (Bauer et al., 2015). In the case of a nuclear accident, like the one that happened in Chernobyl in 1986, it is important to have a numerical weather prediction model that can predict the atmospheric conditions and hence the transportation of the radioactivity to know the location of a possible fallout.

1.1.1 The weather during the Chernobyl accident and transportation of radioactivity

At the time of the accident, the air around Chernobyl was calm and the sky was clear, and there was little vertical motion (Persson et al., 1987). After the explosion, the radioactive debris was either in gaseous form or attached to other particles with the heavier particles located at lower heights (Persson et al., 1987).

Over the first days, there were an overall southeasterly wind above 1000 meters height, causing the radioactive debris to move towards Scandinavia, reaching Sweden on the 27^{th} of April (Persson et al., 1987). On the 28^{th} of April the warm air kept moving towards Norway with a southeasterly wind (Saltbones, 1986).

The wind direction turned on the 30^{th}, going towards the south west, and continuing to be north-easterly until the 1^{st} of May. Then on the 5^{th} of May the winds turned and blew towards Scandinavia again (Saltbones, 1986). In the end it was estimated that six percent of the radioactive cesium that was released from the reactor was deposited in Norway (Backe et al., 1986).

The main deposition of radioactive debris over Norway came from the initial release on the 26^{th} of April and happened during the first four days, and the worst nuclear particle release from the accident cite is thought to have been over by the 5^{th} of May 1986 (Saltbones, 1986).

1.1.2 Modelling of The Transportation of Radioactivity

With the ongoing war in Ukraine, there is an heightened risk of another nuclear accident. To be prepared for the potential radioactive fallout, the Norwegian Meteorological Institute (MET) is running a preparedness modelling system based on a weather prediction model and a radioactive dispersion model. To be able to alert the population and enforce necessary precautions in case of an accident, we need to know how accurate the results are and how the models can be improved.

The Center for Environmental Radioactivity (CERAD) "studies the harmful effects of radiation on organisms and the ecosystem as a whole, to improve the protection of people and environment" (NMBU, 2022). As a part of the work on CERAD, The Norwegian Meteorological Institute (MET) assessed a model for the dispersion of radioactive particles after the Chernobyl accident to test their preparedness modelling system.

The MetCoOp Application of Research to Operations at Mesoscale (AROME) model was used to perform a hindcast of the weather in the time after the accident and is based on a downscaling of the ERA5 data. The ERA5 data is a reanalysis produced by the European Council for Medium-Range Weather Forecasts (ECMWF) from 1940 to present time (Hersbach et al., 2020). Then MET used the SNAP model explained in Bartnicki et al. (2011), a particle dispersion model, that uses these weather predictions to calculate the movement of the radioactive debris, or the "plume".

1.1.3 Other Studies That Performed Validation of Wind Predictions

Multiple wind prediction verifications have been performed through the years. The MetCoOp AROME model forecasts for Sweden and Norway for one year were evaluated in Müller et al. (2017). They found that the wind speed had a mean absolute error between 1.4 m/s and 2.2 m/s in Norway and between 1.2 m/s and 1.6 m/s in Sweden. Furthermore, they found that the error seemed to decrease with higher wind speeds (Müller et al., 2017).

Pentikäinen et al. (2022) evaluated the wind parameters predicted by numerical weather models by using doppler lidars. The weather model that was being evaluated was the the operational global integrated forecast system (IFS). They found that the wind direction performed well, but the error in wind direction increased rapidly with slower wind speeds, especially for wind speeds below 2 m/s (Pentikäinen et al., 2022).

Haakenstad et al. (2021) investigated a 15 year hindcast of the North sea and the Barents sea, from 2004 to 2018. The hindcast was produced by the AROME HARMONIE model an it was run on a

downscaling of the ERA5 data. They compared the 10 meter wind predictions to ground stations, using around 200 000 measurements per year, finding a mean error between 0 m/s and -0.5 m/s and a mean absolute error between 1.2 m/s and 2.1 m/s. In 2004, there were fewer measurements with the number of measurements around 70 000, and both the mean error and the mean absolute error were at their highest in 2004 (Haakenstad et al., 2021).

Raskob et al. (2010) used masts to measure wind in different locations in Denmark and Germany at different heights, and compared the measured wind direction averaged over 10 minutes to wind direction predictions. These wind direction predictions were produced by a a numeric weather prediction model made by the Danish Meteorological Institute. They found varying errors, and at some places the error was close to zero. However, they found an error in wind direction as high as 25 degrees in flat terrain with a higher error in mixed terrain (Raskob et al., 2010).

1.1.4 Radiosonde Observations

To verify numerical weather prediction models, observations are needed. At the time of the Chernobyl Accident, radiosondes were important instruments for atmospheric observations (Ivanov, 1991). Radiosondes are balloons filled with either hydrogen or helium carrying measuring equipment (Milrad, 2018). The data from these measurements are a big part of the data that is used to train and verify numerical weather models, and its therefore essential that these measurements are accurate (Laroche and Sarrazin, 2013).

The radiosonde typically do not drift more than a few kilometers horizontally in the lower troposphere from its launching position. However, it can have moved around 5 kilometers horizontally by the time it is in the mid troposphere, and in the upper troposphere the radiosonde typically can have drifted around 20 km from its launching position (Seidel et al., 2011). Further, it can move as far as 50 kilometers from its launch point when it reaches the lower stratosphere (Seidel et al., 2011). Because of this, Laroche and Sarrazin (2013) tested the impact of adjusting the radiosonde observations for horizontal displacement on numerical weather predictions. They found that the error was between 0.6 m/s and 1.6 m/s for the zonal wind. To be able to do this they described a method that calculates the horizontal displacement of the radiosonde using its horizontal and vertical speed. In the end they found that there were significant improvements to short range forecasts in the upper troposphere and stratosphere when the radiosonde observations were adjusted for horizontal displacement.

1.2 Motivation and Research Questions

Many physical and chemical processes are important for the transportation of radioactive gases and particles in the atmosphere. The parameter errors that would be most influential in dispersion modelling are discussed in Leadbetter et al. (2020). They concluded that error in wind direction would influence the results the most, together with error in release rate of the radioactivity from the site of the accident. Second came wind speed, release timing of the radioactivity and release height of the radioactivity. Also, Saltbones (1986) discussed how the wind speed and direction decides where and how fast gases and particles are moved and where the radioactivity can interact with clouds and precipitation, and this greatly determines where the radioactivity is deposited. This shows how errors in wind speed and wind direction predictions can lead to a wrong mapping of the radioactive fallout after a nuclear accident.

The increasing resolution of weather models means that the horizontal drift of radiosondes could be more significant for verifying numerical weather predictions. The radiosondes have been shown to move between 10 and 20 km from their initial starting position (Laroche and Sarrazin, 2013). This could impact the evaluation because the radiosonde observation is compared to the wrong model grid point and consequently can give the wrong error when subtracting the observation from the prediction.

Keeping this in mind, the two main aims of this thesis are:

1. Investigating the error in the wind speed and wind direction predicted by the MetCoOp AROME model for the time period after the Chernobyl accident, using radiosonde data with and without adjusting for horizontal displacement.

2. To look more closely at specific atmospheric soundings to investigate the error in wind direction along the transportation of the radioactivity over the first 4 days, using radiosonde observations with horizontal drift. What can these errors mean for the transportation of the radioactive debris?

Chapter 2

Theory

In this chapter the weather model that is being investigated is presented. However, to understand the weather model and the resulting wind predictions, a short discussion on pressure, wind and thermodynamic properties is given. Then follows an overview of numerical weather prediction models and methods for validation of wind predictions. Thereafter, a presentation of the Chernobyl accident including a brief explanation of radioactivity and some significant radioactive particles is given. Lastly, an overview of what a radiosonde is and how it was used as a measuring instrument in different countries in 1986 is presented. If not referenced separately, information for the vertical structure of the atmosphere, pressure and geopotential height, and wind is taken from the following textbooks: Wallace and Hobbs (2006), R. Stull (2017), R. B. Stull (1988) and Eliassen and Pedersen (1977).

2.1 The Vertical Structure of The Atmosphere

The Atmosphere can be divided into different parts depending on key processes as shown in figure 2.1. From the surface to around 10 km height is the troposphere. Eighty percent of the mass in the atmosphere is located in the troposphere where temperature usually decreases by around 7 degrees per km. There is a lot of vertical movement in the troposphere, and small solid and liquid particles usually have a residence time of a few days or a few weeks before they are deposited at the surface of the earth. At a typical height of 10 km, there is a rapid change from the moist air in the troposphere to a less moist and more ozone rich air. This is the stratosphere, and the area where the troposphere and the stratosphere meet is the tropopause. In the stratosphere there is less vertical mixing and almost no mixing with the air in the troposphere. Therefore, if a particle is in the stratosphere, it can take more than a year before it reaches the surface of the earth. This is because there is an increasing temperature gradient inhibiting warm air to rise. Most clouds will not be able to penetrate the tropopause, and radiosondes usually burst in mid stratosphere. Above the stratosphere is the mesosphere, ranging from around 50 to 80 kilometers. Then there is the thermosphere, which ranges from 80 kilometers to above 100 kilometers. Lastly, above the thermosphere lies the exosphere.

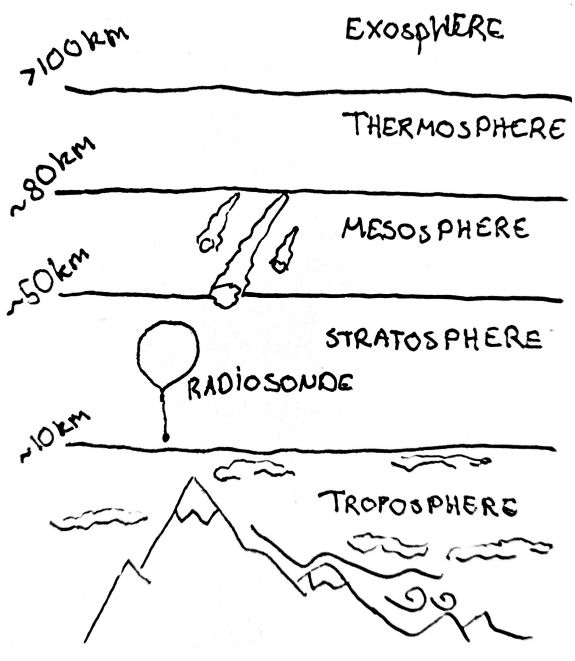

Figure 2.1: The vertical layers in the atmosphere

2.2 Pressure and Geopotential Height

The atmosphere is a mixture of gasses and particles trapped by the earth‘s gravitational field. The gravitational field exerts a force on the air giving rise to pressure. Pressure is equal to the force per area. SI units for pressure are Pascals, and more commonly expressed in hecto Pascals(hPa), weakening exponentially from around 1013 hPA at sea level as the distance from the surface increases. For many applications it is useful to know areas of constant pressure which are denoted as isobars.

Thermodynamics is a large part of atmospheric science since the atmosphere is made out of gasses. Because of the composition of gases and the average temperature and pressures, the gases in the atmosphere can in most instances be considered ideal and follow approximately the same rules and display the same properties as ideal gases. Therefore the ideal gas law can be used,

$$PV = mRT, \tag{2.1}$$

where P is the pressure, V is the volume of the air, m is the mass, R is a constant depending on the composition of the gas and is called the gas constant, and T is the temperature in Kelvin (Wallace and Hobbs, 2006). The gas constant for moist air is larger than that of dry air, and depends on the amount of water vapor in the air. Therefore it can be complicated to obtain the

exact gas constant for moist air. To simplify things, a virtual temperature is created so that the dry gas constant can be used and expressed in the ideal gas law as follows,

$$PV = mR_dT_v, \tag{2.2}$$

where R_d is the dry air gas constant and T_v is the virtual temperature (Wallace and Hobbs, 2006). The virtual temperature is therefore the temperature that the dry air must have to have the same density as the moist air at the same pressure and can be defined by,

$$T_v = \frac{T}{1 - (e/p)1 - \epsilon)}, \tag{2.3}$$

where T is the actual temperature, ϵ is the molecular weight of water divided by the molecular weight of dry air and is equal to 0.662, e is the partial pressure of the moist air and p is the actual pressure (Wallace and Hobbs, 2006).

A slab of air with thickness dz will have a force acting on it due to the decrease in pressure dp. This force is pushing the air up. However the gravitation is pulling on the mass of the slab. If there is no vertical acceleration, there will be a balance in these forces,

$$-dp = g\rho dz, \tag{2.4}$$

where ρ is the density of the air slab (Wallace and Hobbs, 2006). To raise this slab from sea level to its current height a force is excerted, and the magnitude of this force is called the geopotential and is notated by Φ. The work that must be done to raise 1kg from z to dz can therefore be expressed by

$$d\Phi = gdz, \tag{2.5}$$

and the geopotential can be expressed by,

$$\Phi(z) = \int_0^z gdz, \tag{2.6}$$

where g is the gravitational force at a certain height and dz is the distance the mass has been moved (Wallace and Hobbs, 2006). Geopotential height is the distance this mass is lifted and can be expressed as,

$$Z \equiv \frac{\Phi(z)}{g_0} = \frac{1}{g_0}\int_0^z gdz \tag{2.7}$$

where g_0 is the gravitational force at the surface of the earth (Wallace and Hobbs, 2006). From this equation one can find the change in geopotential height in two layers as shown in Wallace and Hobbs (2006). This leads to the following expression,

$$Z_2 - Z_1 = \frac{R_d \overline{T}}{g_0} \ln\left(\frac{p_1}{p_2}\right), \tag{2.8}$$

where $Z_2 - Z_1$ is the difference in geopotential height from layer 1 with pressure p_1, to layer 2 with pressure p_2 (Wallace and Hobbs, 2006). This equation is called the hypsometric equation and is applied in this study to find the height in different model layers when only the pressure is known.

2.3 Wind

Wind is the horizontal movements of air in the atmosphere and it is characterized by its speed and direction. Microscale wind is often described as winds with an extension of 2 mm up to 2 km and with a time span from 1 second to an hour. Then there are mesoscale winds, being 2 km to above 200 km horizontal movement systems with a time span from just under one hour up to 1 month. There are many different forces acting on the air creating movement. This section will explain four of the most important forces that affects the wind speed and wind direction: The pressure gradient, the Coriolis force, the centripetal force and turbulent drag.

The pressure gradient is a force resulting from the pressure difference between two areas of different pressure. Difference in pressure is created by differences in temperature or density. Hot air expands and becomes less dense than the surrounding air, leading the warm air to rise up and creating an area of low pressure. The opposite happens with cooling as the air becomes denser allowing more air to fill the same space. The air going from high to low pressure is being affected by the horizontal pressure gradient determining the wind speed. This is what creates wind on the larger scales. However, the Coriolis force, resulting from the rotation of the earth, also acts on the air parcel disturbing its direction and speed.

The Coriolis force is often referred to as a fictitious force because there is no real force acting on the air. When the earth is rotating around its own axis, the wind will follow the earths rotation. Areas of the earth closer to the poles will have slower rotation speed than the areas closer to the equator because of a smaller radius. There will be conservation of angular momentum as the air moves across the latitudinal lines causing the wind to bend. For example, if the air moves from Spain to Norway the air coming from Spain will have a higher speed in the direction of rotation than the earths surface in Norway making it bend eastward. This causes the air on the northern hemisphere to leave low pressure towards the left, and to leave low pressure towards the right on the southern hemisphere.

The coriolis force balances the pressure gradient force in the opposite direction, making the air flow parallel to the isobars. Simply put, the big wind systems are created by the air around the equator being heated up faster than the air at the poles due to the spherical shape of the earth. This makes the air flow from the equator to the poles, but being deflected by the Coriolis force to the right on the northern hemisphere and to the left on the southern hemisphere.

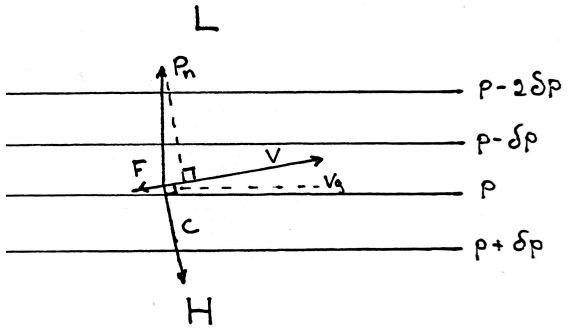

Figure 2.2: Geostrophic wind affected by friction on the northern hemisphere. The solid horizontal lines are the isobars

The free atmosphere is where the air is not affected by the friction of the earths surface. However, when the air experiences friction from the surface of the earth as shown in in figure 2.2, the air will go slightly more towards low pressure to balance out the forces. F is the friction working in the opposite direction of the velocity. C is the Coriolis force working in the opposite direction of P_n, the pressure component that is normal to the velocity vector, and V_g is the geostrophic velocity component. The height where the friction stops having an effect on the wind direction and wind speed is around 1 to 2 kilometers and the area below this is called the atmospheric boundary layer. The resistence caused by the ground, trees, mountains etc makes the air slow down. This friction can be called the turbulent drag force and works in the opposite direction of the wind. This is usually what creates wind on microscale. In the Atmospheric boundary layer, the air will be affected by the topography, creating micro scale winds and is below the free atmosphere. Therefore the horizontal wind fields are more homogeneous as the height increases.

In any circular motion there is force pointing towards the centre of the circle. This the centripetal force. The force acting in the opposite direction is the centrifugal force. If the isobars are bent the centrifugal force will affect the force balance between the Coriolis force and the pressure gradient force. This causes the wind to follow the curved isobars and is referred to as gradient wind.

Turbulence in the boundary layer is often a type of wind that occurs close to the ground due to solar heating or obstacles such as buildings and can be characterized by the rapid changes in motions of the air. The intensity of the turbulence can be found dividing the standard deviation of the wind speed by the mean wind as in the following expression,

$$I = \frac{\sigma_M}{\overline{M}}, \tag{2.9}$$

where I is the turbulence intensity, σ_M is the standard deviation of the wind speed and $\overline{M}$ is the mean wind speed (R. B. Stull, 1988). This means that the turbulence intensity will increase as the mean speed becomes lower.

2.4 Numerical Weather Prediction Models

Every day, numerical weather prediction models are used to predict weather all over the world. These models use numerical techniques to solve partial differential equations that represent the laws of physics to describe fluid flow and the development of different variables with space and time. To solve the equation its common to either use Lagrangian techniques where the object is followed by the coordinate system or Eulerian techniques where one looks at a fixed volume. The resolution of the model grid can vary from around 30 kilometers to 2 kilometers, and different numerical weather models have different strengths and weaknesses (Bauer et al., 2015).

The numerical weather prediction model examined in this thesis is the MetCoOp Application of research to Operations at Mesoscale (AROME) model. The AROME model was developed by the French Meteorological Institute, and put in operation at MET through a collaboration between the Swedish Meteorological and Hydrological Institute, and the Norwegian meteorological institute, referred to as MetCoOp, for day to day weather forecasting (Müller et al., 2017).

ERA5 has a horizontal resolution of 31km which does not contain phenomena at mesoscale such as thunderstorms and urban effects (Hersbach et al., 2020, R. B. Stull, 1988). The MetCoOp AROME model has a horizontal resolution of 2.5 km and produces hourly hindcasts. The wind field is improved from the ERA5 data being able to catch more topographically determined air flow (Haakenstad et al., 2021).

2.4.1 Horizontal coordinates

When looking at the wind speed and direction from the numerical weather prediction models, they are usually represented in Cartesian coordinate system consisting of a xy plane, where x is the number of model grid cells from the Greenwich meridian towards the east and y is the number of model grid cells from the equator towards the north as shown in figure 2.3.

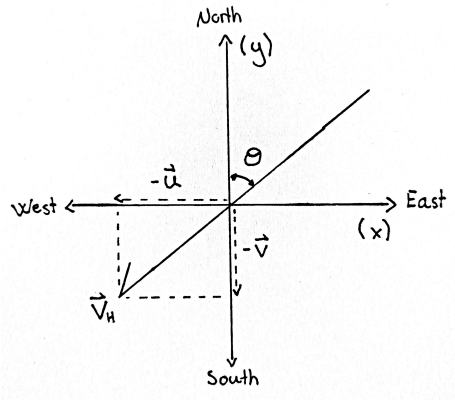

Figure 2.3: The wind directions in the model output. The wind direction represented by the angle θ from north. The wind arrow in this figure is showing a northeasterly wind and would be represented by negative wind speeds in both x and y direction. The remaining quantities in the figure are defined in the text

The wind arrow has a speed $\vec{V}_H$ and is represented by its angle from North, θ. It can further be decomposed into the vector $\vec{u}$ along the x axis and the vector $\vec{v}$ along the y axis. The winds are usually defined by the direction it is coming from. Wind that is coming from the north is northerly wind. If it is coming from south east it is southeasterly and so on.

The spherical earth is projected onto a two dimensional cartesian plane for efficient computations and visualizations. There are many different types of projections. In the hindcast examined in this thesis the Lambert conic projection is used. This is when the earth is projected onto a cone and then unfolded. This projection is conformal meaning that any two intersecting curves will have the same angel as in the spherical projection.

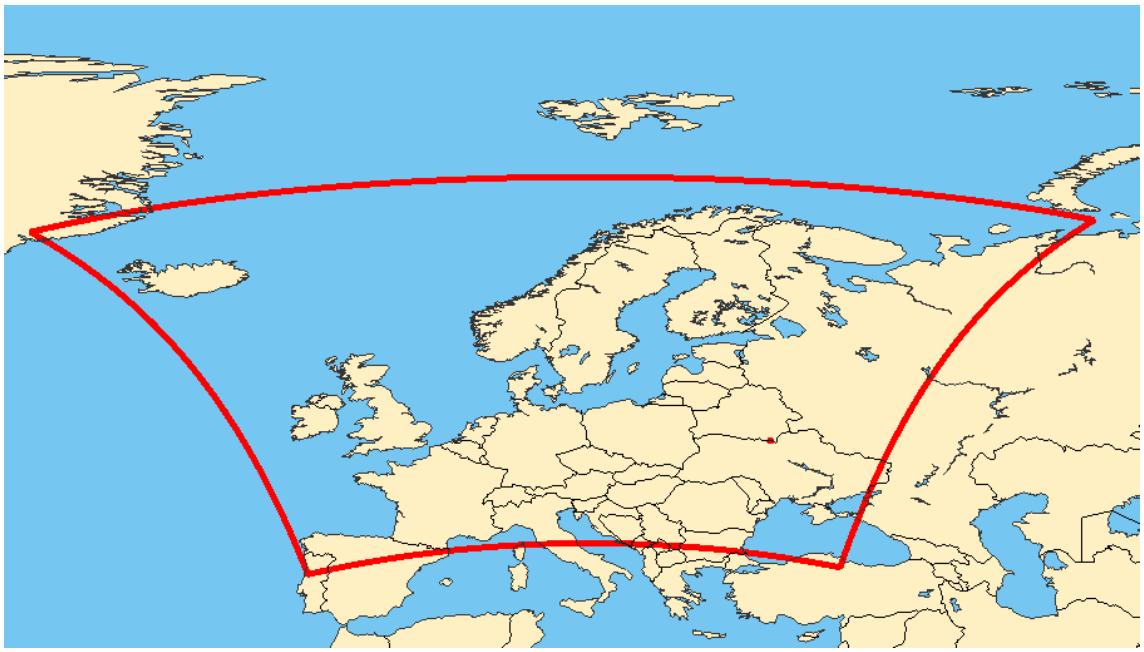

Figure 2.4: A Lambert conic projection shown on a geographic projection representing the model area for the hindcast looked at in this thesis. Retrieved from Diana

Since the earth is spherical it is normal to use spherical coordinates as shown in figure 2.5. Latitude is the angle from the centre of the earth away from the equator ϕ_0, and is denoted by ϕ. Longitude is the angle from the center of the earth away from the Greenwich central meridian λ_0 and is denoted by λ.

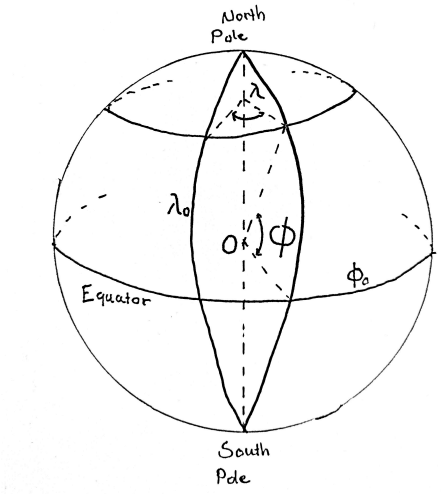

Figure 2.5: Spherical coordinates. See text for explanation of the quantities ϕ, ϕ_0, λ, λ_0

Latitude and longitude can be related to the change in x and y by the following equations,

$$dy = r_e d\phi, \tag{2.10}$$

where dy is the change in y direction and r_e is the average radius of the earth (Wallace and Hobbs, 2006). The radius at the current latitude, can be found using the following expression,

$$r = r_e cos(\phi), \tag{2.11}$$

$$dx = r * d\lambda cos(\phi), \tag{2.12}$$

where ϕ_k is the latitude in the current height level and λ_k is the longitude in the current height level (Wallace and Hobbs, 2006). dx and dy are the changes in y and x position in meters, r_e is the earth's radius and r is the radius at the current latitude.

2.4.2 Vertical Coordinates

Surfaces of constant pressure will at some points intersect with the ground because of uneven topography. Instead of putting the model layers at different heights, the levels can be represented by the σ coordinate. This coordinate is equal to p/p_s, where p_s is the surface pressure and p is the pressure at the current level. The σ coordinate will therefore be a number between zero and one, starting at 1 at ground level and being zero at the top of the atmosphere. In the MetCoOp AROME model there is used a hybrid coordinate shown in figure 2.6 which is a modification of the sigma coordinate, being represented by a monotonic function $\eta(p, p_s)$ also being 1 at ground level and zero at the top of the atmosphere (Simmons and Burridge, 1981). The AROME MetCoOp model has 65 vertical layers starting at 65 at ground level and ending at 1. The model also has half layers representing the values in between two levels ('Harmonie Vertical Model Layer Definitions', n.d.).

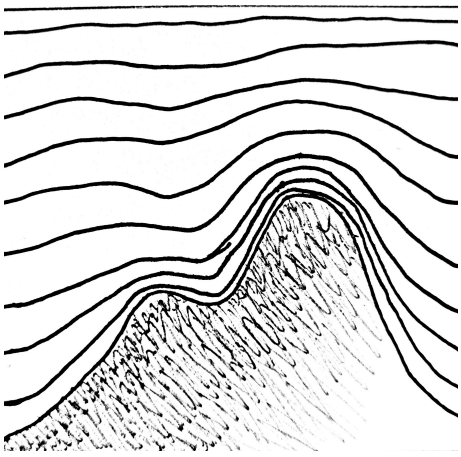

Figure 2.6: The hybrid levels are shown by the dark lines

2.5 Validation of Wind Predictions

Since wind predictions are used in transport calculations of air pollution and radioactivity, the correctness of the model predictions is of utmost importance (Wilks, 2011). There are many types of verification for numerical weather predictions. In this section the more common measures for accuracy are presented. To identify the over prediction or under prediction made by the model in one single prediction, one can use the error(E),

$$E = C - O \tag{2.13}$$

where O is the observation, and C is the prediction (Wilks, 2011).To find the over prediction and under prediction made by the model for a group of observations and prediction, one can use the mean error(ME),

$$ME = \frac{1}{N}\sum_i C_i - O_i \tag{2.14}$$

where N is the sample size, O_i is the i_{th} observation, and C_i is the i_{th} prediction. The error is then summed over all observations and predictions for $i \in \{0, 1, 2, .., N\}$ (Wilks, 2011). This is the same as the bias. If there is no over or under prediction the mean error will sum to zero. A common scalar accuracy measure is the mean absolute error,

$$MAE = \frac{1}{N}\sum_i |C_i - O_i|, \tag{2.15}$$

which equals the magnitude of the error of the forecast or hindcast (Wilks, 2011). Further, the mean square error is also a common measure,

$$MSE = \frac{1}{N}\sum_i (C_i - O_i)^2, \tag{2.16}$$

The mean square error will be more sensitive to bigger errors since the error term is squared (Wilks, 2011). Lastly, the root mean square error can also be used, and is the square root of the mean square error (Wilks, 2011). The root mean square error can be expressed by,

$$RMSE = \sqrt{\frac{1}{N}\sum_i (C_i - O_i)^2}. \tag{2.17}$$

The statistical methods discussed here are spatially dependent and require the variables to have the same position in space and time. Therefore the model data has to be interpolated as to have the same time, x and y position and height as the observations. Linear interpolation is a method that finds the value of a variable in between grid points. To do simple one-dimensional interpolation we have an arbitrary variable y where we want to find a new variable $\hat{y}$ that is $y_i < \hat{y} < y_{i+1}$, and another variable x that is already known in the desired position. Then $\hat{y}$ can be found using the

following equation,

$$\hat{y}(x) = y_i + \frac{(y_{i+1} - y_i)(x - x_i)}{(x_{i+1} - x_i)}, \tag{2.18}$$

retrieved from Kong et al. (2020).

2.6 The Chernobyl Accident and Radioactivity

At 26.04.1986 01:23 local time, during a system test, reactor 4 at the Chernobyl power plant exploded due to overheating and the failure to cool down the core of the reactor (Saltbones, 1986). Following the explosion the reactor started burning, continuing the emission of radioactive debris, and an essential amount of the radioactivity had been emitted after 24 hours (Saltbones, 1986).

The fuel of the Chernobyl nuclear reactor was low enriched uranium (Saltbones, 1986). Uranium easily accepts additional protons or neutrons and becomes unstable. When an element is unstable the goal is to become stable. This can cause the nuclei to decay into two daughter nuclei emitting particles, getting rid of the excess energy. This is called fission. If the daughter nuclei is still unstable, like Cesium 137 which is a decay product of Uranium, the nuclei will part again. This will go on until the elements are stable, and this is referred to as a decay chain. In a nuclear reactor, fission is induced producing heat energy. This energy is collected and converted into electricity (Lilley, 2013). Radioactivity can be measured in Becquerel(Bq) where one Bq is one nuclear fission per second Næumann and Gaare, 1991).

The half life of any radioactive material is how much time it takes for the material to reduce itself to 50 percent through decay. Iodine 131 held the biggest fraction of the emissions from the accident, being responsible for emitting $0.67 * 10^{18} Bq$ (Persson et al., 1987). It was also in gaseous form and represented the majority of radioactivity in the air and the fallout the first day. However, Iodine 131 only has half life of around 8 days and it will therefore disappear relatively quickly (Næumann and Gaare, 1991). Cesium 137 was responsible for the emission of $0.037 * 10^{18} Bq$ but has a half life of 30 years, and will have therefore stayed in the environment for much longer (Næumann and Gaare, 1991, Persson et al., 1987).

2.7 Radiosondes

Radiosondes are an important source of data for validation of the numerical weather prediction models at different height levels. In 1986 the radiosondes would send radio signals to nearby stations, and these signals would then be interpreted (Ivanov, 1991). These Radiosondes typically gather data about wind speed, wind direction, relative humidity and temperature, and height averaged over a vertical distance (Milrad, 2018). They are usually released at 2 meters height and would burst around 30 000 meters (Milrad, 2018). The suggested standard vector error is assumed to have up to 3 m/s errors in the lower troposphere and 5 m/s errors in the upper stratosphere (McGrath et al., 2006).

In 1986 there were different types of radiosondes in use. Ivanov (1991) presented different radiosonde types in different countries, and discussed the errors in the radiosondes from Finland and USSR. In the USSR the meteorite system with a MARS radiosonde and the AVK-1 system with a MRZ radiosonde for atmospheric soundings were in use (Ivanov, 1991). They are estimated to have an ascent rate of between 5 and 6 m/s. The radar height measurements were used to calculate pressure, then the position of the radiosonde could be attained, and from this the wind speed and direction could be calculated. For the MARS radiosonde the position data from the radiosonde had to be manually typed into a computer. Then the wind speed and wind directions were averaged over an increasing vertical area with height. The MRZ was a more modern radiosonde that could make measurements with much shorter time intervals than the MARS. It also carried a small computer that could make direct calculations of wind speed and wind direction mid launch. Both of the radiosonde types are known to have timing shifts in the measurements. For the Meteorite system, typos was a reported issue because of manually inscribing the measurements into the computer (Ivanov, 1991).

In Finland they used Vaisala RS80-15N radiosonde with DigiCORA ground equipment. DigiCORA calculates the wind speed and the wind direction using an averaging period of 4 minutes. Furthermore, the DigiCORA system also has an automatic control of data quality. This was consequently a more modern system in 1986 compared to the USSR system (Ivanov, 1991).

Chapter 3

Data and Methods

In this section the model results from the hindcast for the timperiod after the Chernobyl accident and the radiosonde observation data are presented. Then the methods that are used to compare the predictions and the observations are explained. The time period for which the data is interpolated is 25.04.1986 12 UTC to 08.05.1986 00 UTC. The vertical sections examined are: from 10 meters to the last atmospheric sounding measurement(around 20km), from 0-1000 meters, and from 1000 to 5000 meters height for the specific radiosonde stations. Interpolation was performed in visual studio code using Python 3.11.0. For the statistical analysis and data investigation jupyter notebook was used, also with python 3.11.0. Diana, a graphical display software of MET, is used to make figures showing the dispersion of cesium 137 during the first 4 days. All information without a reference is retrieved from resources at the MET and largely encompasses technical details and information about the hindcast preformed for the time period after the Chernobyl accident.

The code developed in the work on this master thesis and the files discussed in this chapter are located in the following github repositiory:

https://github.com/Norahelgeland/Master-in-Environmental-Physics-and-Renewable-Energy-2023.git

3.1 Processing of The Meteorological Model Data

The hindcasts for the Chernobyl accident were run for the period 25.04.1986 to 15.05.1986 covering 21 days. Every hindcast was run for 18 hours storing the data every hour. Including the initial analysis at 0 hours this resulted in 19 time steps available for each run. The 18 hours hindcasts were started at 00 UTC and 12 UTC for the 21 days period giving an overlap of six hours for each run. The first 6 hours of each run have been considered spin up time and are not used in the analysis of the transportation of the radioactivity. In the present analysis the model data after 12 hours of hindcast (at 00 and 12 UTC) are retrieved for comparison with radiosondes, since the radiosonde data is available at these time intervals. As an example, this means that when looking at data from 00 UTC on the 26th of April 1986, the data corresponds to the 12 hours hindcast initiated at 12 UTC on the 25th of April. The data is stored in *grib* files and to open the files, *Xarray* is used. The *Xarray* library has been used throughout all of the scripts to process and conduct operations on the model data.

The model output does not contain geometrical height, and the different levels are expressed in hybrid coordinates. This is explained in section 2.4.2. To be able to compare the model results to the radiosonde data, the heights need to be found for each time step. It is therefore necessary to find the height in each half layer.

The constants ap and b are contained in each model grid point in each full level k and can be used to calculate the pressure in each half layer $k_{1/2}$ ('Harmonie Vertical Model Layer Definitions', n.d.). The constants in the half levels are known at the top of the atmosphere and at ground level: $a(k=0)_{1/2}=0$ and $a(k=65)_{1/2}=0$, while $b(k=65)_{1/2}=1$ and $b(k=0)_{1/2}=0$ ('Harmonie Vertical Model Layer Definitions', n.d.). Consequently a and b can be found in the next half layer $(k-1)_{1/2}$ if the previous half layer $(k)_{1/2}$ is known by the following expressions,

$$a(k-1)_{1/2} = 2a(k) - a_(k)_{1/2}, \tag{3.1}$$

$$b(k-1)_{1/2} = 2b(k) - b(k)_{1/2}. \tag{3.2}$$

where k is every full layer ('Harmonie Vertical Model Layer Definitions', n.d.). The pressure half layers can then be found by the following expression,

$$p(k)_{1/2} = a_(k)_{1/2} - b(k)_{1/2} p_s(x,y), \tag{3.3}$$

where $p_s(x,y)$ is the surface pressure as a function of its location in the x y grid ('Harmonie Vertical Model Layer Definitions', n.d., Simmons and Burridge, 1981). Then the virtual temperature is calculated for each grid point. The pressure in each half layer can be related to the geopotential height through the hypsometric equation as explained in section 2.2. Equation 3.4 can then be used to find the geopotential height in each half level as shown in the following expression,

$$Z(k-1)_{1/2} = Z(k)_{1/2} - \frac{R_d \overline{T}(k)_{1/2}}{g_0} \ln\Big(\frac{p(k-1)_{1/2}}{p(k)_{1/2}}\Big), \tag{3.4}$$

where g_0 is $9.81 m/s$. These equation are then implemented in *make_geopot_levs.py*. This script calculates the geopotential heights for all grid points and writes it to *netcdf* files.

The model output includes the wind components in the north-south and east-west directions, being represented by the variables *x_wind_ml* and *y_wind_ml* respectively. These variables are available in the hybrid levels and are further used to calculate the wind speed V_h and the wind direction θ.

The model uses a Lambert conic projection with its center at 15 degrees East and 63.5 degrees North. The model grid is rotated with varying angles away from the longitudinal lines. Because of this the wind direction has to be changed to fit the projection of the Radiosonde wind direction. The rotation angles for all grid points are kept in a data file obtained from the AROME group at MET. This angle will be added to or subtracted from the wind direction depending on if the radiosonde is located on the eastern or western side of the central meridian.

3.2 The Transportation of Radioactivity From Chernobyl

A presentation of the transportation of the plume to Scandinavia during the first four days is given here, since this is the basis for selection of radiosonde stations for model validation. Diana is a graphical software at MET that makes it possible to plot model results in an easy way. Hence it is possible to look at the transportation of the emissions and the wind field as predicted by the model for the first four days. To model the transportation of radioactivity The Severe Nuclear Accident program (SNAP) model is used at MET (Bartnicki et al., 2011). Figure 3.1 shows the spread of cesium 137 at 26.04.1986 12 UTC and figure 3.2 shows the spread at 27.04.1986 20 UTC. These two figures are chosen because they can represent a summary of the path of the radioactivity. The dispersion of cesium 137 at 27.04.1986 20 UTC is shown since this is around the time when the plume reaches Sweden as described in Persson et al. (1987).

The rest of the figures, for a more in depth illustration of the path, are presented in Appendix A, showing the position of the plume for different times between 26.04.1986 00 UTC and 29.04.1986 00 UTC. They show primarily a southeasterly wind for the first few days over Belarus and the Balkan countries. This persists until 28.04.1986 12 UTC when there is a large variability in wind direction over Belarus and the Balkan countries. The wind over Scandinavia is mostly southerly or southeasterly. In northern Scandinavia there is a lot of variability in the wind direction after the 27^{th} of April. Also two figures, 8 and 9, with the deposition of cesium 137 as a result from the dispersion calculations are shown. The majority of the deposition is seen in Sweden and some in southeastern part of Norway.

In figure 3.1 the dispersion of cesium 137 at 26.04.1986 12 UTC is shown. The plume is being transported by southeasterly and southerly winds towards the Balkan sea passing through the west of Belarus and into Lithuania. From the wind arrows it looks like the plume will be transported towards Finland making a bow. The hybrid level is 0.884509 which corresponds to around 1200 meters height.

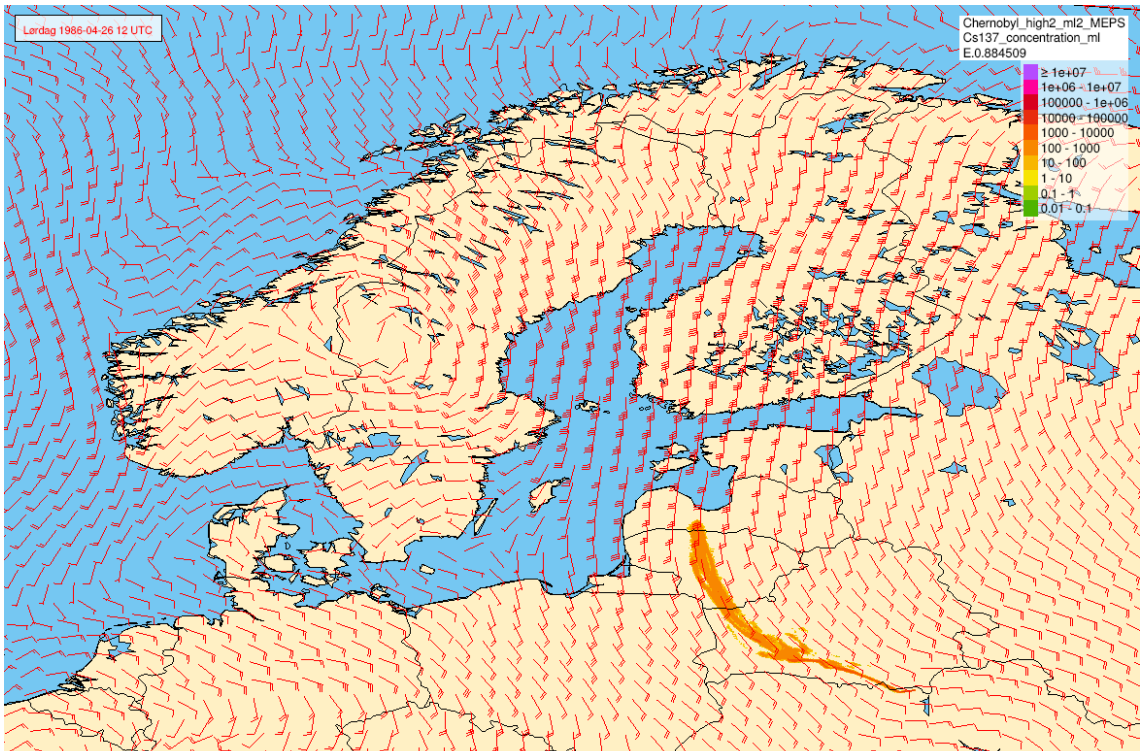

Figure 3.1: The Cs137 concentration in Bq/m^3 at around 1000 meters height at 26.04.1986 12 UTC. Retrieved from the SNAP and AROME model runs

In figure 3.2 the dispersion of cesium 137 at 27.04.1986 20 UTC is shown. It can be seen that the middle of the the plume is touching the coastline of Sweden. The bow has been pushed away from the Balkan countries towards Scandinavia because of southeasterly wind towards Finland over the Balkan sea and southeasterly/easterly wind closer to Chernobyl. There are some small scale changes in wind direction in the area of the accident. The hybrid level value is 0.86138 which corresponds to around 1200 meters height.

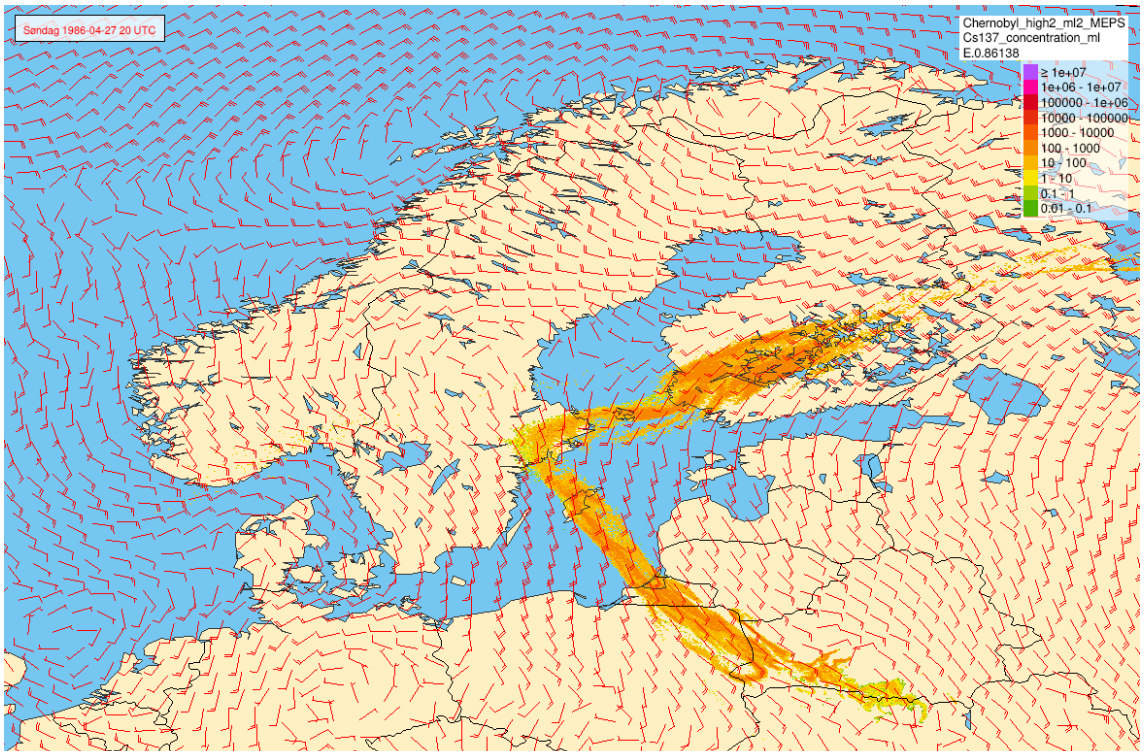

Figure 3.2: The Cs137 concentration in Bq/m^3 at around 1200 meters height at 27.04.1986 20 UTC. Retrieved from the SNAP and AROME model runs

3.3 The Radiosonde Data

The Radiosonde data that is used to evaluate the hindcast is retrieved from the University of Wyoming's web page ('University of Wyoming', n.d.), which contains all available radiosondes in the world and their station number and location. The radiosonde data is available for 00 UTC and for 12 UTC and is accessed by typing in the radiosonde station number and the date and time.

Since we are looking at the Chernobyl accident and the transportation of particles towards Scandinavia, the Radiosondes have to be limited to a relevant area based on the position of the plume showed in the previous section. The chosen area is between 48 and 80 degrees North, and 10 to 40 degrees East. The stations that are located inside the selected area are written to a csv file called *filtered_stations.csv*. The resulting radiosonde stations are shown in figure 3.3. The code developed for this can be found in *filter_stations.py*.

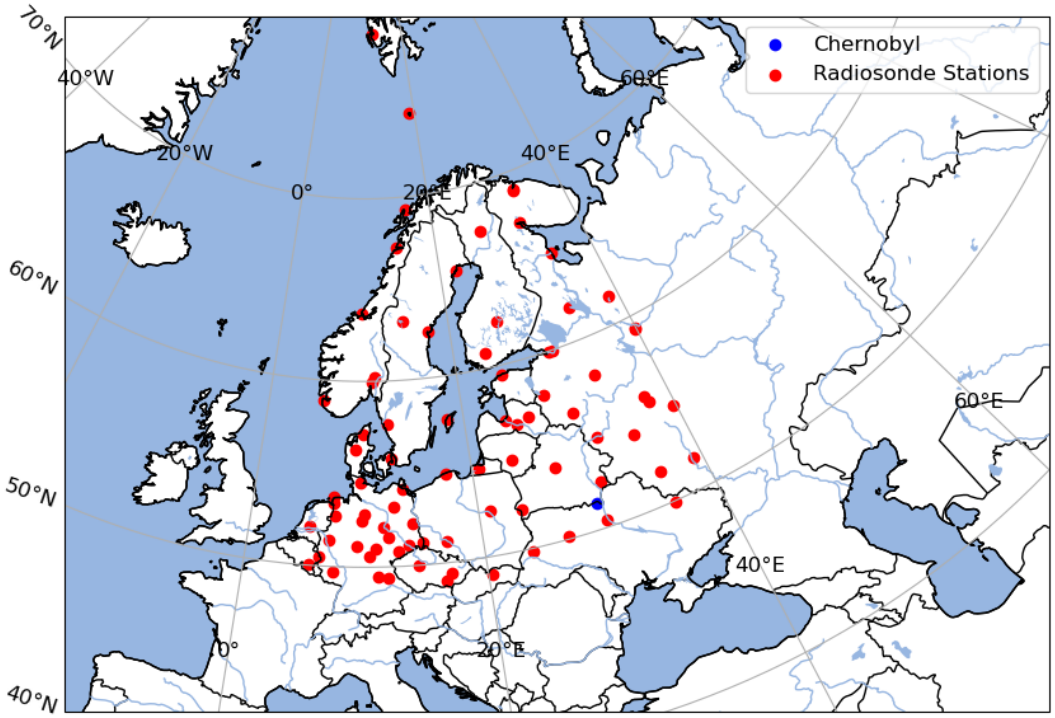

Figure 3.3: The locations of the radiosonde Stations in the selected area plotted in red. Chernobyl is plotted in blue.

The data from each radiosonde station shown in figure 3.3 are written to files for each time point in the selected time span. This results in 26 time steps holding approximately 45 radiosondes. It varies which radiosondes have measurements at which times. Some of them will carry data at every time step, while other only have data every other day. This is implemented in the python script *get_sonde_data.py*. Some of the code is retrieved from Blaylock, 2015, with some modifications.

The data sets have varying resolution, and many of the data sets that are created contain a large fraction of missing values(NaN values). It is observed that the data is mostly missing at the last height levels of the sounding and in a few files the data is missing by four or more data points for height levels in the middle of the sounding.

Since some of the data sets contain large amounts of missing values, there needs to be a few criteria for which data files are applied. First, only the data sets that contain more than 10 data points below 5000 meters are accepted. However, this ended up with discarding too many atmospheric sounding files. Seeing that most files had nine or eight points below 5000 and one or two points more below 7000 meters, the limit was expanded to 7000 meters. This assures that there are enough sounding files to work with while also containing enough data below 5000 meters. Since the winds are changing more up until 10000 meters and most of the data is missing in the first data points, interpolation is ruled out. These NaN values are difficult to replace in a way that will not cause extra error. Therefore, the second criteria is that the data has to have less than thirty percent NaN values in the height levels below 10000 meters and less than three missing values in the first 10 values.

After these criteria have been fulfilled, the number of files that are left to be used in the analysis

are shown in table 3.1.

Table 3.1: Available and accepted radiosonde files for each time and date

Time	Available Sounding Files	Accepted Files
1986-04-25T12	39	33
1986-04-26T12	41	34
1986-04-27T00	41	38
1986-04-27T12	39	34
1986-04-28T00	41	36
1986-04-28T12	46	27
1986-04-29T00	45	31
1986-04-29T12	49	26
1986-04-30T00	44	38
1986-04-30T12	51	34
1986-05-01T00	44	32
1986-05-01T12	44	32
1986-05-02T00	48	28
1986-05-02T12	50	28
1986-05-03T00	43	32
1986-05-03T12	45	31
1986-05-04T00	0	0
1986-05-04T12	45	34
1986-05-05T00	47	29
1986-05-05T12	50	36
1986-05-06T00	47	29
1986-05-06T12	49	34
1986-05-07T00	49	23
1986-05-07T12	50	37
1986-05-08T00	45	35
1986-04-26T00	41	31

A radiosonde object is created in python. The object will have the location, time and data sets of the radiosonde as attributes. The Radiosonde Class also contains a function that, when executed, will calculate the horizontal displacement of a radiosonde in each height layer. This is done by first calculating the speed in x and y direction from the wind angle and wind speed that are provided in the data set. From the decomposed wind speed, the following equations can be used to find the new x and y position.

$$x_k = x_{k-1} + (t_k - t_{k-1})\frac{(u_k - u_{k-1})}{2}, \tag{3.5}$$

$$y_k = y_{k-1} + (t_k - t_{k-1})\frac{(v_k - v_{k-1})}{2}, \tag{3.6}$$

where x_k is the x position in the current height level k, x_{k-1} is the x position in the previous

height level, and $t_k - t_{k-1}$ accounts for the time difference between the previous height level and the current height level. u is the x component of the wind speed and $u_k - u_{k-1}$ accounts for the change in wind speed from the previous height level to the current (Laroche and Sarrazin, 2013). The same can be done to find the current y position with v being the y component of the wind speed. It is assumed that the radiosonde is ascending with a rate of 5m/s as suggested in Laroche and Sarrazin (2013).

Then by using the change in x and y position, the new longitude and latitude for each height can be found by using the relationships between x, y, and latitude and longitude as explained in section 2.4.1.

These new variables will be added to the data set. Another built-in function of the radiosonde class will generate a data set in the same way, but will neglect horizontal displacement and simply use the initial latitude and longitude for all heights. This function is made so that the analysis with radiosondes with horizontal displacement can be compared to the analysis with radiosondes without horizontal displacement. Both functions will fill in missing values by backward and front fill since the data is missing from the edges and larger parts in the middle of the data sets. Lastly, knots are converted to meters per second. This is implemented in the developed program *Radiosonde_class.py*.

A number of radiosonde stations are chosen for a closer investigation at certain time points. They are chosen visually from figures 1-9, to follow the movement of the radioactive spread of cesium 137. Since the largest deposition in Scandinavia happened during the 28th and 29th of April, the wind direction is looked at every 12 hours between the 26th and 29th resulting in a total of 8 timesteps. Some of the close by stations were not available for the first day. The radiosonde station in Kiev for example, which is the closest station to the site of the accident, was not sent up until 27.04.1986 12 UTC, the day after the accident. However, the selected stations are shown in table 3.2.

Table 3.2: Radiosonde Stations that are chosen for AROME model validation following the plume towards Scandinavia

Time	latitude	Longitude	City/Country	Station Code
1986-04-26T00	52.45N	31.00E	Gomel/Belarus	33041
1986-04-26T00	49.93N	36.28E	Kharkov/Russia	34300
1986-04-26T00	53.87N	27.53E	Minsk/Belarus	26850
1986-04-26T12	53.87N	27.53E	Minsk/Belarus	26850
1986-04-26T12	56.97	24.07	Riga/Latvia	26422
1986-04-26T12	54.75N	17.53E	Leba/Poland	12120
1986-04-27T00	54.70N	20.62E	Kaliningrad/Russia	26702
1986-04-27T00	52.12N	23.68E	Brest/Belarus	33008
1986-04-27T00	53.87N	27.53E	Minsk/Belarus	26850
1986-04-27T00	59.45N	24.80E	Tallin/Estland	26038
1986-04-27T12	54.70N	20.62E	Kaliningrad/Russia	26702
1986-04-27T12	59.45N	24.80E	Tallin/Estland	26038
1986-04-27T12	57.65N	18.35	Visby/Sweden	2591
1986-04-28T00	57.67N	12.30	Goteborg/Sweden	2527
1986-04-28T00	57.65N	18.35	Visby/Sweden	2591
1986-04-28T00	60.20N	11.10	Gardermoen/Norway	1384
1986-04-28T12	57.65N	18.35	Visby/Sweden	2591
1986-04-28T12	62.53N	17.47	Sundsvall/Sweden	2365
1986-04-29T00	57.65N	18.35	Visby/Sweden	2591
1986-04-29T00	65.55N	22.13	Lulea/Sweden	2185
1986-04-29T00	57.67N	12.30	Goteborg/Sweden	2527
1986-04-29T12	65.55N	22.13	Lulea/Sweden	2185
1986-04-29T12	57.67N	12.30	Goteborg/Sweden	2527

3.3.1 Testing The Horizontal Displacement Function and Investigating Vertical Speed of Radiosonde

The Horizontal displacement function was tested by using high resolution radiosonde data from Søråsfeltet in Ås provided by MET. The data set from Søråsfeltet in Ås was up until 25000 meters height and had 2526 time points. There is a measurement every two seconds. It also contains the exact position in latitude and longitude in every measurement. Therefore it can be used to see if the latitude and longitude predicted by the code implemented in *Radiosonde_class.py* is correct.

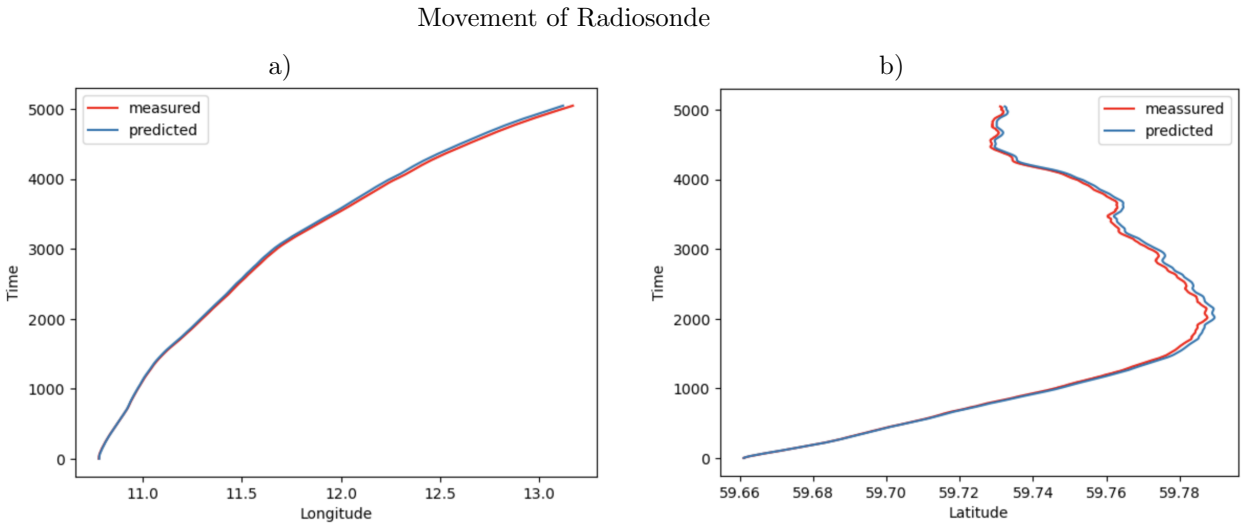

Figure 3.4: a) Movement of radiosonde along the latitudinal lines as predicted by the class function(blue) and as measured by the radiosonde(red) plotted against time from launch in seconds. b) Movement of radiosonde as predicted by the class function(blue) and as measured by the radiosonde(red) along the longitudinal lines plotted against time from launch in seconds

Along the longitudinal lines, it can be seen that the biggest difference is around 0.002 degrees which equals Approximately 200 meters. There is no apparent difference along the latitudinal lines.

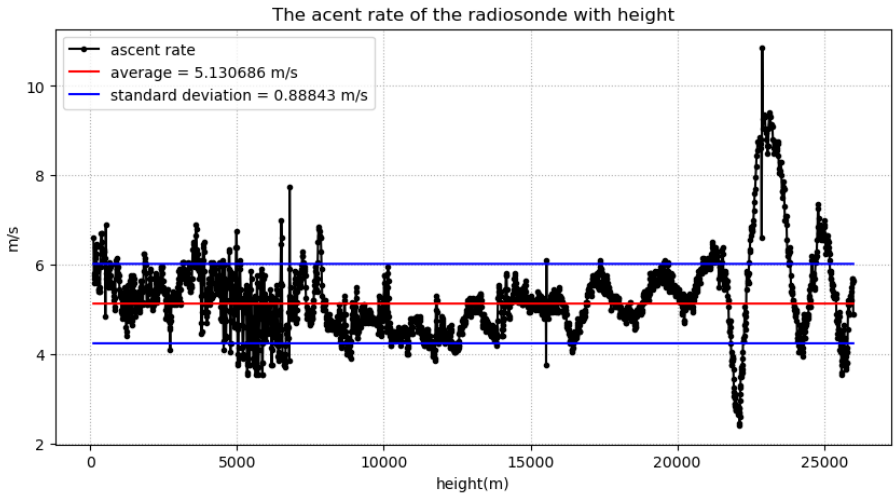

Figure 3.5: The ascent rate of the Radiosonde plotted in black. The average ascent rate and the standard deviation is plotted in red and blue respectively.

The average speed is 5.1 m/s which is the same as the average found in Laroche and Sarrazin

(2013). It is therefore continued to be used as an overall ascent rate. The code for this test was developed in the jupyter notebook file *Horizontal_displacement_test.ipynb*

3.4 Interpolation

As explained in section 2.5, the values in the model grid needs to be interpolated to have the same position in space and time as the radiosonde observations before preforming statistical analysis. Figure 3.6 shows the position of the radiosonde relative to the model grid. If the Radiosonde makes an observation of wind direction $\hat{w}$ in that point, the observation will have position $(\hat{x}, \hat{y}, \hat{h}, \hat{t})$. First the predicted wind direction w, is interpolated in the four nearest grid points in the xy plane between h_1 and h_2, resulting in four grid points having height position $\hat{h}$. Secondly these values are interpolated along the x axis, between x_1 and x_2 and obtain two variables having positon $\hat{x}$ along the x axis. Then the same is then done along the y axis. Lastly, the previous steps have to be taken for the two nearest timepoints, so that it can be interpolated along time, and finally obtain a value in position $(\hat{x}, \hat{y}, \hat{h}, \hat{t})$.

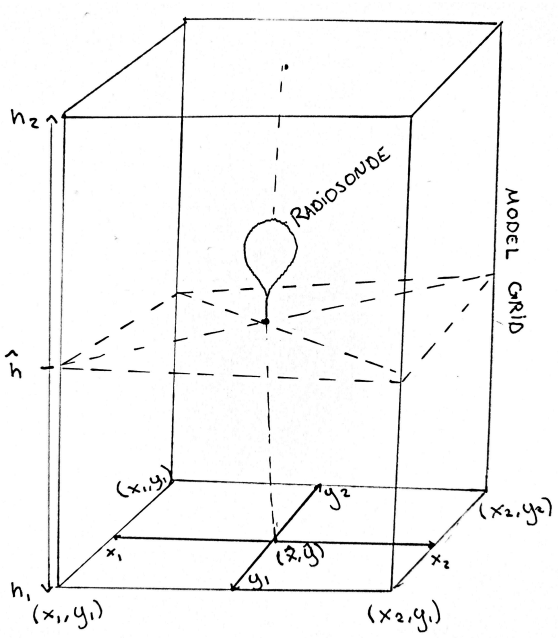

Figure 3.6: The position of a radiosonde relative to the model grid

This process is repeated for *x_wind_ml* and *y_wind_ml* presented in section 3.1, and for each radiosonde in each timestep. The wind direction is found by using geometric properties. Further it has to be repeated for wind speed. For the wind speed, the *x_wind_ml* and the *y_wind_ml* variables are interpolated in the same way as for the wind direction. Then the Pythagoras rule is used to calculate the wind speed. For both the wind speed and the wind direction, the x_wind_10m and the y_wind_10m variables are added to the pre interpolated data since the model data has its first

data point around 30 meters and the radiosondes often has their first data point below 30 meters. Since the lowest model level is at 10 meters height, all radiosonde measurements before 10 meters height are not included in the analysis.

The results are placed in *netcdf* files corresponding to the radiosonde station and the time and date of the sounding. Then the same is done, but without horizontal drift. This is done by simply letting the radiosonde ascend in a completely straight vertical line as explained in the previous subsection. The code is developed in the python file *interpolation.py*

3.5 Statistical Analysis

In the validation procedure of the model the interpolated model predictions are compared to the corresponding radiosonde observations. For the comparison the mean absolute error and mean error, explained in section 2.5, are used. The mean absolute error is chosen as a way to look at the average error over many predictions. For example, over all heights and soundings, or over all time and dates. Mean error is used in the same way, but gives also an indication to if there are any over predictions or under predictions.

To investigate the radiosonde stations, each atmospheric sounding, including all available measurements, from the separate stations are subtracted from the corresponding interpolated data points in the model predictions results, then the absolute of these errors are found before averaging over all errors for each station to find the mean absolute error. Then this is presented in a scatter plot to see if there are any stations with high errors compared to the other stations. Special attention is then paid to radiosondes with a larger mean absolute error than the majority of the other radiosondes. The results from these radiosondes are then included and excluded to see the effect on the correctness of the analysis. This is done with the data adjusted for horizontal displacement of the radiosonde observations.

The absolute error and mean error per timepoint is found by comparing the model prediction data with the corresponding radiosonde observation data. Each wind speed and wind direction in each sounding is subtracted from the corresponding interpolated data point in the model predictions results, to find the error. This is done for all heights with available radiosonde observations. Then the errors and the absolute of the errors are averaged over all data points in the same timepoint. This is done with both the data adjusted for horizontal displacement of the radiosonde observations and the data without adjustment.

To investigate the mean error and mean absolute error at different heights, height bins of 500 meters width are defined. The first bin starting at 10 meters height and ending at 500 meters height, and the last bin ending at 5010 meters height. The error and absolute error is then found by subtracting the radiosonde observations from the corresponding interpolated model prediction. Then averaging over all errors and mean errors in the same height bin to produce mean error and mean absolute error at different height intervals. The bin width of 500 meters height is chosen so that there will be enough data in each bin. The errors are plotted in a line plot against the middle height in the height bin. This is done with both the data adjusted for horizontal displacement of the radiosonde observations and the data without adjustment.

To investigate the error in the wind direction in the selected atmospheric soundings from table

3.2, the wind directions are plotted in two polar plots for each atmospheric sounding. One polar plot is for vertical levels from 10 to 1000 meters height, and one polar plot is from 1000 meter to 5000 meters height. Each radiosonde observation and corresponding interpolated model prediction is represented by two separate dots representing the rotation from north, θ, of the wind arrow as explained in section 2.4.1. The wind arrow can be found by drawing a line through the dot and origo as visualized in figure 2.3. To summarize the information from the polar plots, the mean absolute error is found for each selected atmospheric sounding in table 3.2 by subtracting the radiosonde observations from the corresponding model prediction and averaged over all errors between 10 and 1000 meters and between 1000 and 5000 meters. This is only done for the analysis with adjusting for horizontal displacement in the radiosonde observations.

For mean error in wind direction, positive bias is when the predictions are rotated less than 180 degrees clockwise from the observation. Negative bias is when the predictions are rotated less than 180 degrees counterclockwise from the observation. The maximum mean absolute error and mean error for the wind direction is 180 degrees.

The code for implementing the statistical analysis was developed in the jupyter notebook file *statistical_analysis.ipynb*.

Chapter 4

Results

In this chapter a scatter plot analysis of the mean absolute errors in the AROME model predictions for each radiosonde station is presented. Then a presentation of the mean error and mean absolute error in the wind speed and wind direction predicted by the AROME model, with focus on the hindcast around the Chernobyl accident is given. This was done with and without adjusting for horizontal displacement of the radiosonde observations. Then it looks more closely on specific atmospheric soundings to investigate the potential errors in modelled transportation of radioactivity to Norway over the first four days using radiosonde observations with horizontal drift.

4.1 Evaluation of the AROME MetCoOp Model Wind Direction and Wind Speed

4.1.1 Scatter Plot Analysis of mean absolute error in the AROME model results per Radiosonde Station

To investigate the radiosonde stations, the average of the absolute of the difference between the model predictions and the radiosonde observations is taken over all soundings and heights for each radiosonde station as explained in section 3.5. The resulting mean absolute error is shown for the wind direction and the wind speed in figure 4.1 and 4.2. If the overall error is large, there could be faulty observations from these stations. Therefore it is useful to investigate potential outliers.

Each dot represents a radiosonde station and the mean absolute error is plotted along the longitude. The country codes are explained in table 4.1.

Table 4.1: Country Codes retrieved from the ISO 3166-1 alpha-2 standard

country code	country
BE	Belgium
BY	Belarus
CZ	Czechia
DE	Germany
DK	Denmark
FI	Finland
NL	Netherlands
NO	Norway
PL	Poland
RU	Russia
SE	Sweden
SK	Slovakia
UA	Ukraine

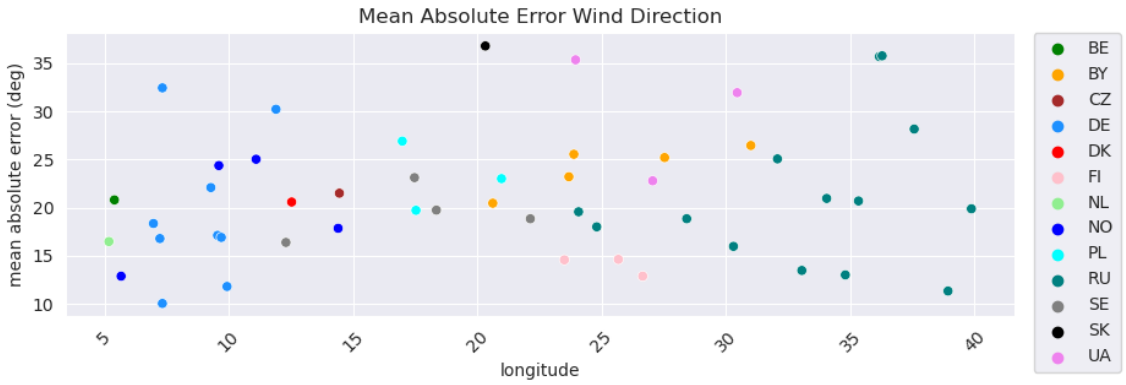

Figure 4.1: Mean absolute error in wind direction in each radiosonde station over all heights, and all time and dates. Each radiosonde station is represented by a dot, and the color represent the country. The analysis is preformed with adjusting for horizontal displacement of the radiosonde observations

In figure 4.1 it can be seen that for most of the radiosonde stations AROME has a mean absolute error between 10 and 30 degrees. However, some Russian, Ukrainian and Slovakian stations having higher values. The radiosonde stations with a mean absolute error higher than 30 degrees are shown in table 4.2. These stations are considered outliers because of high errors compared to the other radiosonde stations.

Table 4.2: Stations with a mean absolute error above 30 degrees

city/country	station code	MAE Wind Direction (deg)
Idar-Oberstein/Germany	10618	30.4
Kuemmersbruck/Germany	10771	30.2
Kursk/Russia	34009	35.7
Kharkov/Russia	34300	35.8
Poprad/Slovakia	11952	36.8
Kiev/Ukraine	33345	31.9
L'viv/Ukraine	33393	35.4

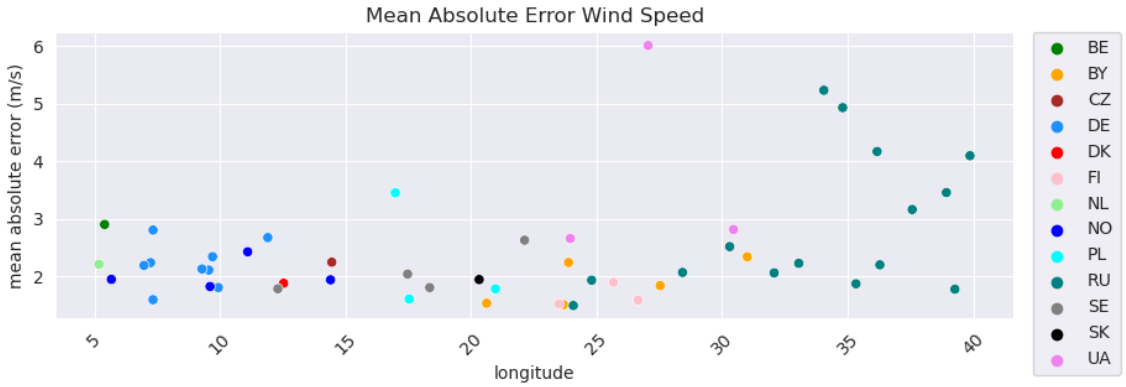

Figure 4.2: Mean absolute error in wind speed in each radiosonde station over all heights and all time and dates. Each radiosonde station is represented by a dot, and the color represent the country. The analysis is preformed with adjusting for horizontal displacement of the radiosonde observations

In figure 4.2 it can be seen that the mean absolute errors for some of the Russian and Ukrainian stations are going towards 6 m/s, while the other stations are below 3 m/s. Therefore all stations with an mean absolute error of above 3 m/s are considered outliers and are presented in table 4.3.

Table 4.3: Stations with a mean absolute error above 3 m/s

city/country	station code	MAE Wind Speed (m/s)
Wroclaw/Poland	12425	3.4
Kem/Russia	22522	4.9
Kargopol/Russia	22845	3.5
Bologoe/Russia	26298	5.2
Vologda/Russia	27037	4.1
Moscow/Russia	27612	3.2
Kursk/Russia	34009	4.2
Sepetovka/Ukraine	33317	6.0

The turbulence intensity is known to increase if the wind speed is very low as shown in section 2.3 equation 2.9. The model is not able to catch turbulence and low speeds can therefore cause large deviations between model and measurements. To see the effect of removing the outliers and the

soundings with an average speed below 1000 meters of less than 2m/s, the mean absolute error is found both with removing these soundings and without removing them. The stations from table 4.2 are only removed for the wind direction analysis, and the stations in table 4.3 are only removed from analysis of the wind speed. This is done for the wind speed per timestep, wind direction per timestep, and wind speed for each height with bin width of 500 meters height. They are made as explained in section 3.5. The resulting plots are shown below in figure 4.3, 4.4 and 4.5.

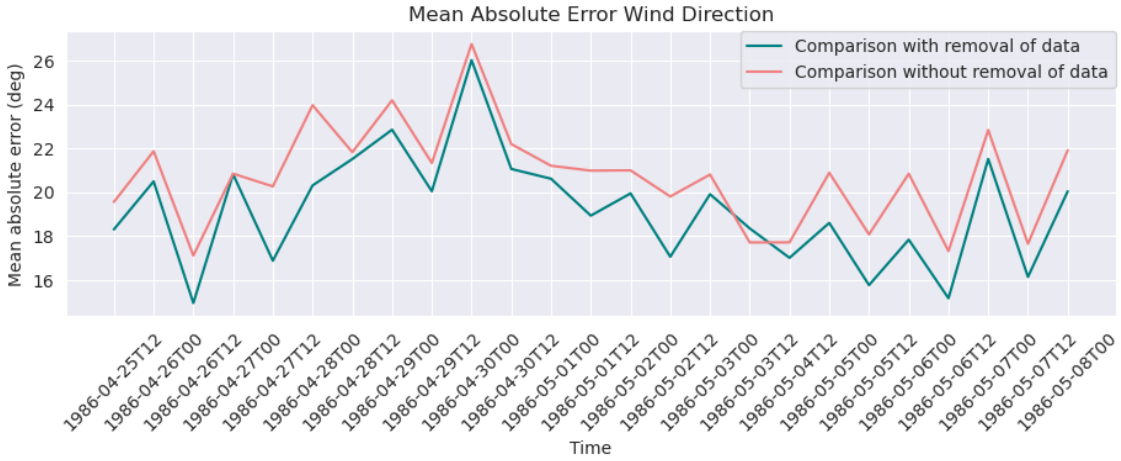

Figure 4.3: Mean absolute error in wind direction for all radiosondes and all heights in each time point. The green line showing the mean absolute error for the data with removal of outliers and soundings with mean speed below 2 m/s before 1000 meters. The red line shows the mean absolute error for the data without removal. The analysis is preformed with adjusting for horizontal displacement of the radiosonde observations

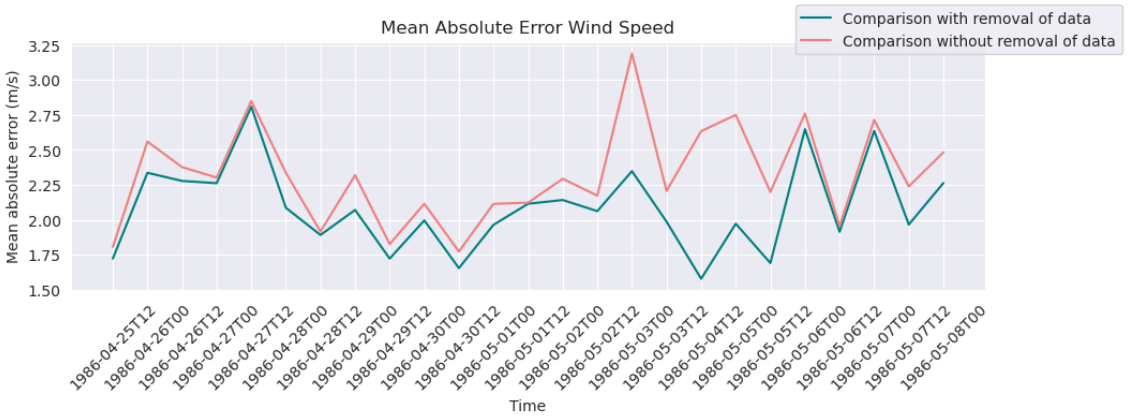

Figure 4.4: Mean absolute error in wind speed for all radiosondes and all heights in each time point. The green line showing the mean absolute error for the data with removal of outliers and soundings with mean speed below 2 m/s before 1000 meters. The red line shows the mean absolute error for the data without removal. The analysis is preformed with adjusting for horizontal displacement of the radiosonde observations

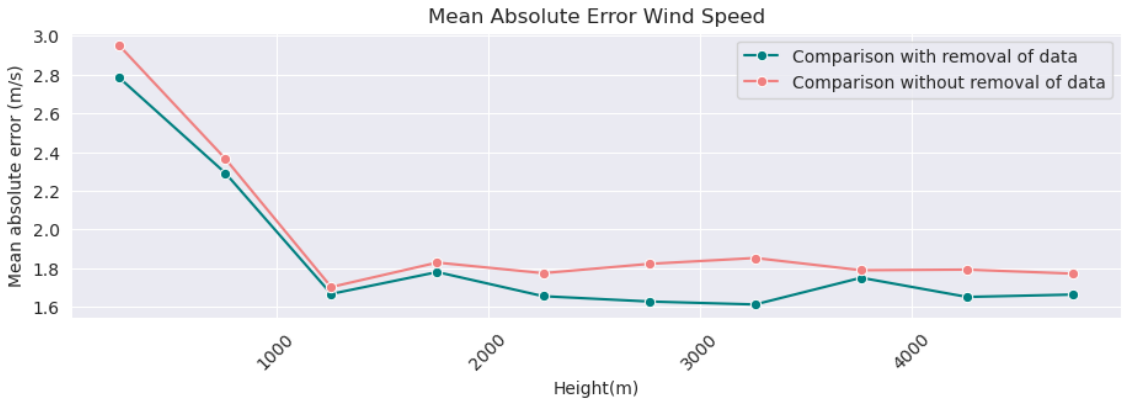

Figure 4.5: Absolute error in wind speed averaged over height bins of 500 meters resulting in mean absolute error per height. The green line showing the mean absolute error for the data with removal of outliers and soundings with mean speed below 2 m/s before 1000 meters. The red line shows the mean absolute error for the data without removal. The analysis is preformed with adjusting for horizontal displacement of the radiosonde observations

Removing the radiosonde stations from tables 4.2 and 4.3 and the soundings with low speeds as explained in the previous paragraph seem to lower the mean absolute error for all of the comparisons between the observations and predictions shown in figures 4.3, 4.4 and 4.5. In figure 4.4, a peak in mean absolute error at 03.05.1986 00 UTC is removed, making the mean average error more even across all dates and overall smoothing the plot.

4.1.2 The Error in Wind Speed and Wind Direction Per Timestep

For all plots in this section the stations with an average speed lower than 2 m/s below 1000 meters are not used. Also the stations with an average mean absolute error in wind direction larger than 30 degrees are not used for the analysis of the wind direction. The radiosonde stations with an average mean absolute error in wind speed larger than 3 m/s are not included in the analysis of the wind speed.

To evaluate the error in the wind speed and the wind direction by comparing it with the corresponding radiosonde observations, mean error and mean absolute error for each data point is calculated as explained in section 3.5. The mean error and mean absolute error for wind direction over all radiosondes and heights is plotted in figures 4.6 and 4.7. The mean error and mean absolute error in wind speed over all radiosondes and heights are shown for each time step in figures 4.8 and 4.9.

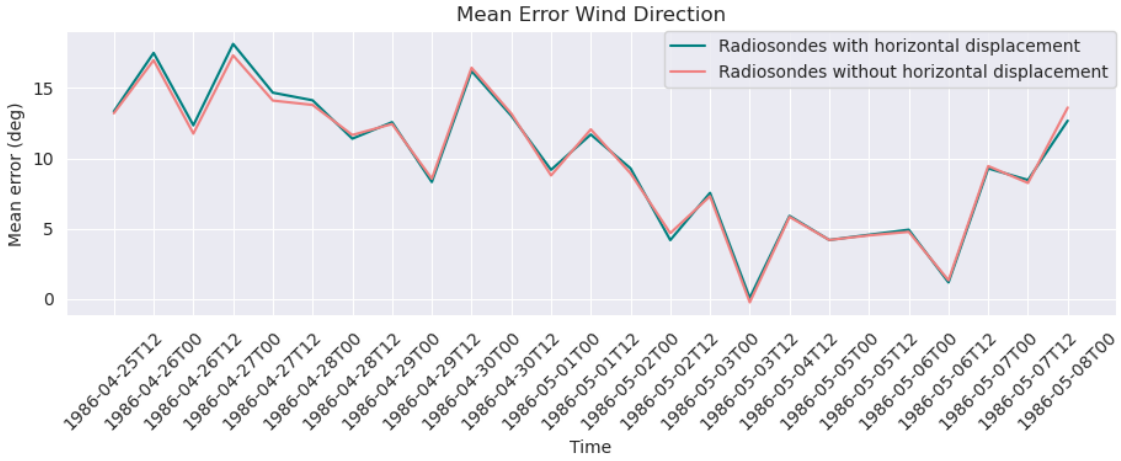

Figure 4.6: Mean error in wind direction of all radiosondes and all heights plotted for each time and date UTC. The red line showing the analysis done without adjusting for horizontal displacement of the radiosondes. The green line showing the analysis done with adjusting for horizontal displacement of the radiosondes

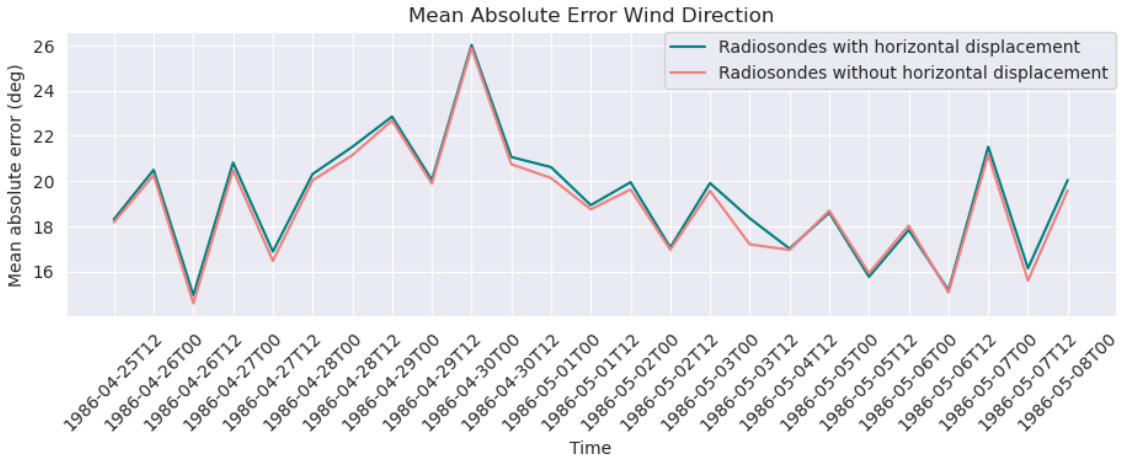

Figure 4.7: Mean absolute error in wind direction of all radiosondes and all heights plotted for each time and date UTC. The red line showing the analysis done without adjusting for horizontal displacement of the radiosondes. The green line showing the analysis done with adjusting for horizontal displacement of the radiosondes ,and is the same as the green line in figure 4.3.

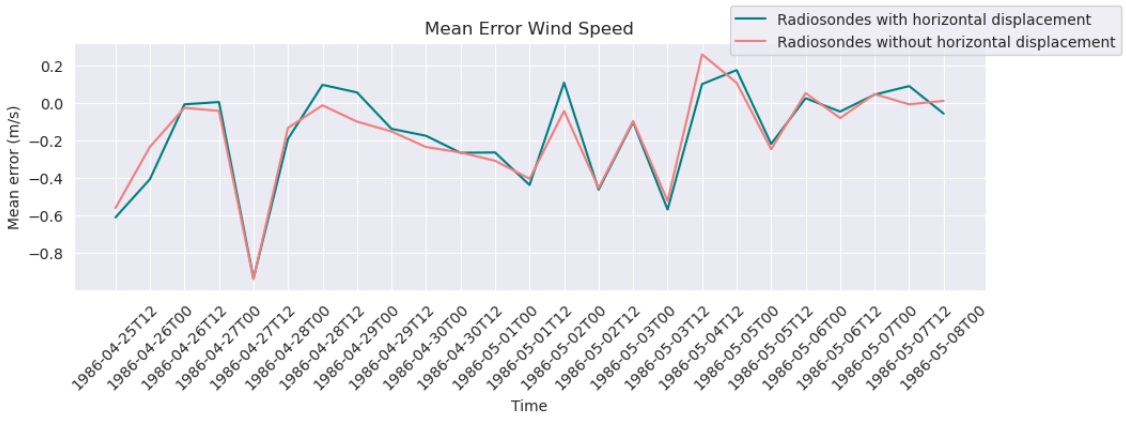

Figure 4.8: Mean error in wind speed of all radiosondes and all heights plotted for each time and date UTC. The red line showing the analysis done without adjusting for horizontal displacement of the radiosondes. The green line showing the analysis done with adjusting for horizontal displacement of the radiosondes

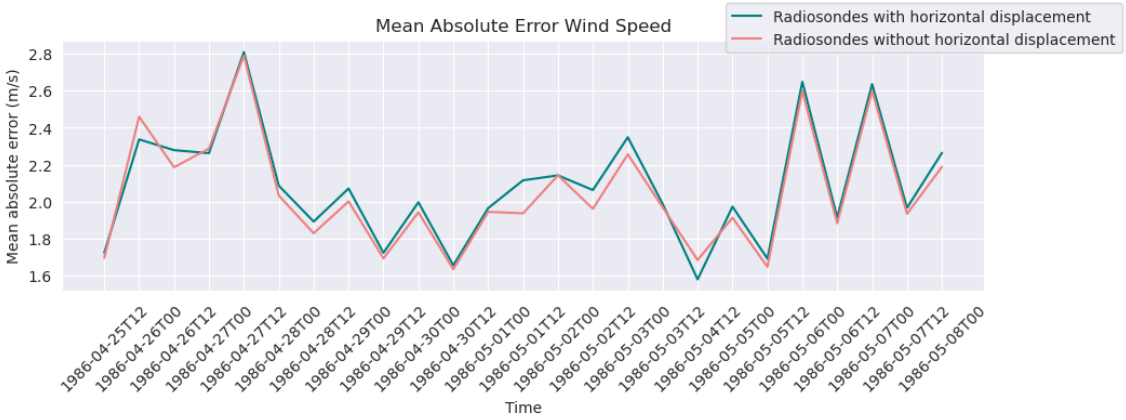

Figure 4.9: Mean absolute error in wind speed of all radiosondes and all heights plotted for each time and date UTC. The red line showing the analysis done without adjusting for horizontal displacement of the radiosondes. The green line showing the analysis done with adjusting for horizontal displacement of the radiosondes, and is the same as the green line in figure 4.4.

From figures 4.6 and 4.7 it can be seen that the difference in error in wind direction between the analysis done with adjusting for horizontal displacement of the radiosondes and the analysis done without adjusting for horizontal displacement of the radiosondes is at most 0.5 degrees for mean error and 1.0 degree for mean absolute error. For the wind speed it can be seen in figure 4.8 and figure 4.9 that the difference is at most 0.2 m/s both for the mean error and for the mean absolute error.

It can be seen in figure 4.6 that there is an overall positive bias for the wind direction. It starts at 17.0 degrees, before going to 0.1 degrees at 03.05.1886 12 UTC and then going back up to 13.5 degrees on 08.05.1986 00 UTC. The mean absolute error can be seen in figure 4.7 to be between 22.5 and 14.5 degrees while going to 26.0 degrees at 30.04.1986 00 UTC.

For the wind speed the mean error, shown in figure 4.8, is mostly below zero, showing a negative bias going to -0.9 at 27.04.1986 12 UTC. Then showing a mean error of 0.2 m/s at 05.05.1986 00

UTC, having a positive bias. The mean absolute error for the wind speed is between 1.6 m/s and 2.4 m/s. However, it goes to 2.8 m/s on 27.04.1986 12 UTC,2.6 m/s on the 06.05.1986 00 UTC, and 07.05.1986 00 UTC.

4.1.3 The Error in Wind Speed and Wind Direction With Height

To compare the radiosonde observations and model predictions for wind speed and wind direction for each height level, the mean error and mean absolute error is calculated for bins of 500 meters in altitude starting from 10 meters height as explained in section 3.5. The mean absolute error is plotted against the height in the middle of the corresponding bin. Mean absolute error and mean error for the wind direction of all radiosondes in all time and dates averaged over the different height bins are shown in figures 4.10-4.13.

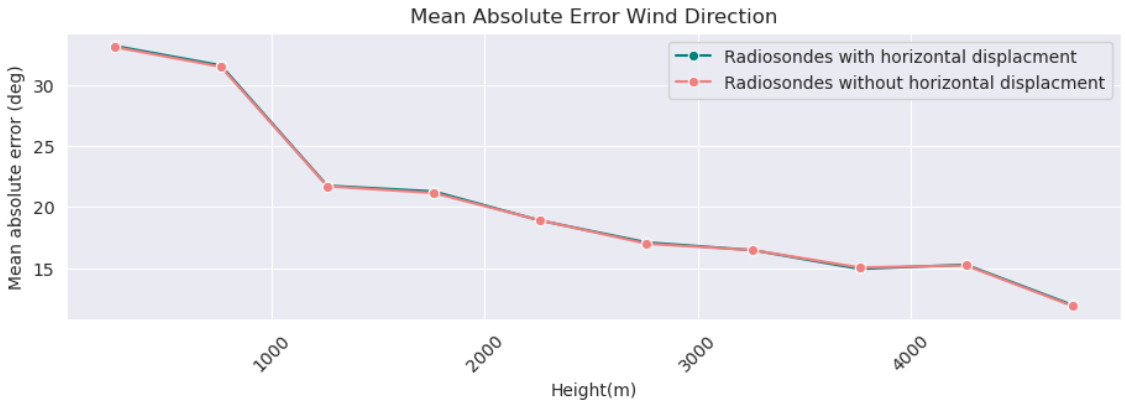

Figure 4.10: Absolute error in wind direction for all soundings averaged over height bins of 500 meters, from 10 to 5010 meters height, resulting in mean absolute error per height. The red line showing the analysis done without adjusting for horizontal displacement of the radiosondes. The green line showing the analysis done with adjusting for horizontal displacement of the radiosondes, and is the same as the green line in figure 4.5.

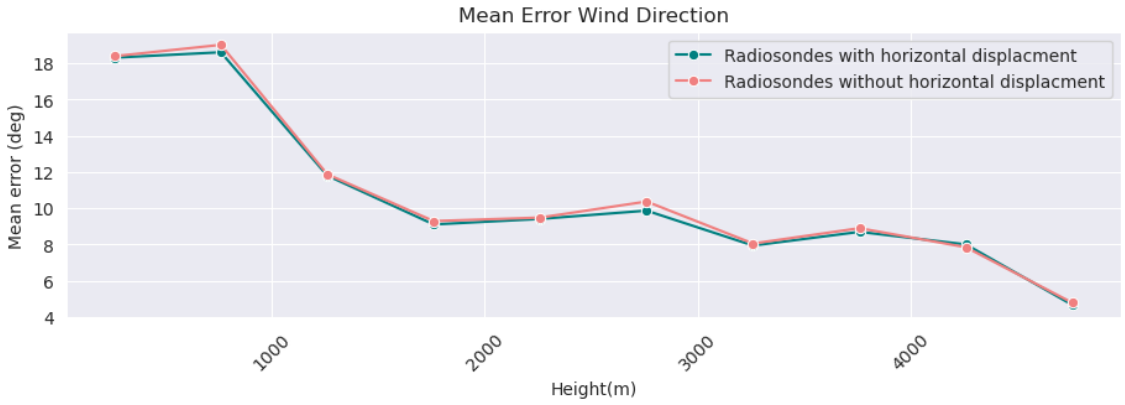

Figure 4.11: Error in wind direction for all soundings averaged over height bins of 500 meters, from 10 to 5010 meters height, resulting in mean error per height. The red line showing the analysis done without adjusting for horizontal displacement of the radiosondes. The green line showing the analysis done with adjusting for horizontal displacement of the radiosondes

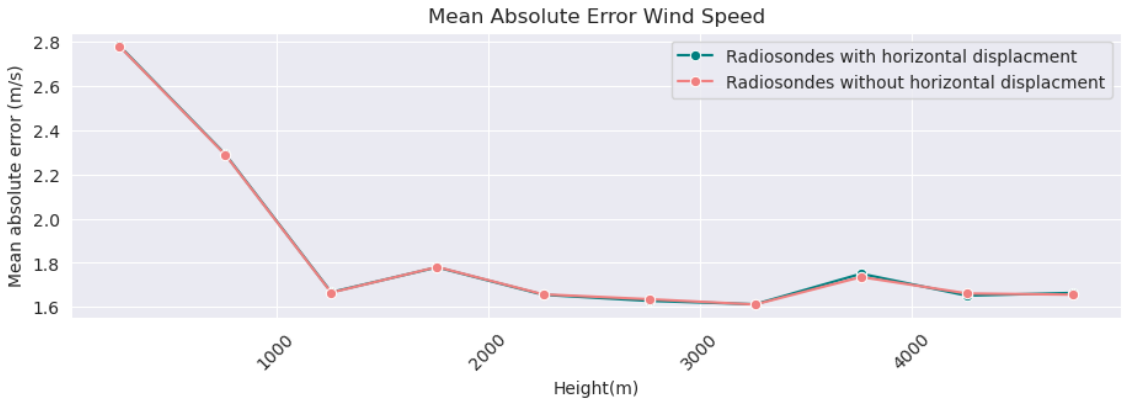

Figure 4.12: Absolute error in wind speed for all soundings averaged over height bins of 500 meters, from 10 to 5010 meters height, resulting in mean absolute error per height. The red line showing the analysis done without adjusting for horizontal displacement of the radiosondes. The green line showing the analysis done with adjusting for horizontal displacement of the radiosondes

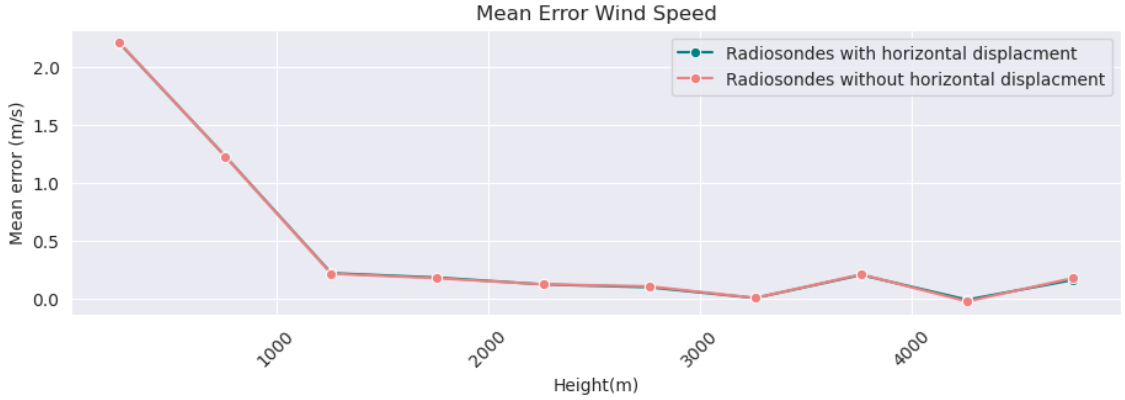

Figure 4.13: Error in wind speed for all soundings averaged over height bins of 500 meters, from 10 to 5010 meters height, resulting in mean error per height. The red line showing the analysis done without adjusting for horizontal displacement of the radiosondes. The green line showing the analysis done with adjusting for horizontal displacement of the radiosondes

In figures 4.10 and 4.13, showing the mean absolute error in wind direction and mean error wind speed, there is no visible difference between the analysis with adjusting for the horizontal displacement of radiosonde observations and the analysis without adjusting for horizontal displacement of the radiosonde observations. However in figure 4.11, showing the mean error in wind direction, a differende of 0.3 degrees can be seen.

In figure 4.10 and figure 4.11 there is a larger mean absolute error and mean error below 1000 meters for the wind direction. The mean absolute error in wind direction starts at 34.0 degrees, and is 20.0 degrees at around 2000 meters height and going to 15.0 degrees above 4000 meters height. The mean error in wind direction is positive for all heights and starts at 18.0 degrees, and is 9.5 degrees at 2000 meters height.

In figure 4.12 and figure 4.13 there is also a larger error below 1000 meter height. The absolute mean error is at 2.8 m/s for the comparison between 10 and 510 meters height and 1.6 m/s at a point after 3000 meters. The mean error starts at 2.2 m/s and is between 0.2 m/s and 0 m/s above 1000 meters height.

4.2 Error in Wind Direction Along The Path of The Radioactivity

To look at the error in the movement of the plume during the first four days, some stations are selected along the predicted movement of the radioactivity listed in table 3.2 and as explained in section 3.3. The atmospheric soundings having a mean speed below 1000 meters height of less than 2 m/s are not removed like in the previous section. This is because the observations and predictions from 1000 to 5000 meters height can still be used in the analysis. The mean absolute error and mean wind speed is shown for the selected stations in table 4.4. The mean absolute error is calculated for 0 to 1000 meters height (MAE_1) and from 1000 to 5000 meters (MAE_2). The mean speed predicted by the model is calculated for heights between 0 to 1000 meters (MS_1) and from 1000 to 5000 meters (MS_2) as explained in section 3.5.

Table 4.4: Mean absolute error in wind direction and mean speed for selected stations

Time UTC	City	MAE_1 (deg)	MAE_2 (deg)	MS_1 (m/s)	MS_2 (m/s)
1986-04-26T00	Gomel	23.2	30.7	6.8	12.8
1986-04-26T00	Kharkov	43.8	39.1	3.3	11.0
1986-04-26T00	Minsk	15.5	39.3	3.2	8.4
1986-04-26T12	Minsk	19.7	17.3	4.5	9.6
1986-04-26T12	Riga	17.0	3.2	8.2	10.1
1986-04-26T12	Leba	29.4	14.0	2.8	9.1
1986-04-27T00	Kaliningrad	20.5	1.8	6.6	9.0
1986-04-27T00	Brest	8.7	43.5	4.8	7.7
1986-04-27T00	Minsk	33.2	33.5	3.3	7.5
1986-04-27T00	Tallin	14.4	11.0	7.2	11.0
1986-04-27T12	Kaliningrad	8.1	5.6	7.5	12.1
1986-04-27T12	Tallin	55.6	4.7	6.0	9.0
1986-04-27T12	Visby	26.6	11.3	8.2	10.5
1986-04-28T00	Gothenborg	30.8	6.3	4.1	9.9
1986-04-28T00	Visby	36.0	16.1	4.3	7.6
1986-04-28T00	Gardermoen	38.6	23.0	1.8	10.1
1986-04-28T12	Visby	107.4	22.5	3.1	3.7
1986-04-28T12	Sundsvall	60.4	15.3	3.2	7.2
1986-04-29T00	Visby	175.3	12.5	0.5	8.0
1986-04-29T00	Gotenburg	115.6	16.7	1.7	9.0
1986-04-29T00	Lulea	8.5	11.6	2.6	10.4
1986-04-29T12	Lulea	8.8	21.2	4.0	5.3
1986-04-29T12	Gotenburg	15.4	8.7	2.9	7.1

To take a closer look at the error along the path of the plume, polar plots are made showing the wind direction as predicted by the model and as measured by the radiosondes as explained in section 3.5. This is done for each time step for the selected stations and shown in figures 4.15-4.32.

The polar plots showing very similar wind direction because of proximity will have one figure in the result section and one figure in appendix B. The line connecting the dots in the polar plots have different colors so that they are easier to tell apart when they are very close.

4.2.1 Error in Wind Direction 26.04.1986 00 UTC

The wind direction in Kharkov at 26.04.1986 00 UTC is shown in figure 4.14. Below 1000 meters both the predictions and the observations show a northeasterly wind with a mean absolute error of 43.8 degrees and a mean speed of 3.3 m/s. There is also a positive bias in the model. The observations are showing a more northerly wind than the predictions. Above 1000 meters there is a southeasterly wind with a mean absolute error of 39.1 degrees and a mean speed of 11.0 m/s. The model shows an easterly wind up to 3000 meters then becoming southeasterly. The observations are southeasterly from just above 1000 meters, meaning that there is a negative bias.

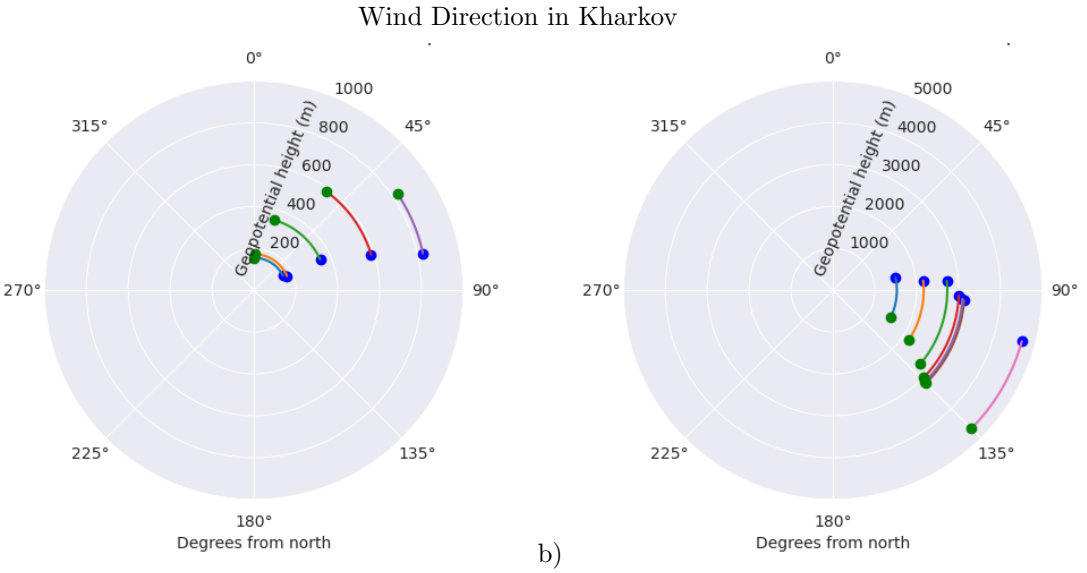

Figure 4.14: Wind direction in Kharkov at 26.04.1986 00 UTC predicted by the model plotted in blue, the measurements done by the radiosonde is plotted in green. a) shows the wind directions below 1000 meters and b) shows the wind directions between 1000 and 5000 meters. The line linking the two dots is the error

The southeasterly and easterly wind over Belarus at 26.04.1986 00 UTC can be seen in the plot showing the wind direction in Gomel (Figure 4.15). The mean absolute error below 1000 meters is calculated to be 23.2 degrees with an average speed of 6.8 m/s. Between 1000 and 5000 meters the mean average error is 30.7 degrees with a mean speed of 12.8 m/s. The figure shows a positive bias below 800 meters, and afterwards shifts to a negative bias above 800 meters height. Below 1000 meters both the observations and the predictions show an easterly wind. Above 1000 meters the observations show a southeasterly wind while the predictions show an easterly wind before showing a northeasterly wind above 4000 meters.

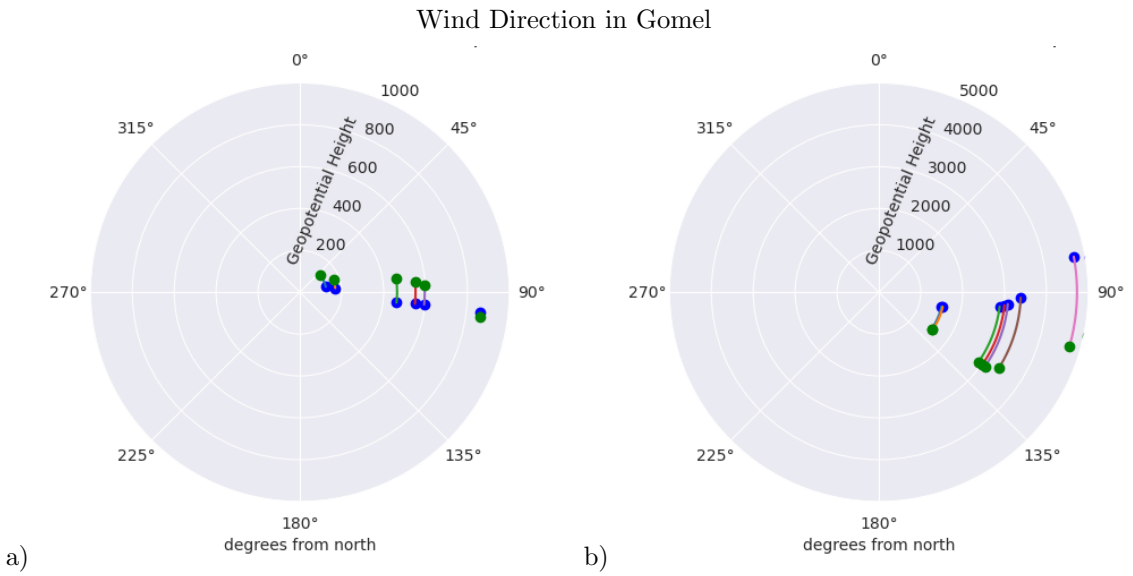

Figure 4.15: Wind direction in Gomel at 26.04.1986 00 UTC predicted by the model in blue, the measurements done by the radiosonde is plotted in green. a) shows the wind directions below 1000 meters and b) shows the wind directions between 1000 and 5000 meters. The line linking the two dots is the error

The wind direction in Minsk at 26.04.1986 00 UTC is similar to the wind direction in Gomel at 26.04.1986 00 UTC as is shown in figure 10 in Appendix B. However, there is a more southerly wind than in Gomel. Below 1000 meters there is a mean absolute error of 15.5 degrees and a mean speed of 3.2 m/s, and a southeasterly wind. Above 1000 meters there is a mean absolute error of 39.3 degrees and mean speed of 8.4 m/s and a southeasterly wind. Below 1000 meters height there is a positive bias. Above 1000 meters height the observations show a more southerly wind while the predictions show a more easterly wind resulting in a negative bias.

4.2.2 Error in Wind Direction 26.04.1986 12 UTC

The wind direction in Riga at 26.04.1986 12 UTC is shown in figure 4.16. The mean error below 1000 meters is 17.0 degrees and the mean speed is 8.2 m/s. Above 1000 meters the mean absolute error is 3.2 and the mean speed is 10.1. Below 1000 meters there is a southeasterly wind. There is a negative bias. Above 1000 meters there is a southerly wind becoming southwesterly above 3000 meters. There is slight negative bias.

The wind direction in Minsk at 26.04.1986 12 UTC is shown in figure 4.17. There is a positive bias below 1000 meters with a southeasterly wind. There is a mean absolute error of 19.7 degrees and a mean speed of 4.5 m/s. Above 1000 meters there is a mean absolute error of 17.3 and a mean speed of 9.6 m/s. There is a negative bias above 1000 meters with a southeasterly wind.

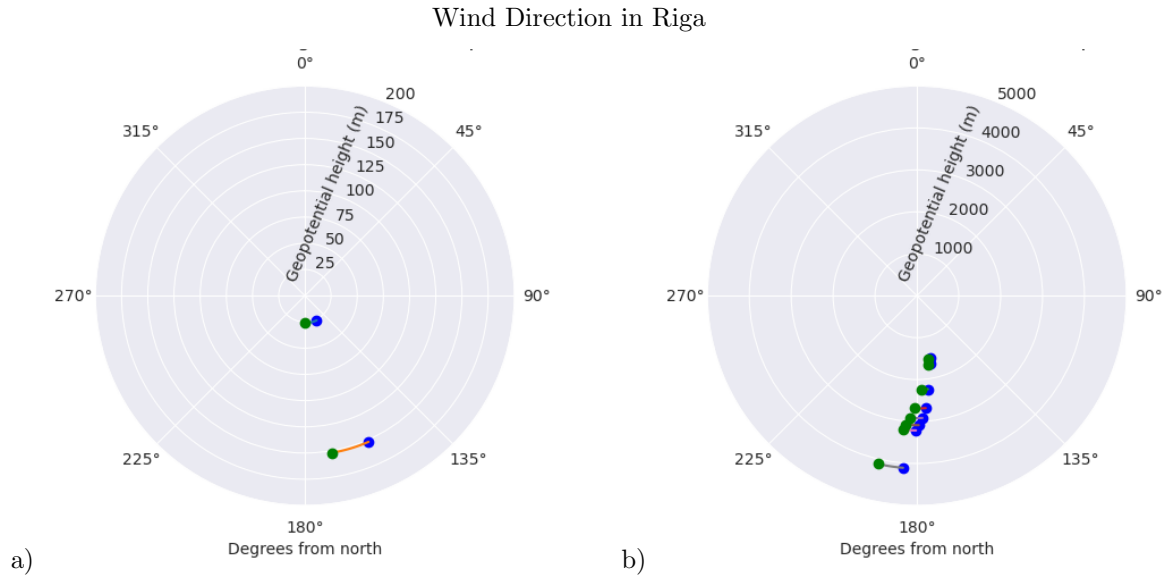

Figure 4.16: Wind direction in Riga at 26.04.1986 12 UTC predicted by the model in blue, the measurements done by the radiosonde is plotted in green. a) shows the wind directions below 1000 meters and b) shows the wind directions between 1000 and 5000 meters. The line linking the two dots is the error.

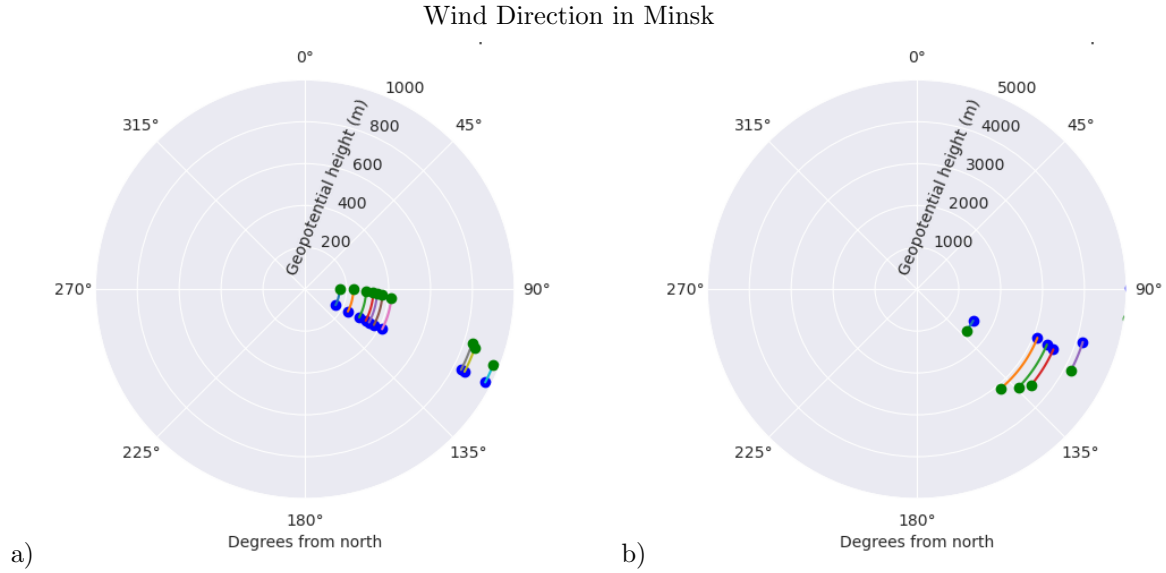

Figure 4.17: Wind direction in Minsk at 26.04.1986 12 UTC predicted by the model in blue, the measurements done by the radiosonde is plotted in green. a) shows the wind directions below 1000 meters and b) shows the wind directions between 1000 and 5000 meters. The line linking the two dots is the error.

The wind direction in Leba at 26.04.1986 12 UTC is shown in figure 4.18. There is a northeasterly wind before changing to a more easterly wind at around 400 meters. The radiosonde observed a northeasterly and easterly wind while the model predicted a southeasterly wind after 400 meters. There is a mean absolute error of 29.4 degrees below 1000 meters and a mean speed of 2.8 m/s, and a positive bias. Above 1000 meters there is a mean absolute error of 14.0 degrees and a mean speed of 9.1 m/s. The observations show a more southwesterly wind while the predictions show a southerly wind resulting in a negative bias above 1000 meters.

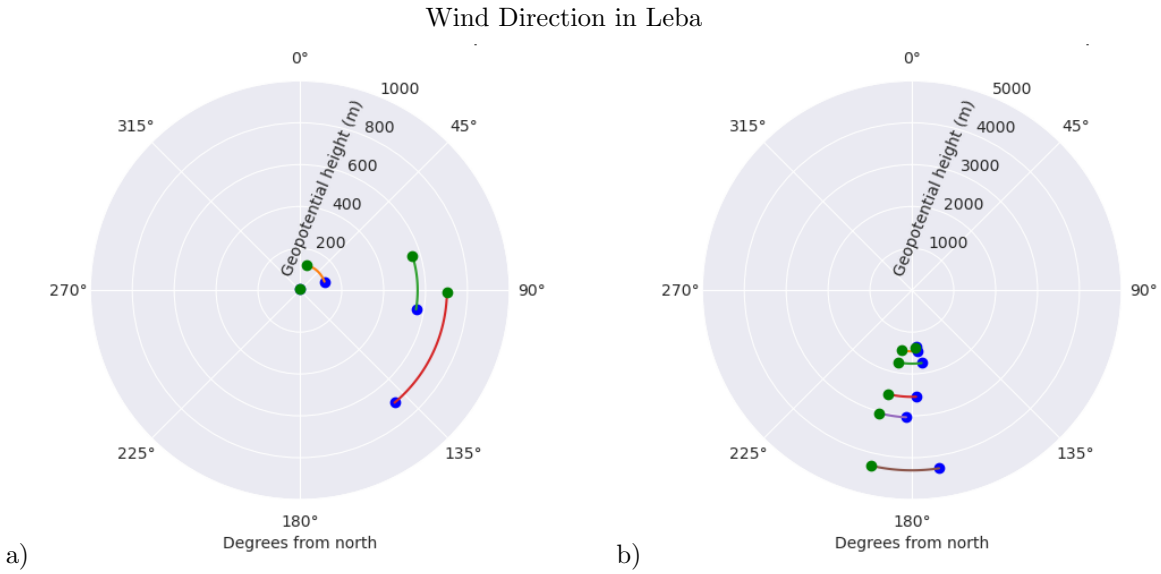

Figure 4.18: Wind direction in Leba at 26.04.1986 12 UTC predicted by the model in blue, the measurements done by the radiosonde is plotted in green. a) shows the wind directions above 1000 meters and b) shows the wind directions between 1000 and 5000 meters. The line linking the two dots is the error.

4.2.3 Error in Wind Direction 27.04.1986 00 UTC

The wind direction in Tallin at 27.04.1986 00 UTC is shown in figure 4.19. There is a southerly wind and positive bias below 1000 meters with a mean absolute error of 14.4 degrees and a mean speed of 7.2 m/s. Above 1000 meters there is a mean absolute error of 11.0 degrees and a mean speed of 11.0 m/s. There is a southwesterly wind above 1000 meters and a negative bias.

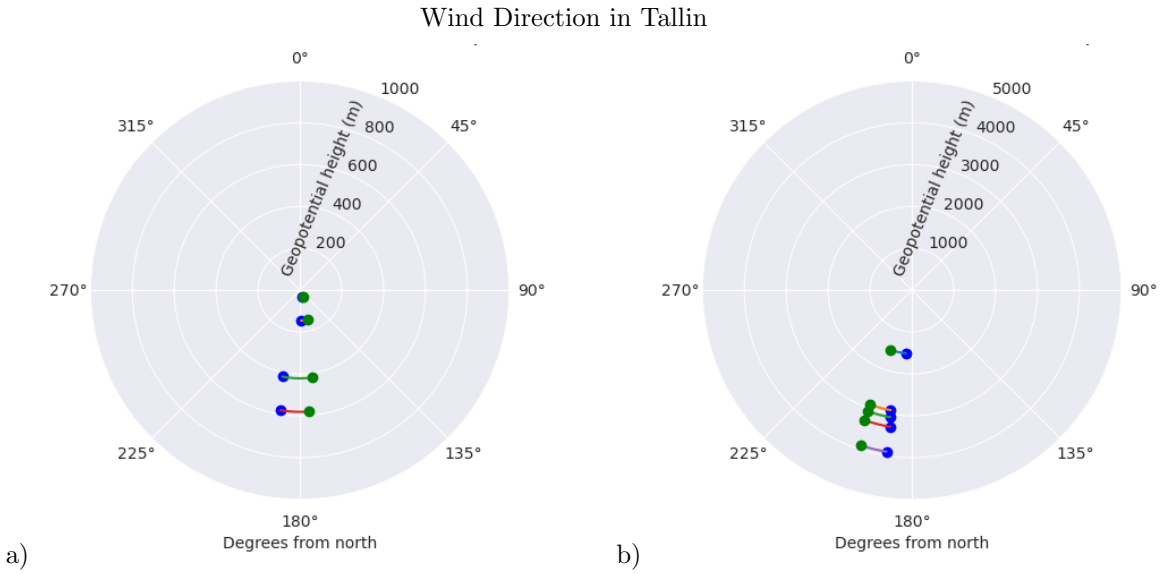

Figure 4.19: Wind direction in Tallin at 27.04.1986 00 UTC predicted by the model in blue, the measurements done by the radiosonde is plotted in green. a) shows the wind directions below 1000 meters and b) shows the wind directions between 1000 and 5000 meters. The line linking the two dots is the error.

The wind direction in Kaliningrad at 27.04.1986 00 UTC is shown in figure 4.20. There is a southeasterly wind below 1000 meters with a positive bias. Further, there is a mean absolute error of 20.5 degrees and a mean speed of 6.6 m/s. Above 1000 meters there is still a southeasterly wind. There is a slight negative bias with a mean absolute error of 1.8 degrees and a mean speed of 9.0 m/s.

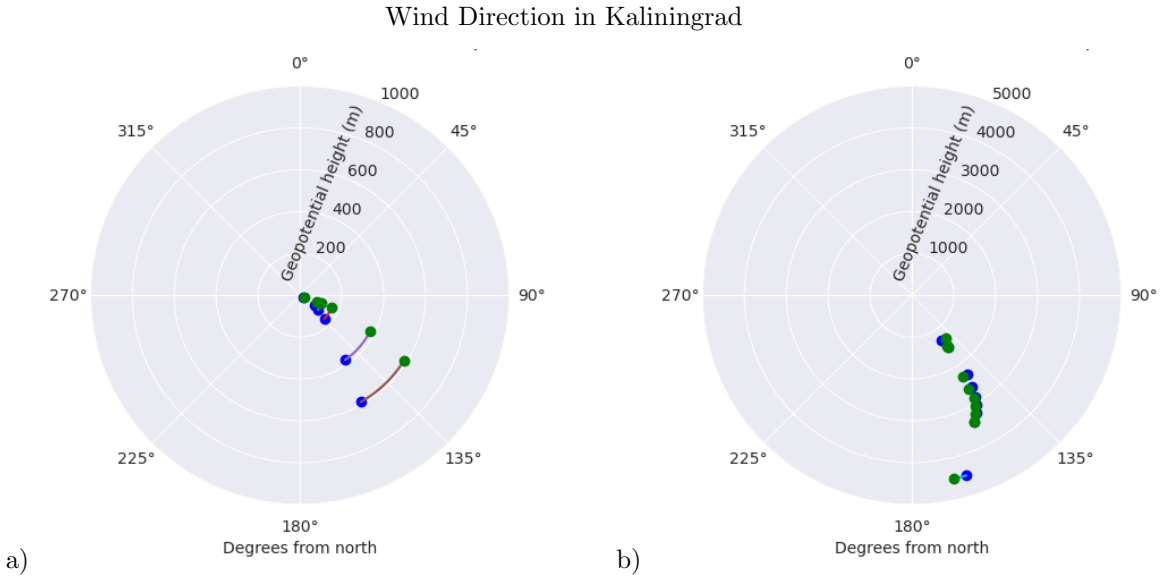

a) b)

Figure 4.20: Wind direction in Kaliningrad at 27.04.1986 00 UTC predicted by the model(blue) and the measurements done by the radiosonde (green). a) shows the wind directions below 1000 meters and b) shows the wind directions between 1000 and 5000 meters. The line linking the two dots is the error.

The wind direction in Brest at 27.04.1986 00 UTC is similar to the wind in Kaliningrad and is shown in figure 11 in appendix B. Below 1000 meters there is a southeasterly and easterly wind with a mean absolute error of 8.7 degrees and a mean speed of 4.8 m/s. Above 1000 meters there are more changes in wind direction. There is an overall negative bias with the observations showing a southeasterly wind before showing an easterly/northeasterly wind above 4000 meters height. Above 1000 meters there is a mean bias of 43.5 degrees and mean speed of 7.7 m/s.

The wind direction in Minsk at 27.04.1986 00 UTC is shown in figure 4.21. Below 1000 meters the observations show an easterly wind and the predictions show a southeasterly wind resulting in a positive bias. There is a mean absolute error of 33.2 degrees and mean speed of 3.3 m/s. Above 1000 meters there is a mean absolute error of 33.5 degrees and a mean speed of 7.5 m/s. Furthermore, there is a negative bias, with the observed wind directions showing a southeasterly wind and the predictions showing easterly wind.

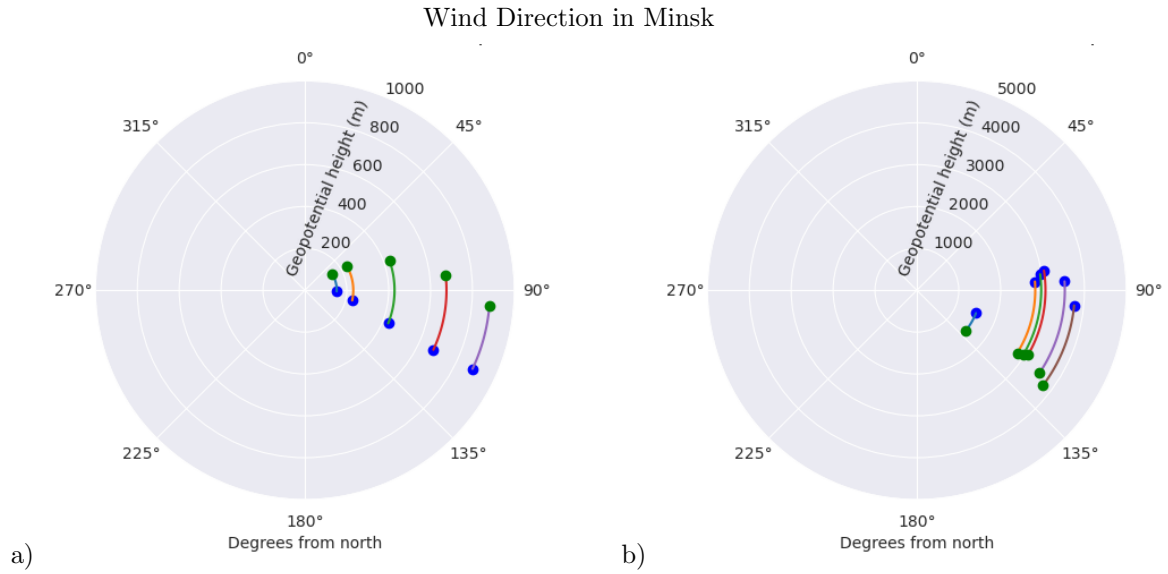

Figure 4.21: Wind direction in Minsk at 27.04.1986 00 UTC predicted by the model in blue, the measurements done by the radiosonde is plotted in green. a) shows the wind directions below 1000 meters and b) shows the wind directions between 1000 and 5000 meters. The line linking the two dots is the error.

4.2.4 Error in Wind Direction 27.04.1986 12 UTC

The wind direction in Kaliningrad at 27.04.1986 12 UTC is shown in figure 4.22. Below 1000 meters there is a southeasterly wind with mean absolute error of 8.1 degrees and a mean speed of 7.5 m/s. Above 1000 meters there is a mean absolute error of 5.6 degrees and a mean speed of 12.1 m/s. Above 1000 meters height there is a southeasterly wind. At around 3000 and 4000 meters height the observations show a southerly wind. There is a negative bias above 3000 meters.

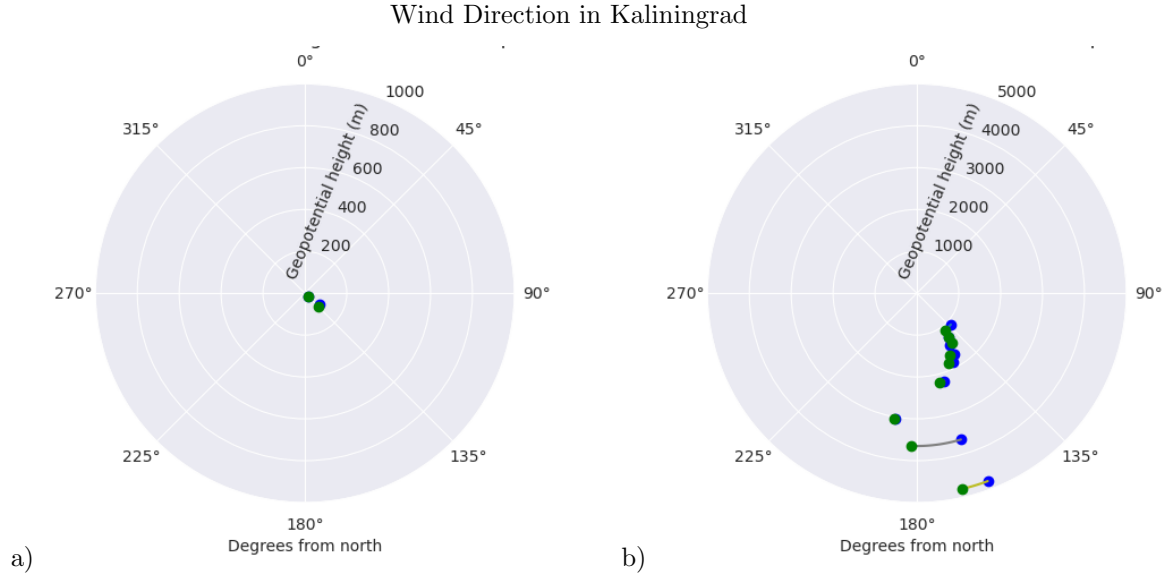

Figure 4.22: Wind direction in Kaliningrad at 27.04.1986 12 UTC predicted by the model in blue, the measurements done by the radiosonde is plotted in green. a) shows the wind directions below 1000 meters and b) shows the wind directions between 1000 and 5000 meters. The line linking the two dots is the error.

The wind direction in Tallinn at 27.04.1986 12 UTC is shown in figure 4.23. The observations show a southwesterly wind below 1000 meters and the predictions show a southerly wind. There is a mean absolute error of 55.6 degrees and a mean speed of 6.0 m/s. Above 1000 meters there is mean absolute error of 4.7 degrees and a mean speed of 9.0 m/s. There is a southwesterly wind above 2000 meters height. There is a negative bias below 1000 meters and a slight negative bias above 1000 meters height.

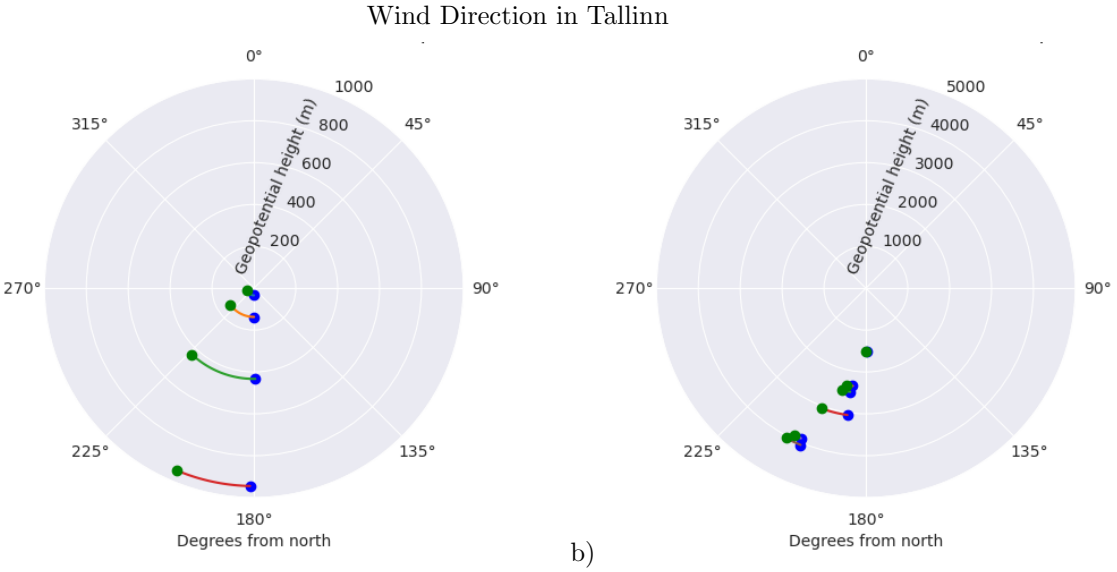

Figure 4.23: Wind direction in Tallin at 27.04.1986 12 UTC predicted by the model (blue) and the measurements done by the radiosonde (green). a) shows the wind directions below 1000 meters and b) shows the wind directions between 1000 and 5000 meters. The line linking the two dots is the error.

The wind direction in Visby at 27.04.1986 12 UTC is shown in figure 4.24. For this station there were only two datapoints below 1000 meters and both were below 100 meters. It is therefore zoomed in on 200 meters. Below 1000 meters there is a southeasterly wind. There is a positive bias, and a mean absolute error of 26.6 degrees and a mean speed of 8.2 m/s. Above 1000 meters there is a southeasterly wind turning to become southwesterly, with the observations turning at around 2000 meters and the predictions turning at around 3000 meters, with a mean absolute error of 11.3 degrees and a mean speed of 10.5 m/s.

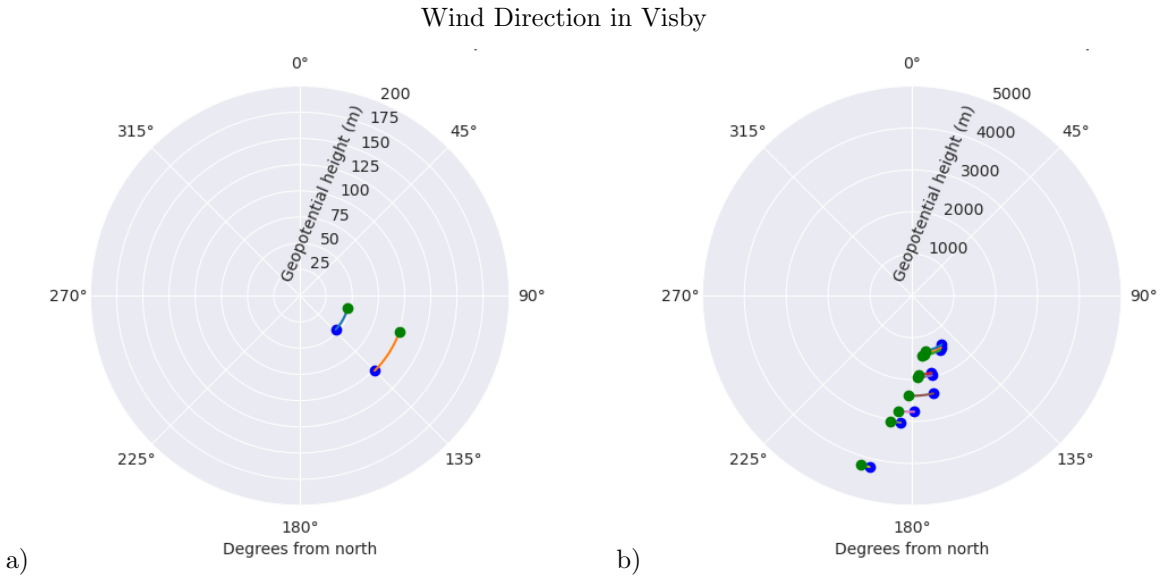

Figure 4.24: Wind direction in Visby at 27.04.1986 12 UTC predicted by the model (blue) and the measurements done by the radiosonde (green). a) shows the wind directions below 1000 meters and b) shows the wind directions between 1000 and 5000 meters. The line linking the two dots is the error.

4.2.5 Error in Wind Direction 28.04.1986 00 UTC

The wind direction in Gothenburg at 28.04.1986 00 UTC is shown in figure 4.25. Below 1000 meters the model predicts a mostly southerly wind while the observations show a southeasterly wind. Therefore, there is a positive bias and mean absolute error of 30.8 degrees and a mean speed of 4.1 m/s. Above 1000 meters the wind is southeasterly. With a southerly wind above 4000 meters, the mean absolute error is 6.3 degrees and the mean speed is 9.9 m/s. There positive bias becomes smaller above 1000 meters.

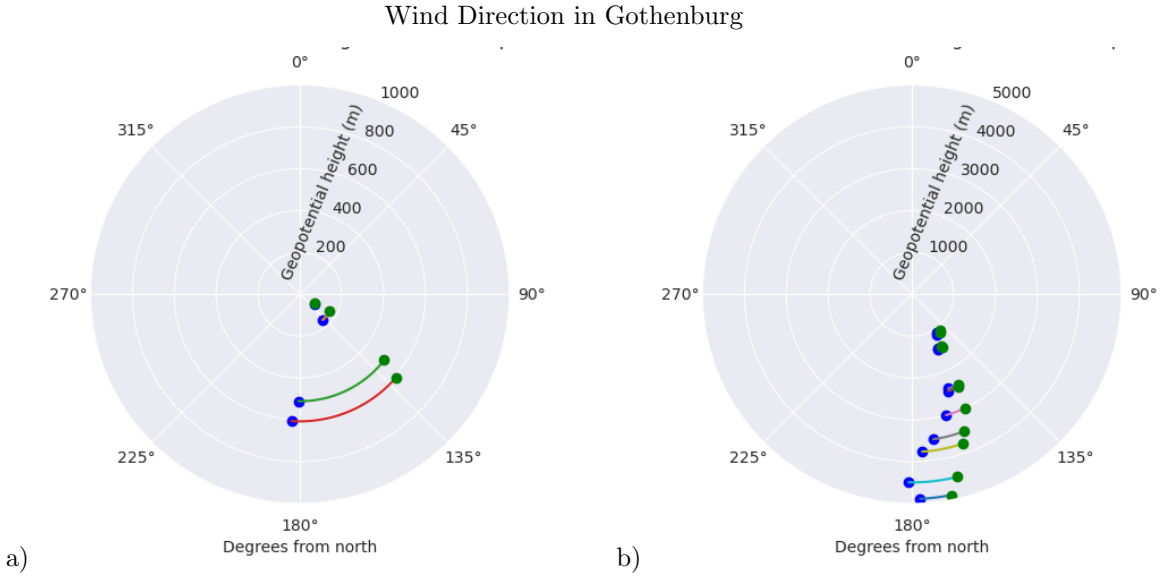

Figure 4.25: Wind direction in Gothenburg at 28.04.1986 00 UTC predicted by the model (blue) and the measurements done by the radiosonde (green). a) shows the wind directions below 1000 meters and b) shows the wind directions between 1000 and 5000 meters. The line linking the two dots is the error.

The wind direction in Visby at 28.04.1986 00 UTC is similiar to the wind in Gothenburg and is shown in figure 12 in Appendix B. Below 1000 meters there is a southeasterly wind with a mean absolute error of 36.0 degrees and a mean speed of 4.3 m/s. There is also a positive bias. Above 1000 meters there is still a southeasterly wind with mean absolute error of 16.1 degrees and a mean speed of 7.6 m/s. The observations are showing a southeasterly wind above 1000 meters.

The wind direction at Gardermoen at 28.04.1986 00 UTC is shown in figure 4.26. Below 1000 meters the predictions show an easterly wind and the observations show a northeasterly wind, meaning there is a positive bias. The mean absolute error below 1000 meters is 38.6 degrees and there is a mean speed of 1.8 m/s. The mean absolute error above 1000 meters is 23.0 degrees and the mean speed is 10.1 m/s. The wind above 1000 meters is southeasterly wind turning towards the east with height, and with a continuing positive bias.

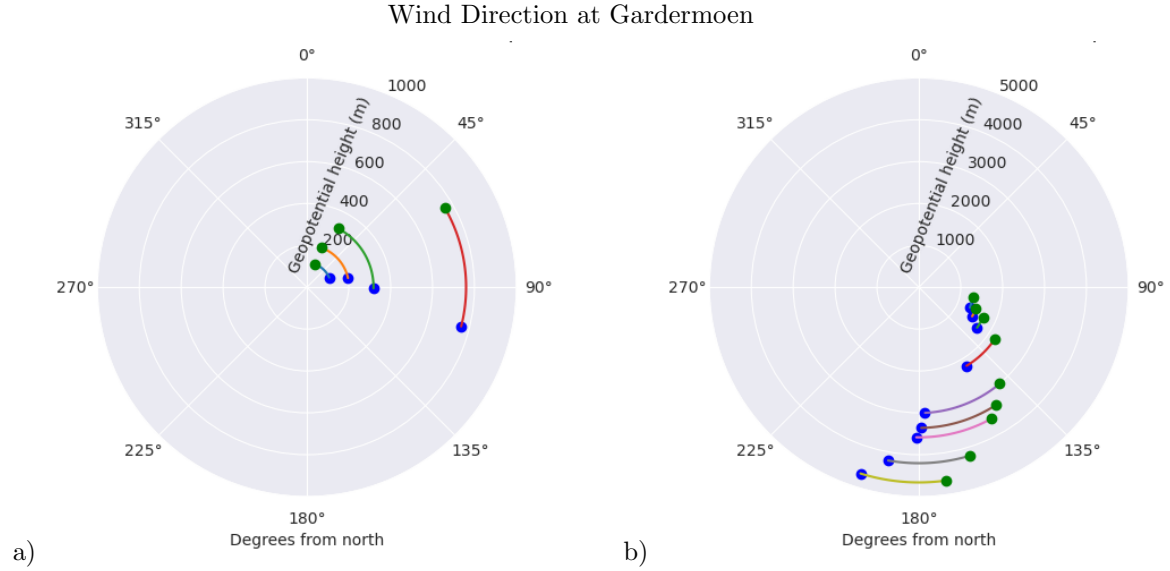

Figure 4.26: Wind direction in Gardermoen at 28.04.1986 00 UTC predicted by the model (blue) and the measurements done by the radiosonde (green). a) shows the wind directions below 1000 meters and b) shows the wind directions between 1000 and 5000 meters. The line linking the two dots is the error.

4.2.6 Error in Wind Direction 28.04.1986 12 UTC

The wind direction in Visby at 28.04.1986 12 UTC is shown in figure 4.27. Below 1000 meters there is a mean absolute error of 107.4 degrees and a mean speed of 3.1 m/s. The predictions show a southeasterly wind and the observations show a westerly wind leading to a negative bias. Above 1000 meters there is a mean absolute error of 22.5 degrees and a mean error of 3.7 m/s. There is a southeasterly wind above 1000 meters. However, the observations show a southwesterly wind between 1000 and 2000 meters height.

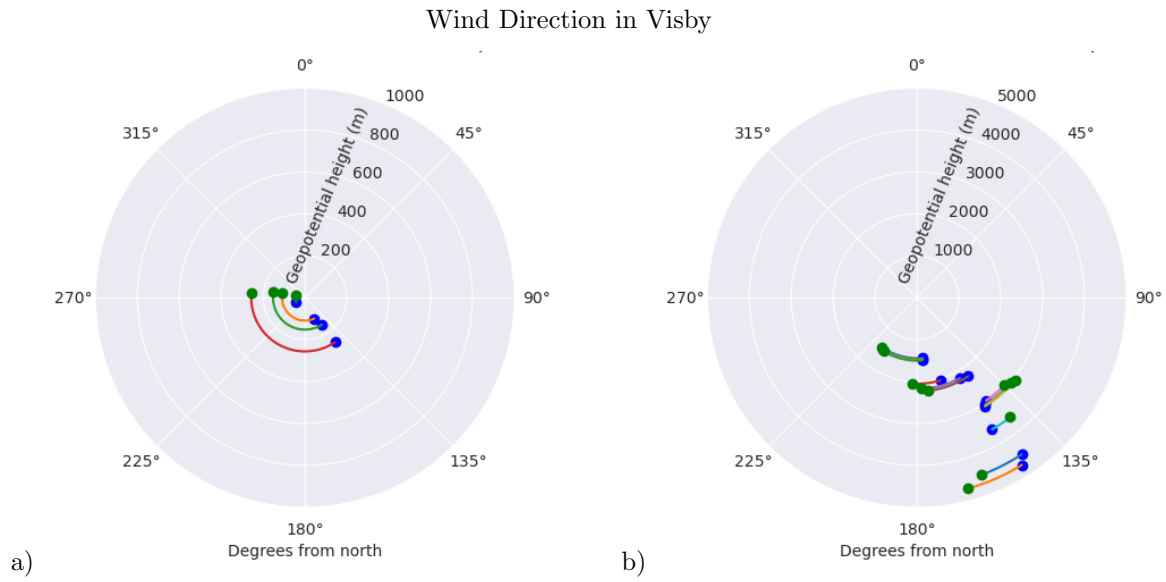

Figure 4.27: Wind direction in Visby at 28.04.1986 12 UTC predicted by the model (blue) and the measurements done by the radiosonde (green). a) shows the wind directions below 1000 meters and b) shows the wind directions between 1000 and 5000 meters. The line linking the two dots is the error.

The wind direction in Sundsvall at 28.04.1986 12 UTC is shown in figure 4.28. Below 1000 meters there is a mean absolute error of 60.4 degrees and a mean speed of 3.2 m/s. There is an observed slight southerly wind and a predicted easterly wind, resulting in a positive bias. Above 1000 meters there is a mean absolute error of 15.3 degrees and a mean speed of 7.2 m/s, and a southwesterly wind.

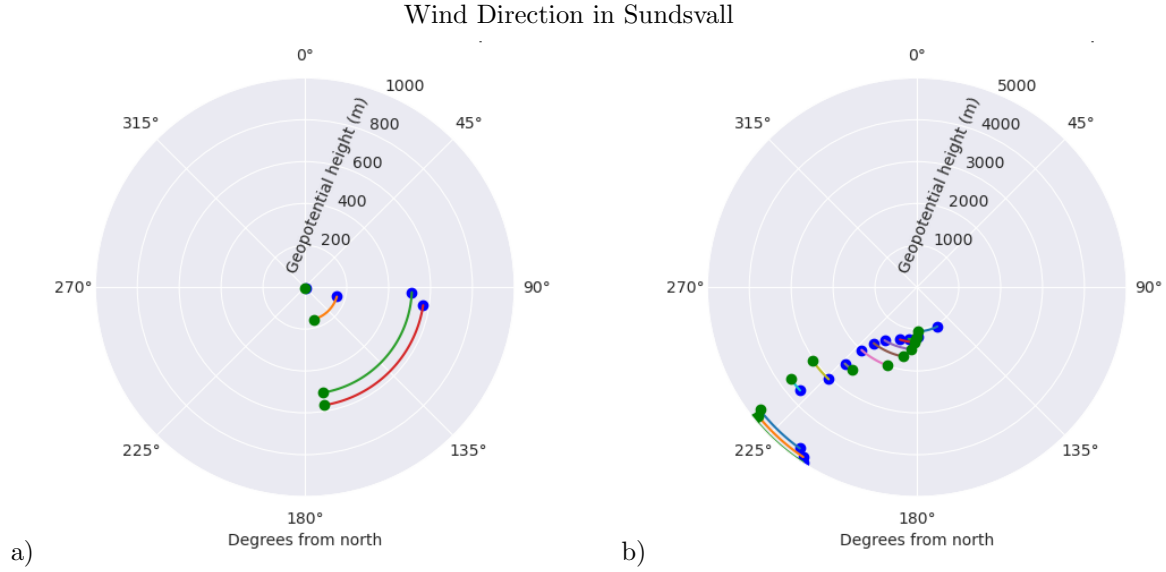

Figure 4.28: Wind direction in Sundsvall at 28.04.1986 12 UTC predicted by the model (blue) and the measurements done by the radiosonde (green). a) shows the wind directions below 1000 meters and b) shows the wind directions between 1000 and 5000 meters. The line linking the two dots is the error.

4.2.7 Error in Wind Direction 29.04.1986 00 UTC

The wind direction in Visby at 29.04.1986 00 UTC is shown in figure 4.29. Below 1000 meters the predictions show a westerly wind while the observations show a southeasterly wind. There is a mean absolute error of 175.3 degrees and mean speed of 0.5 m/s. Above 1000 meters there is a mean absolute error of 12.5 degrees and a mean speed of 8.0 m/s. There is a southwesterly wind. However, the observations show a southeasterly wind between 1000 and 2000 meters height.

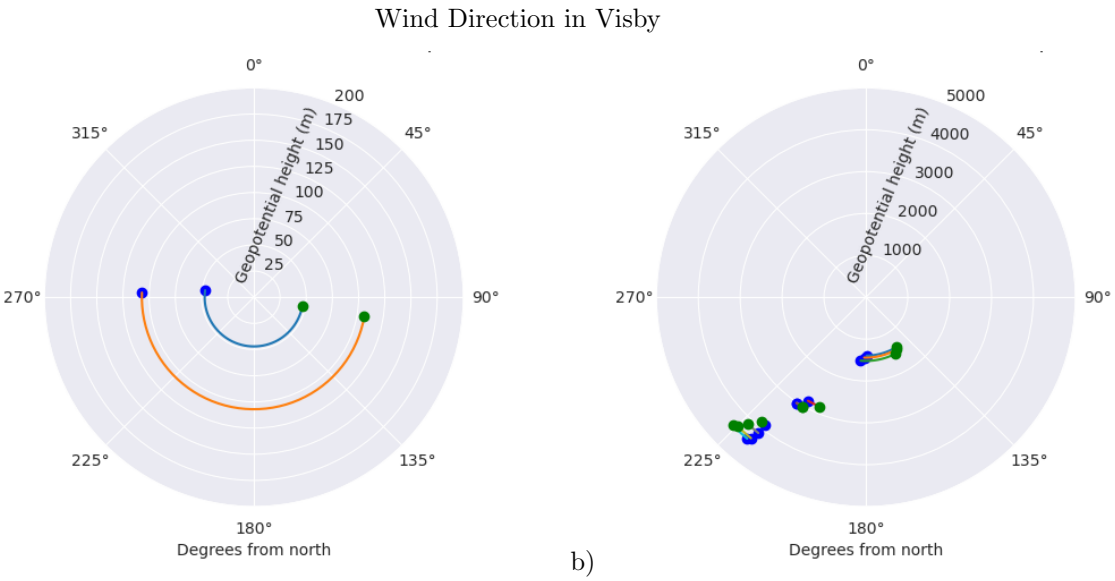

Figure 4.29: Wind direction in Visby at 29.04.1986 00 UTC predicted by the model (blue) and the measurements done by the radiosonde (green). a) shows the wind directions below 1000 meters and b) shows the wind directions between 1000 and 5000 meters. The line linking the two dots is the error.

The wind direction in Gotenburg at 29.04.1986 00 UTC is similar to the wind direction in Visby and shown in figure 13 in Appendix B. Below 1000 meters the predictions show a westerly wind while the observations show an easterly wind. There is a mean absolute error of 115.6 degrees and mean speed of 1.7 m/s. Above 1000 meters there is a mean absolute error of 16.7 degrees and a mean speed of 9.0 m/s. Above 1000 meters there is a southwesterly wind. There is a slight negative bias above 1000 meters height.

The wind direction in Lulea at 29.04.1986 00 UTC is shown in figure 4.30. There is a northeasterly wind and a positive bias below 1000 meters. Further there is a mean absolute error of 8.5 degrees and a mean speed of 2.6 m/s. Above 1000 meters there is a mean absolute error of 11.6 degrees and a mean speed of 10.4 m/s. There is a northeasterly wind below 2000 meters before turning towards a northwesterly wind.

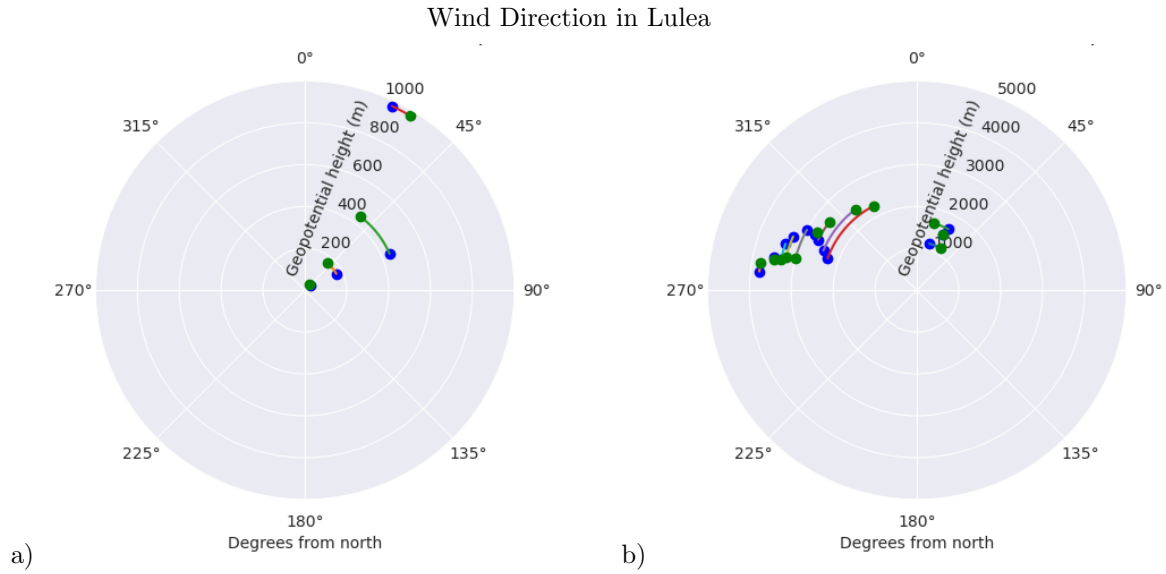

Figure 4.30: Wind direction in Lulea at 29.04.1986 00 UTC predicted by the model (blue) and the measurements done by the radiosonde (green). a) shows the wind directions below 1000 meters and b) shows the wind directions between 1000 and 5000 meters. The line linking the two dots is the error.

4.2.8 Error in Wind Direction 29.04.1986 12 UTC

The wind direction in Lulea at 29.04.1986 12 UTC is shown in figure 4.31. There is a northeasterly wind below 1000 meters and a negative bias. Below 1000 meters there is a mean absolute error of 8.8 degrees and a mean speed of 4.0 m/s. Above 1000 meters there is a mean absolute error of 21.2 degrees and a mean speed 5.3 m/s. Above 1000 meters the wind turns counterclockwise from being northeasterly to being northwesterly, continuing to have a negative bias.

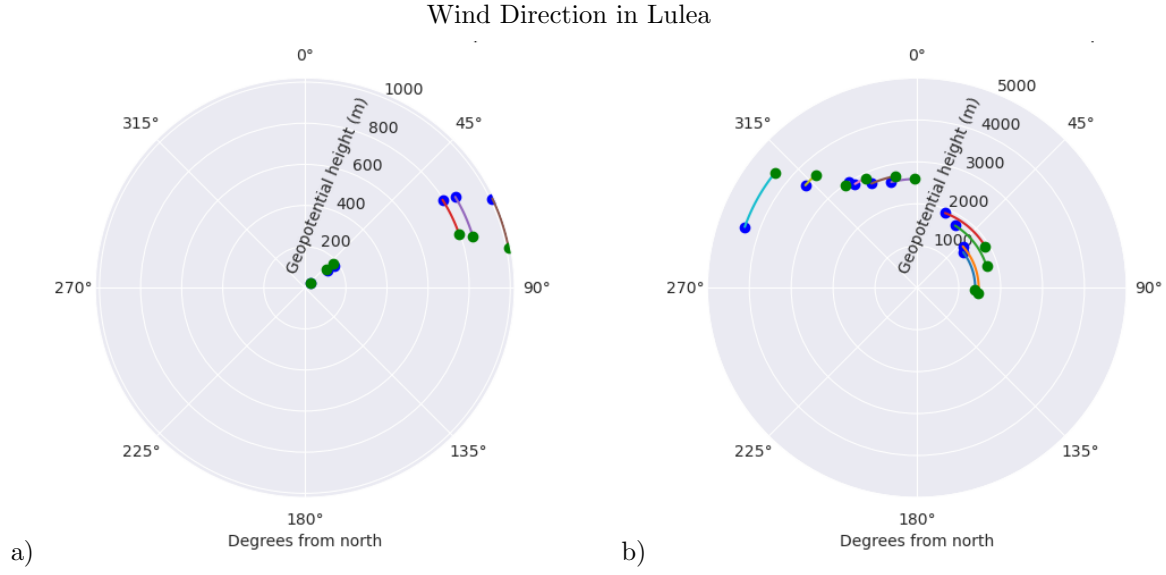

Figure 4.31: Wind direction in Lulea at 29.04.1986 12 UTC predicted by the model (blue) and the measurements done by the radiosonde (green). a) shows the wind directions below 1000 meters and b) shows the wind directions between 1000 and 5000 meters height. The line linking the two dots is the error.

The wind direction in Gothenburg at 29.04.1986 12 UTC is shown in figure 4.32. Below 1000 meters there is a mean absolute error of 15.4 degrees and a mean speed of 2.9 m/s. There is a westerly wind. Above 1000 meters there is a mean absolute error of 8.7 degrees and a mean speed of 7.1 m/s. Above 1000 meters height there is a southwesterly wind. There is a negative bias except for at 1000 meters where there is a positive bias.

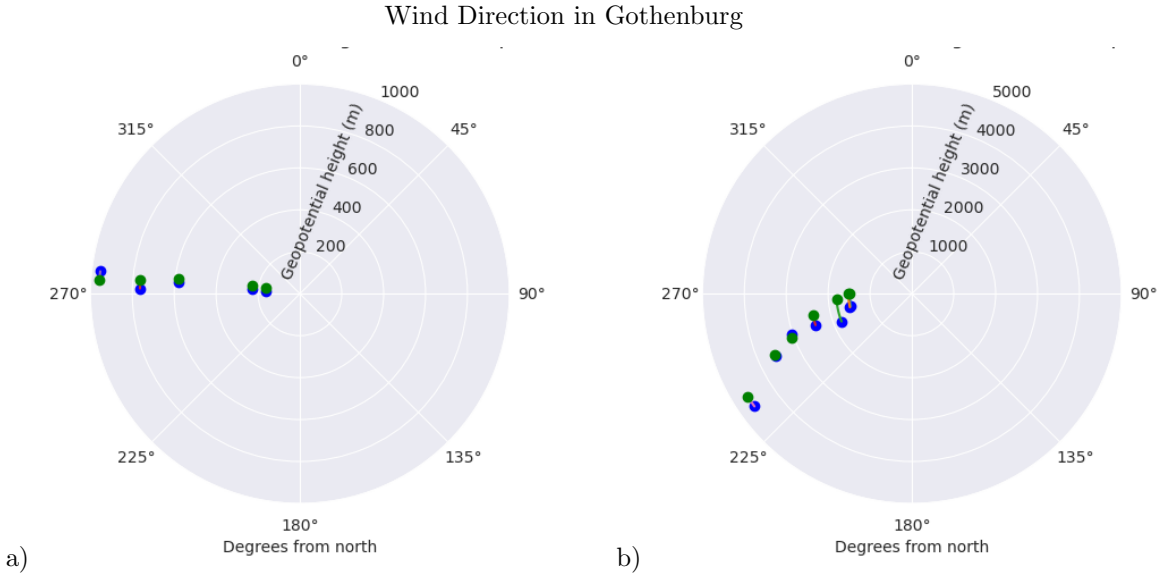

a) b)

Figure 4.32: Wind direction in Gothenburg at 29.04.1986 12 UTC predicted by the model (blue) and the measurements done by the radiosonde (green). a) shows the wind directions below 1000 meters and b) shows the wind directions between 1000 and 5000 meters. The line linking the two dots is the error.

Chapter 5

Discussion

In this chapter it is discussed how the errors in the AROME wind predictions can affect the predictions of the transportation of radioactivity after a nuclear accident. The radiosonde data and some choices of methods are discussed. It is also discussed whether adjusting for the horizontal drift of the radiosonde will impact the error. It is further discussed how the error in predicted wind speed and wind direction found in this thesis compares to other studies.

Moreover, it is discussed whether the transportation is modeled more correctly when the radioactivity is dispersed in higher altitudes. Is this correct when looking at the hindcast for the time period after the Chernobyl accident? Also the possible over prediction or under prediction of rotation in the wind direction from the atmospheric boundary layer to the free atmosphere is discussed.

5.1 The Radiosonde Data

As seen from section 4.1.1 there were higher mean absolute errors in wind speed and wind direction in certain countries. The Ukrainian and Russian radiosondes have high mean absolute errors while Finland is an example of a country with low overall absolute errors. This could indicate systematic error in either the model or in the stations. It could be that the model predicts the weather well in Finland or poorly in Russia. However, not all stations at the same approximate locations have high errors. Assuming that the USSR radiosondes in section 2.7 were also used in Ukraine, the errors could be from typos, and wrong inscription and results. Seeing that the Finnish radiosonde stations were more modern, it could explain why the errors are lower for these atmospheric soundings. Therefore the the largest outliers are removed for the analysis.

The interpolation technique is linear which could lead to errors in the comparison between the radiosonde observations and the model predictions. This method will work best for the days where the wind speed or wind direction will increase or decrease close to linearly with height. For days with very rapid and abruptly changing wind direction between the atmospheric boundary layer and the free atmosphere, or in areas of turbulence, this technique could lead to errors.

There are also other limitations for using radiosonde observations to verify the model predictions. Since it varied when the different radiosonde stations had data, the stations closer to the plume

was not always available. The temporal and spatial distribution of radiosonde observations in the area close to the accident and along the path of the plume is limited. Therefore not all wind directions and wind speed errors are caught in this analysis.

5.2 The AROME MetCoOp model

Adjusting for horizontal displacement of the radiosonde observations was not found to have a large impact on the mean absolute error and mean error for the wind speed and the wind direction. In some instances the radiosondes without horizontal drift had slightly less error, but this difference in error is relatively small compared to the error itself. This could indicate that the model has quite small horizontal variations over the drift distance. Additionally, the closer to the ground the more smaller scale changes in wind direction there are and larger horizontal differences could be expected in the model, but the radiosondes have very little displacement close to the surface. Moreover, as the displacement grows larger with height, the wind fields also grow smoother. Therefore it does not seem necessary to add horizontal displacement when investigating wind direction and wind speed predictions by using radiosonde observations.

The mean error for wind direction per time and date has an overall positive bias when all heights are included, meaning that the predictions are rotated clockwise away from the radiosonde observations. The mean absolute error in wind direction per time and date for all available heights is lower than the mean error. This indicates that these errors are noise or random errors in the radiosonde measurements

The mean error for wind speed per time and date has an overall negative bias, meaning that the model under predicts the wind speed when all heights are accounted for. The mean error is around zero, meaning that the majority of the errors cancel out. This indicates that a large part of the error in wind direction is noise or from random errors in the radiosonde measurements.

It can be seen from the results that the bias in wind direction is bigger for the first few days. This could be due to many factors. It could be because of weather phenomena that is difficult to model, more errors in the radiosonde observations or more microscale weather events that were not caught by either the model or the radiosondes. Since the first few days are important for the transportation towards Scandinavia, this could have had a big impact on how much radioactivity was transported to, for example Norway.

When the error is averaged over all observations in the same height bin, the error in wind direction, both the bias and the mean absolute error below 1000 is larger than the error below 1000 meters height. This correlates with the mesocscale and microscale wind phenomena in the atmospheric boundary level. Also the error in wind speed, when the error is averaged over all observations in the same height bin, is larger below 1000 meters than above 1000 meters height. Then the mean error is around 0 for the above 1000 meters height. This means that the model predicts both the wind speed and wind direction better in the free atmosphere.

Haakenstad et al. (2021) found a mean error of -0.5 m/s and 0 m/s at 10 meter height for a hindcast performed by the AROME MetCoOp model, while the mean error found in this thesis for data below 500 meters was around 2 m/s. The errors found in this thesis are therefore a bit higher. However, the radiosondes measurements of wind speed are assumed to have an error of up to 3

m/s in the mid troposphere and 5 m/s in the upper troposphere. Seeing that Haakenstad et al. (2021) used ground measuring equipment it may indicate that a fraction of the error in wind speed found in this thesis is from the radiosonde.

Müller et al. (2017) found an error between 1.4 and 2.2 m/s between the forecast performed which is similar to the errors found in this thesis. They also found that the error decreased with height which also was observed in the results of this thesis.

The wind direction errors found in Raskob et al. (2010) were slightly lower than the errors found in this thesis for heights below 1000 meters. However, the mean absolute error is higher than the bias by 15 degrees when averaged between 10 and 510 meters height, and above 2000 meters the model has very little bias, meaning that this difference in error could be from random errors, and errors in the observations.

5.3 The Movement of The Radioactivity

From table 4.4 it can be seen that soundings with a mean speed predicted by the model below 2 m/s has a very high mean absolute error, often being close to 180 degrees. The low speed causes high variability which makes it impossible to compare the radiosonde observations with the model results as explained in section 2.3. The polar plots showing the wind direction below 1000 meters of these atmospheric soundings are not used further in the discussion.

AT 26.04.1986 00 UTC the wind prediction in the area around the accident above 1000 meters shows an overall more southerly wind than the model predictions which could mean that the plume was going more north than predicted by the model during the first hours. However, if the radioactivity is situated below 1000 meters, it would be transported more towards the west or even towards the south, and in Gomel both the model and the observations show an easterly wind below 1000 meters height, transporting the radioactivity towards Poland.

At 12 UTC on the same day the northernmost part of the plume has reached the beginning of the Balkan countries. The wind is going towards Finland along the the northernmost part of the plume, both below and above 1000 meters with small errors in the AROME wind predictions. Alongside Poland close to where the plume is moving there is a more southwesterly wind observed above 1000 meters. Below 1000 meters there is high variability. The wind coming from Belarus is observed to be more southeasterly than the predictions, pushing the radioactivity above 1000 meters more towards Scandinavia. Below 1000 meters a more easterly wind is observed than predicted, transporting the radioactivity again more towards Poland.

At 27.04.1986 00 UTC the plume is moving over the Baltic sea and there is very little error above 1000 meters, showing that the middle of the plume is being transported towards the northwest and towards Scandinavia, while the northernmost part of the plume is being transported towards Finland and the northern part of Russia. The errors in wind direction are also small below 1000 meters height, however, the winds over the Balkan sea are observed to be more easterly than the predictions. At 12 UTC the same day the observations below 3000 meters show a southeasterly wind across the Baltic sea towards Scandinavia with small errors. The northernmost part of the plume is still being transported towards Finland and north of Russia both above and below 1000 meters. Closer to Sweden the winds around 1000 meters are transporting the radioactivity towards

the north with the observations being more southerly than the predictions. However, the wind below 1000 meters is observed to be almost easterly, transporting the radioactivity towards the south of Norway.

At 28.04.1986 00 UTC the wind is observed to go towards the north of Sweden above 1000 meters, below 1000 meters observing more easterly wind, and the winds over the south of Norway being southeasterly around 1000 meters and with small errors. Below 1000 meters there are more errors and an observed more easterly wind than predicted by the AROME model in the south of Sweden. At 28.04.1986 12 UTC the observations are showing a more variable wind direction than the model above 1000 meters. The observations are more southerly and southwesterly than the predictions between 1000 and 3000 meters in the middle of Sweden. The radioactive debris that has already reached the middle of Scandinavia could therefore have been transported more towards the north. In northern Sweden there is little error above 1000 meters height showing a southerly/southeasterly wind, and below 1000 meters the observations are southerly with the predictions being 90 degrees off towards the north. Therefore the radioactivity below 1000 meters could be transported more towards the north than predicted.

At 29.04.1986 00 UTC the winds around 1000 meters are observed to be more southeasterly than predicted by the model close to the south of Sweden. In the north of Sweden the wind is northeasterly around 1000 meters and below with the observations showing slightly more easterly transportation than predicted, which would lead to the radioactivity being transported more towards Norway. At 29.04.1986 12 UTC the wind direction in the north of Sweden is more easterly than predicted between 800 and 2000 meters height, which could lead to more of the radioactivity in this height being transported towards Norway than predicted by the model. In the south of Sweden the wind is now mainly westerly, transporting the radioactivity back across the Baltic sea.

11 out of 23 of the selected atmospheric soundings show positive bias below 1000 meters and negative bias after 1000 meters. This wind changes its direction as we move away from the surface of the earth in the atmospheric boundary layer because of friction and the Coriolis force. This could indicate that the model under predicts this change in wind direction. Additionally, there are small errors around 1000 meters for all the polar plots.

There is an observed more northward transportation of the plume during the first hours, if the radioactivity is in the free atmosphere. A more northward transportation would have led to more of the debris being transported towards Finland and the north of Russia while a more westward wind below 1000 meters height would have led more of the debris towards the south of Scandinavia. Then the radioactivity above 1000 meters would be transported to the north of Sweden with little errors in wind direction. The radioactivity below 1000 meters would have been directly transported towards Norway as it reaches Sweden. Then the radioactivity in the north of Sweden would have been transported more southwestward towards the middle of Norway. The vertical position of the radioactivity is therefore shown to be very important for determining the path. In the end it can be said that depending on if the radioactivity is below 1000 meters or above it could be transported more westward or more northward according to the radiosonde observations.

The mean absolute error is lower above 1000 meters as discussed in the previous section which means that the predictions above 1000 meters are more consistent between the observations and the model predictions. Depending on the vertical position of the radioactivity, the radioactivity could move more as the model is predicting or there could be more deviation.

Overall, the errors in wind direction presented in the result section could lead to a change in deposition pattern inside a region. This depends on the wind speed and the vertical position of the radioactivity, seeing that a higher wind speed would lead the model to predict a displacement of the radioactivity further away from the actual deposition.

5.4 Further Work

When applying a weather prediction model to the dispersion of radioactivity, many parameters of the weather prediction model could be important for the quality of the dispersion calculations. In this thesis the focus has been on validating the wind speed and the wind direction, and discuss the consequences of the errors in the prediction for the dispersion after the Chernobyl accident. Other parameters, such as precipitation, vertical winds, convection and turbulence would be interesting for further investigations. For further analysis also the vertical placement and movement of the radioactivity during the transportation should be included.

More advanced statistical tests could be performed to the data to find more specifically where the error lies as explained in Wilks (2011) and Klug et al. (1992).

It is recommended to compare the AROME MetCoOp model predictions in detail with the ERA5 reanalysis. It would be interesting to study if ERA5 has similar type of errors with height as the AROME model both with respect to wind direction and wind speed. Also the vertical distribution after the initial explosion should be investigated, and possible outcomes with different initial heights should be tested.

Chapter 6

Conclusion

This thesis aimed to investigate how well the MetCoOp Arome model wind speed and wind direction for the hindcast during the Chernobyl accident compared with radiosonde observations. The comparison was carried out both with and without taking horizontal drift of the radiosondes into account. By analysing the meteorological model results the wind speed and wind direction errors were seen to be larger during the first few days after the accident than later when averaging over all radiosondes and all height levels in each timepoint. Among the radiosondes the Russian and Ukrainian radiosondes showed the largest discrepancy with the model. This resulted in seven radiosonde stations from Russia, Ukraine and Slovakia being discarded from the analysis of the wind direction and eight radiosonde stations from Russia, Ukraine and Poland being discarded from the analysis of the wind speed.

The wind speed in the AROME model had small errors compared to the assumed error in radiosonde measurements and similar errors compared to other similar studies (Haakenstad et al., 2021; Müller et al., 2017). The error in wind direction found in this thesis was slightly larger compared to the error found in a similar study (Raskob et al., 2010). However, when the difference between the mean absolute error and bias is assumed to be from the radiosonde observations, the error in wind direction found in this thesis is similar compared to Raskob et al. (2010). The mean absolute error in wind speed and wind direction, considering all radiosonde measurements, was larger below 1000 meters than above. The mean error went towards zero after 1000 meters height for the wind speed and for the wind direction it became relatively small meaning that the model predicted the wind well in the free atmosphere.

Adjusting for the horizontal displacement of the radiosonde did not lead to any significant difference in the mean absolute error and mean error of the wind speed and wind direction predictions. Therefore, the conclusion from this study is that in comparing radiosonde observations with the AROME model it is not necessary to include horizontal displacement of radiosonde observations for analysing wind speed and wind direction predictions.

Furthermore, this thesis aimed to look more closely on specific atmospheric soundings to investigate the error in wind direction along the path of the plume after the Chernobyl accident over the first 4 days using radiosonde observations with horizontal drift. The main question being: What does this mean for the transportation of the radioactivity? Many of the selected atmospheric soundings had

an under prediction of the rotation of wind angle when moving from the atmospheric boundary layer to the free atmosphere leading to errors in the predicted wind direction compared to the radiosonde observations.

The radioactivity above 1000 meters height was shown to be transported more northward according to the radiosondes observations than predicted by the model due to the errors in wind direction along the path of the radioactivity. Below 1000 meters there could have been a more westward transportation than predicted by the model due to the errors in wind direction. Then later the radiosondes showed a more westward/southwestward movement across Sweden towards the middle of Norway than what was predicted by the model.

Since the error is smaller above 1000 meters and the wind direction changes around 1000 meters, the errors in the transportation of radioactivity, due to errors in the predicted winds, is largely dependent on where the radioactivity is located vertically. Therefore, for the future, it would be interesting to investigate how the vertical distribution of radioactivity could interact with possible errors in the vertical wind distribution predicted by the weather model. Also, there should be attempts to compare the wind direction with other data such as the ERA5 data set to further investigate possible errors. Lastly, since this model is used for emergency preparedness, the area for the predicted deposition of radioactivity should be expanded to make up for the possible errors in the wind direction.

Bibliography

Backe, S., Bjerke, H., Rudjord, A., & Ugletveit, F. (1986). Nedfall av cesium i norge etter ts-jernobylulykken. *National Institute of Radiation Hygiene, Østerås*.

Bartnicki, J., Haakenstad, H., & Hov, Ø. (2011). Operational snap model for remote applications from nrpa. *Norwegian Meteorological Institute. Report*, 12–2011.

Bauer, P., Thorpe, A., & Brunet, G. (2015). The quiet revolution of numerical weather prediction. *Nature*, *525*(7567), 47–55.

Blaylock, B. (2015). Plotting sounding data from university of wyoming's website [Accessed: 2023-05-12].

Eliassen, A., & Pedersen, K. (1977). Meteorology. an introduction course. vol. 1: Physical processes and motion. *Oslo*.

Haakenstad, H., Breivik, Ø., Furevik, B. R., Reistad, M., Bohlinger, P., & Aarnes, O. J. (2021). Nora3: A nonhydrostatic high-resolution hindcast of the north sea, the norwegian sea, and the barents sea. *Journal of Applied Meteorology and Climatology*, *60*(10), 1443–1464.

Harmonie vertical model layer definitions [Accessed: 2023-04-18]. (n.d.).

Hersbach, H., Bell, B., Berrisford, P., Hirahara, S., Horányi, A., Muñoz-Sabater, J., Nicolas, J., Peubey, C., Radu, R., Schepers, D., et al. (2020). The era5 global reanalysis. *Quarterly Journal of the Royal Meteorological Society*, *146*(730), 1999–2049.

Ivanov, A. (1991). Wmo international radiosonde comparison-phase iii-dzhambul, ussr, 1989 final report. *WMO Instruments and Observing Methods Report*, (40).

Klug, W., Graziani, G., Grippa, G., Pierce, D., & Tassone, C. (1992). *Evaluation of long range atmospheric transport models using environmental radioactivity data from the chernobyl accident: The atmes report: Workshop*. Elsevier Applied Science.

Kong, Q., Siauw, T., & Bayen, A. (2020). *Python programming and numerical methods: A guide for engineers and scientists*. Academic Press.

Laroche, S., & Sarrazin, R. (2013). Impact of radiosonde balloon drift on numerical weather prediction and verification. *Weather and forecasting*, *28*(3), 772–782.

Leadbetter, S., Andronopoulos, S., Bedwell, P., Chevalier-Jabet, K., Geertsema, G., Gering, F., Hamburger, T., Jones, A., Klein, H., Korsakissok, I., et al. (2020). Ranking uncertainties in atmospheric dispersion modelling following the accidental release of radioactive material. *Radioprotection*, *55*(HS1), S51–S55.

Lilley, J. (2013). *Nuclear physics: Principles and applications*. John Wiley & Sons.

McGrath, R., Semmler, T., Sweeney, C., & Wang, S. (2006). Impact of balloon drift errors in radiosonde data on climate statistics. *Journal of climate*, *19*(14), 3430–3442.

Milrad, S. (2018). 4 - upper-air observations. In S. Milrad (Ed.), *Synoptic analysis and forecasting* (pp. 41–47). Elsevier. https://doi.org/https://doi.org/10.1016/B978-0-12-809247-7.00004-1

Müller, M., Homleid, M., Ivarsson, K.-I., & et. al. (2017). Arome-metcoop: A nordic convective-scale operational weather prediction model. *Weather and Forecasting*, *32*(2), 609–627.

Næumann, R., & Gaare, E. (1991). Måling av radioaktivitet etter tsjernobyl-katastrofen. *TSJERNOBYL*, *2*, 16.

NMBU, R. (2022). Welcome to cerad [Accessed: 2023-04-18].

Pentikäinen, P. S. S., O'Connor, E. J., & Ortiz-Amezcua, P. (2022). Evaluating wind profiles in a numerical weather prediction model with doppler lidar. *Geoscientific Model Development Discussions*, 1–31.

Persson, C., Rodhe, H., & De Geer, L.-E. (1987). The chernobyl accident: A meteorological analysis of how radionuclides reached and were deposited in sweden. *Ambio*, 20–31.

Raskob, W., Hugon, M., Astrup, P., & Mikkelsen, T. (2010). Comparison of nwp prognosis and local monitoring data from npps. *Radioprotection*, *45*(5), S97–S111.

Saltbones, J. (1986). *The chernobyl reactor accident* (tech. rep.). Norske Meteorologiske Inst.

Seidel, D. J., Sun, B., Pettey, M., & Reale, A. (2011). Global radiosonde balloon drift statistics. *Journal of Geophysical Research: Atmospheres*, *116*(D7).

Simmons, A. J., & Burridge, D. M. (1981). An energy and angular-momentum conserving vertical finite-difference scheme and hybrid vertical coordinates. *Monthly Weather Review*, *109*(4), 758–766.

Stull, R. (2017). *Practical meteorology: An algebra-based survey of atmospheric science - version 1.02b*. Univ. of British Columbia.

Stull, R. B. (1988). *An introduction to boundary layer meteorology* (Vol. 13). Springer Science & Business Media.

University of wyoming [Accessed: 2023-04-18]. (n.d.).

Wallace, J. M., & Hobbs, P. V. (2006). *Atmospheric science: An introductory survey* (Vol. 92). Elsevier.

Wilks, D. S. (2011). *Statistical methods in the atmospheric sciences* (Vol. 100). Academic press.

Appendix

A Model Results Not Included in The Method Section Showing The Path of The Plume

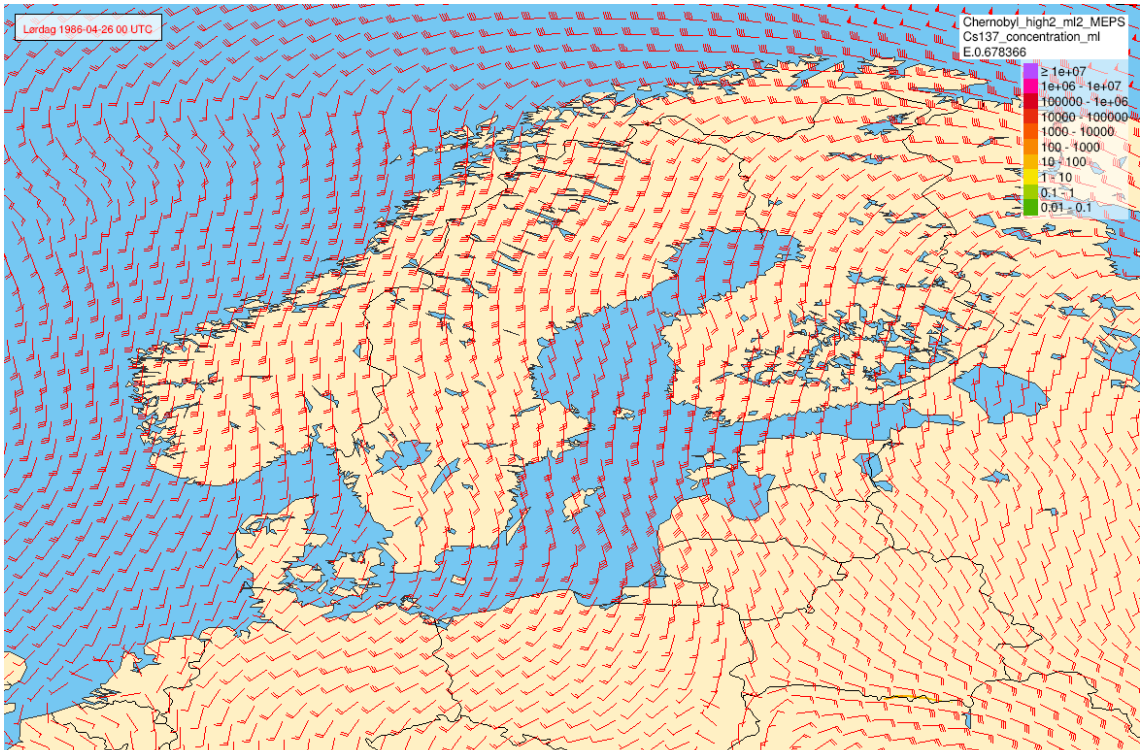

Figure 1: The Cs137 concentration in Bq/m^3 at around 4000 meters height at 26.04.1986 00 UTC. Retrieved from the SNAP and AROME model runs

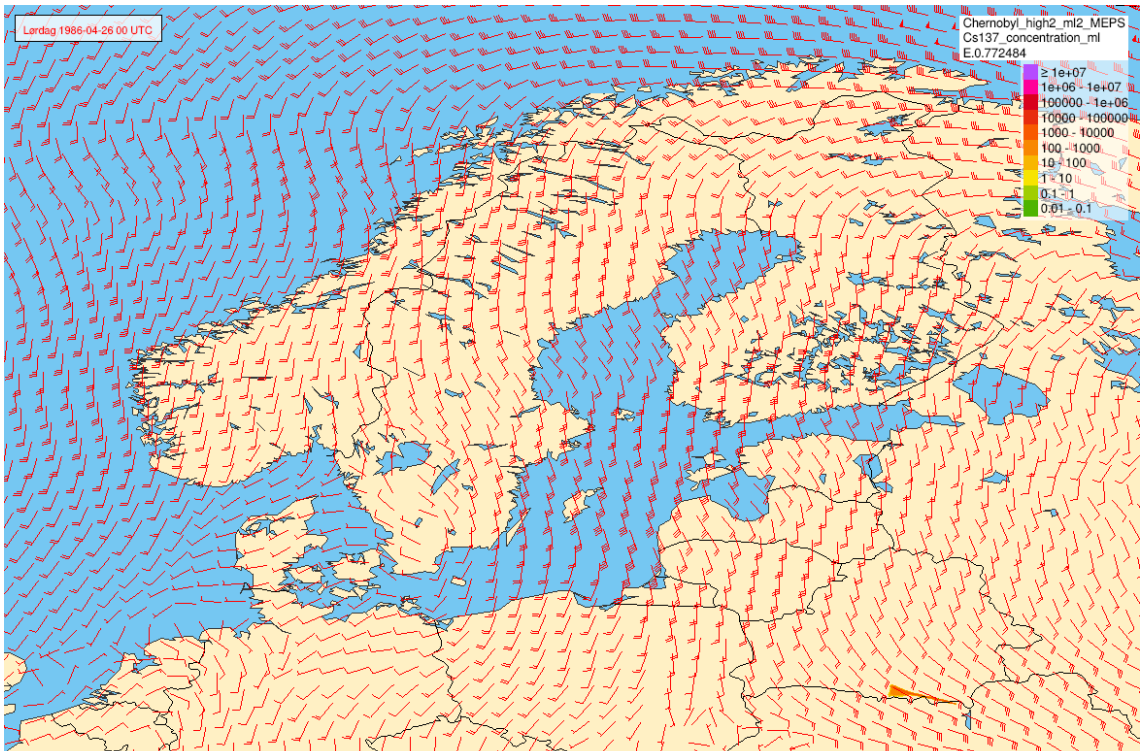

Figure 2: The Cs137 concentration in Bq/m^3 at around 2000 meters height at 26.04.1986 00 UTC. Retrieved from the SNAP and AROME model runs

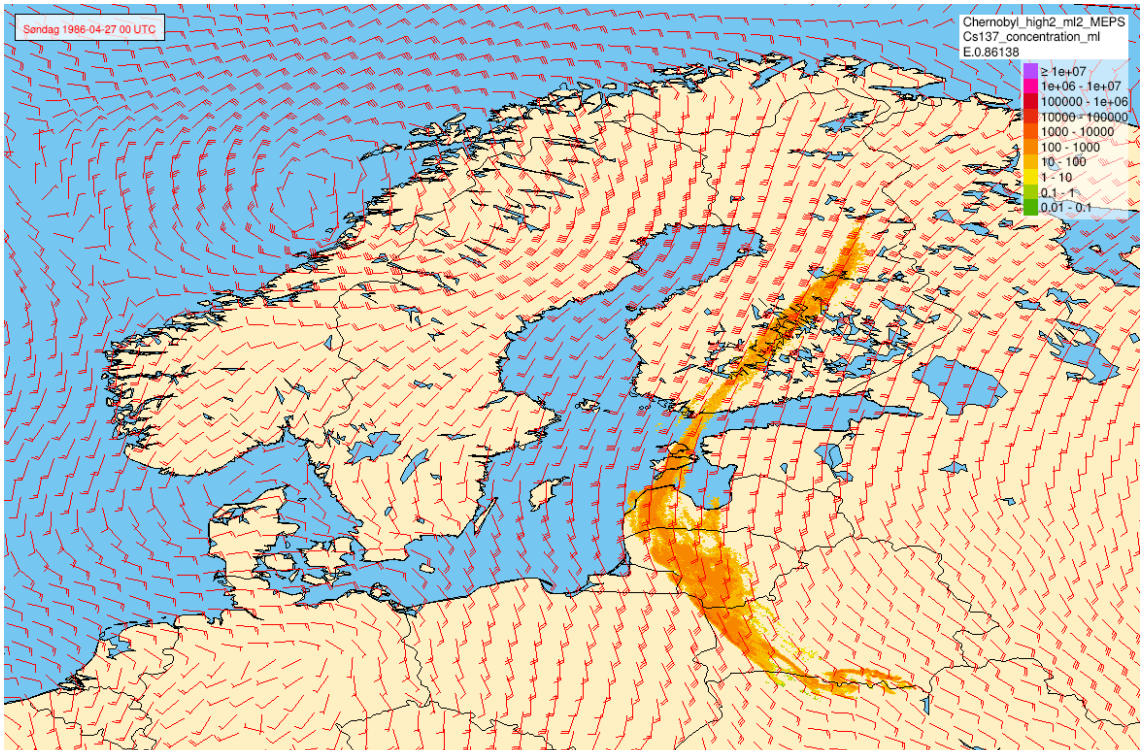

Figure 3: The Cs137 concentration in Bq/m^3 at around 1200 meters height at 27.04.1986 00 UTC. Retrieved from the SNAP and AROME model runs

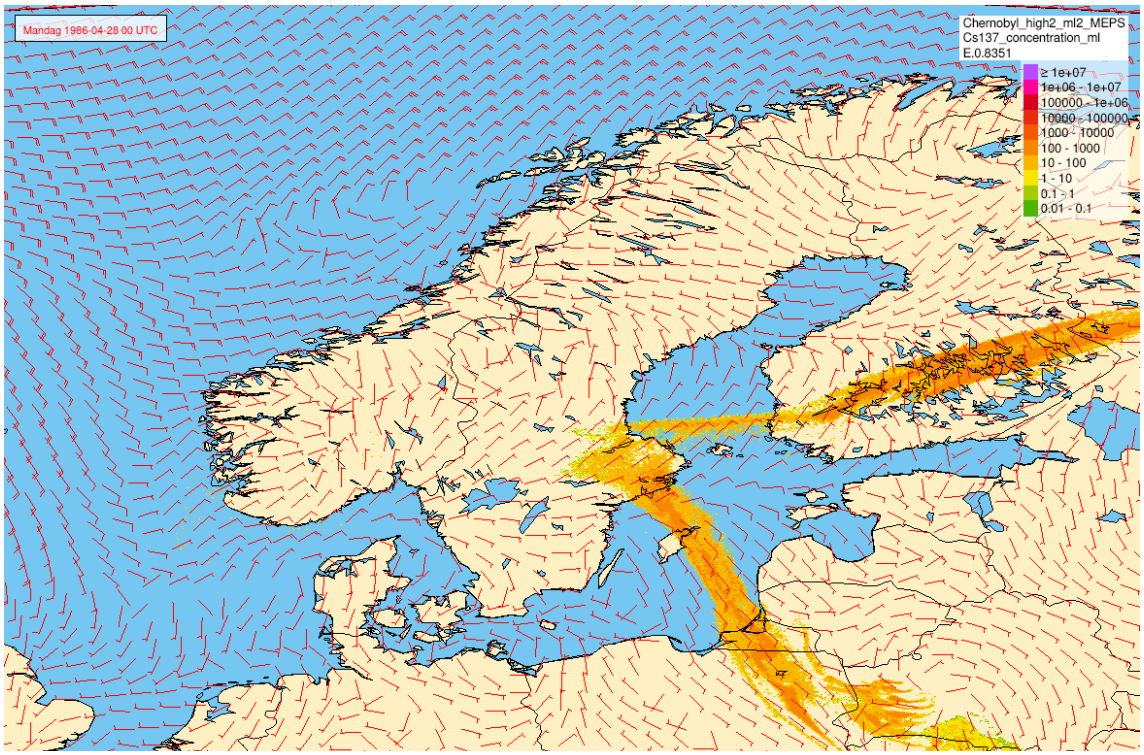

Figure 4: The Cs137 concentration in Bq/m^3 at around 1500 meters height at 28.04.1986 00 UTC. Retrieved from the SNAP and AROME model runs

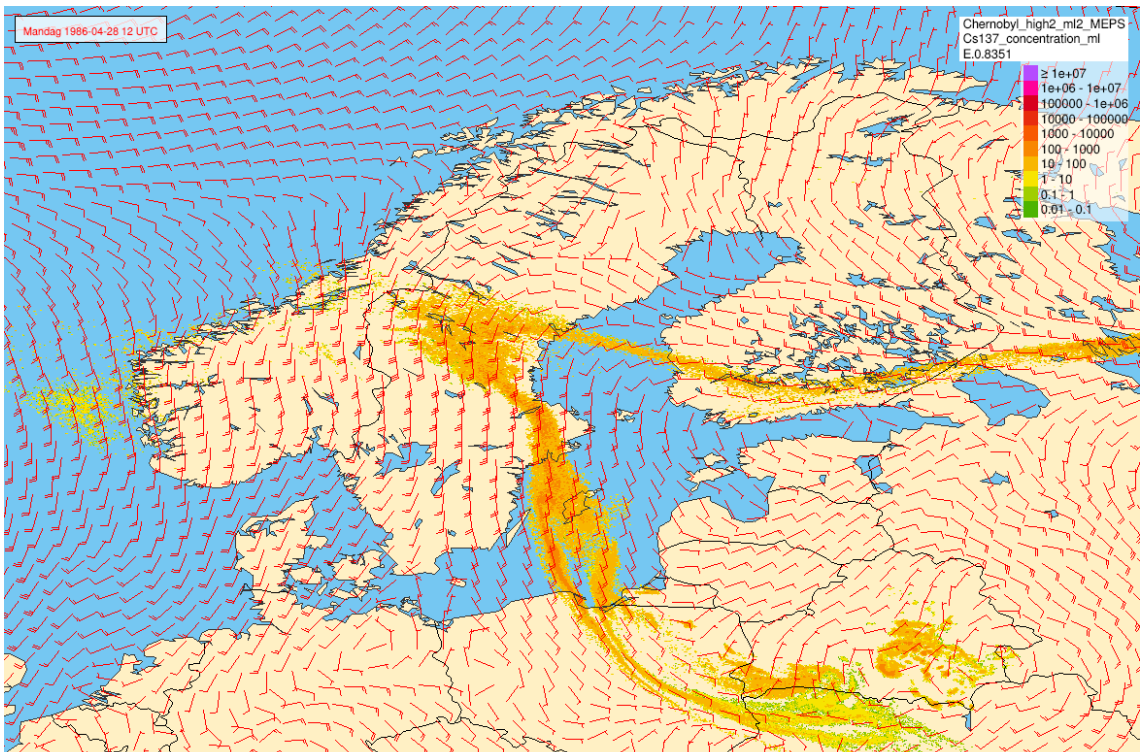

Figure 5: The Cs137 concentration in Bq/m^3 at around 1600 meters height at 28.04.1986 12 UTC. Retrieved from the SNAP and AROME model runs

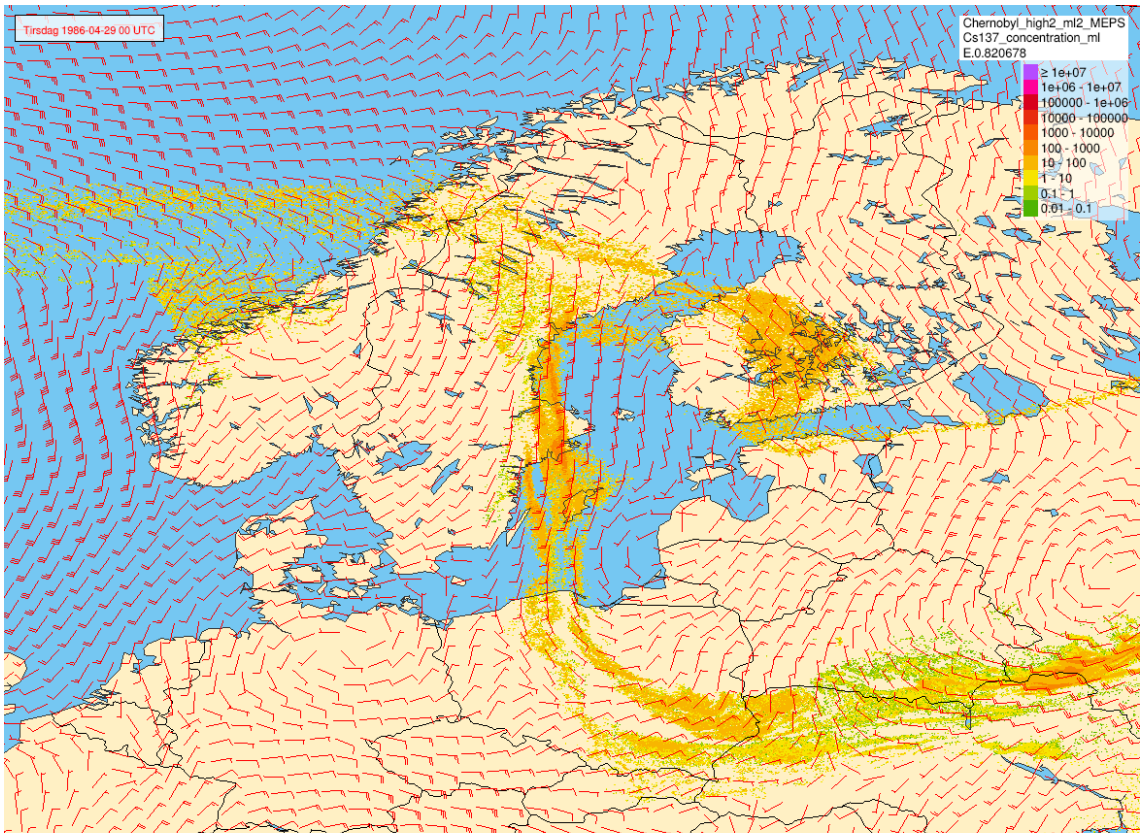

Figure 6: The Cs137 concentration in Bq/m^3 at around 1600 meters height at 29.04.1986 00 UTC. Retrieved from the SNAP and AROME model runs

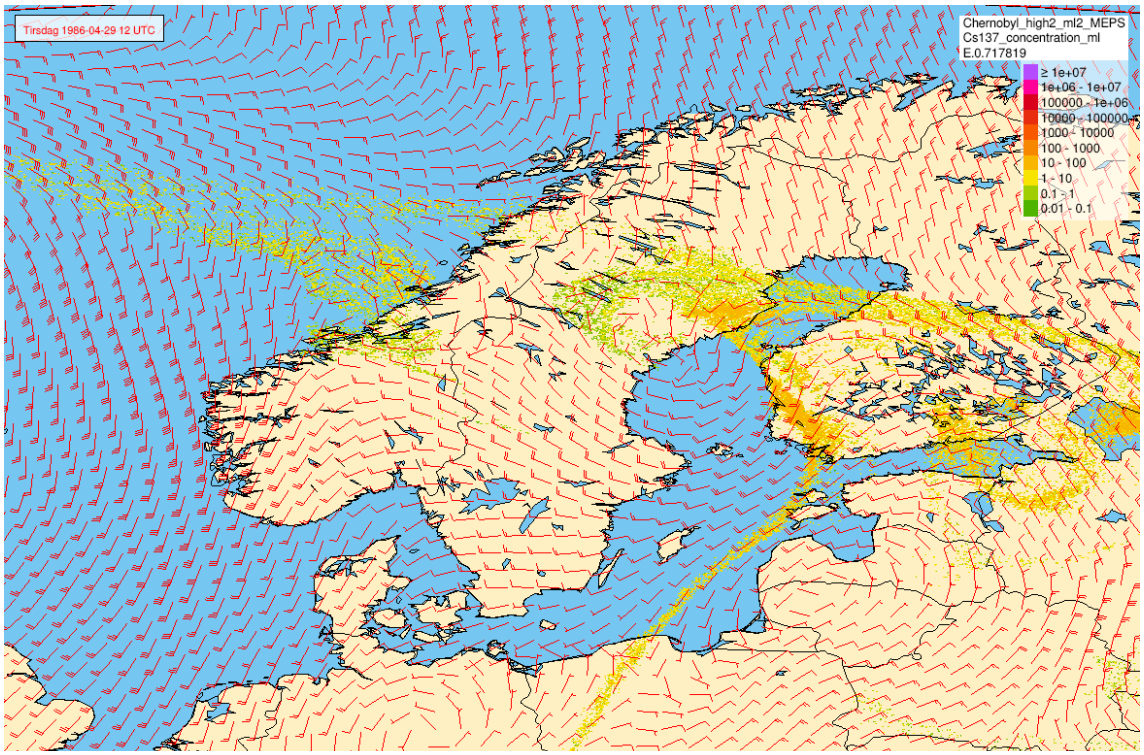

Figure 7: The Cs137 concentration in Bq/m^3 at around 1500 meters height at 29.04.1986 12 UTC. Retrieved from the SNAP and AROME model runs

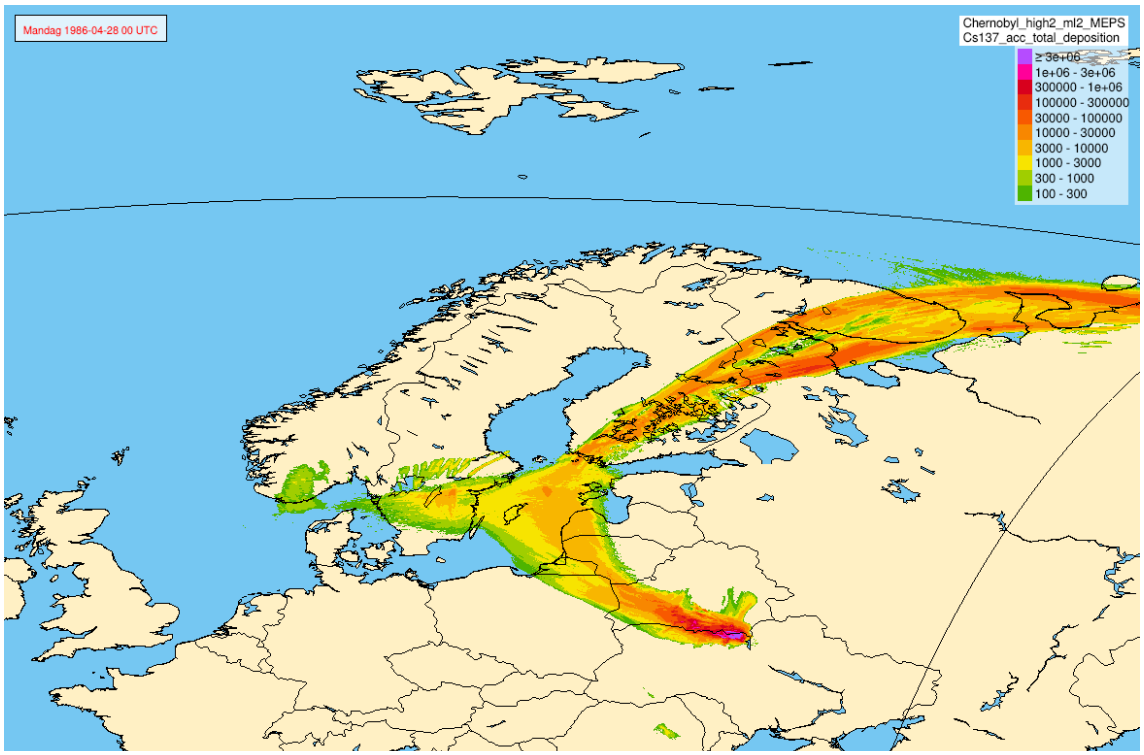

Figure 8: The total accumulated deposition of cesium 137 at 00 on the 28^{th} of April. Retrieved from Diana

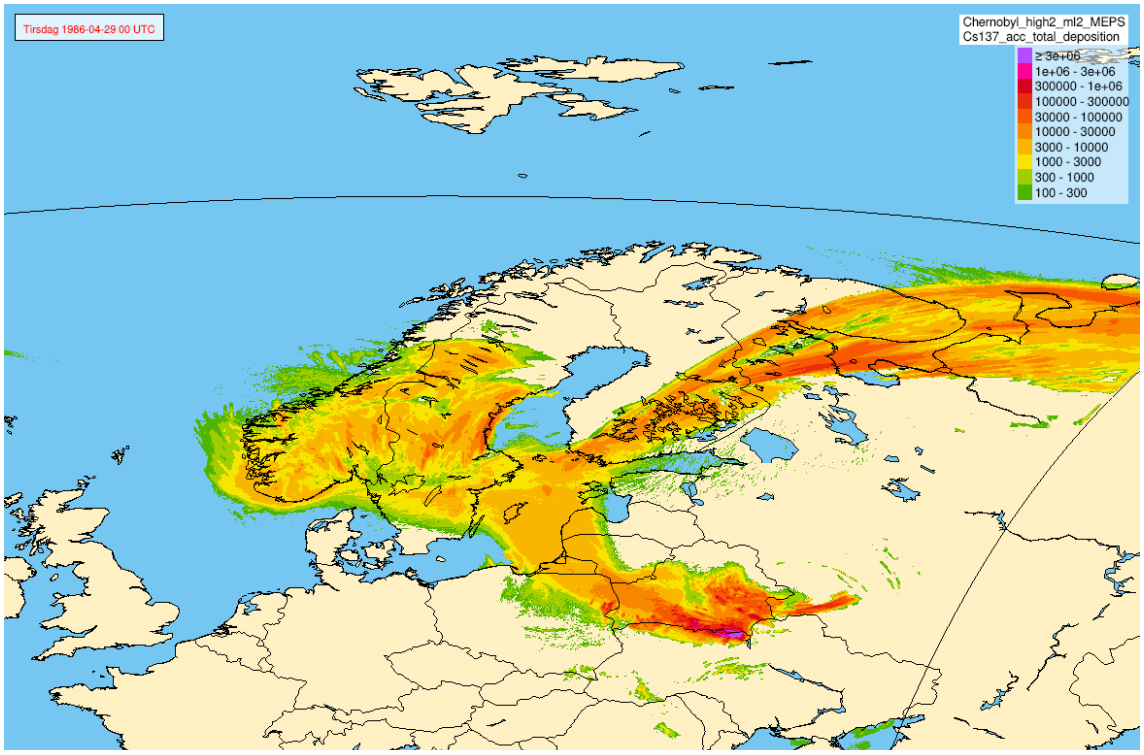

Figure 9: The total accumulated deposition of cesium 137 at 00 on the 29^{th} of April. Retrieved from Diana

B Atmospheric Soundings not included in the results

B.1 Error in Wind Direction 26.04.1986 00 UTC

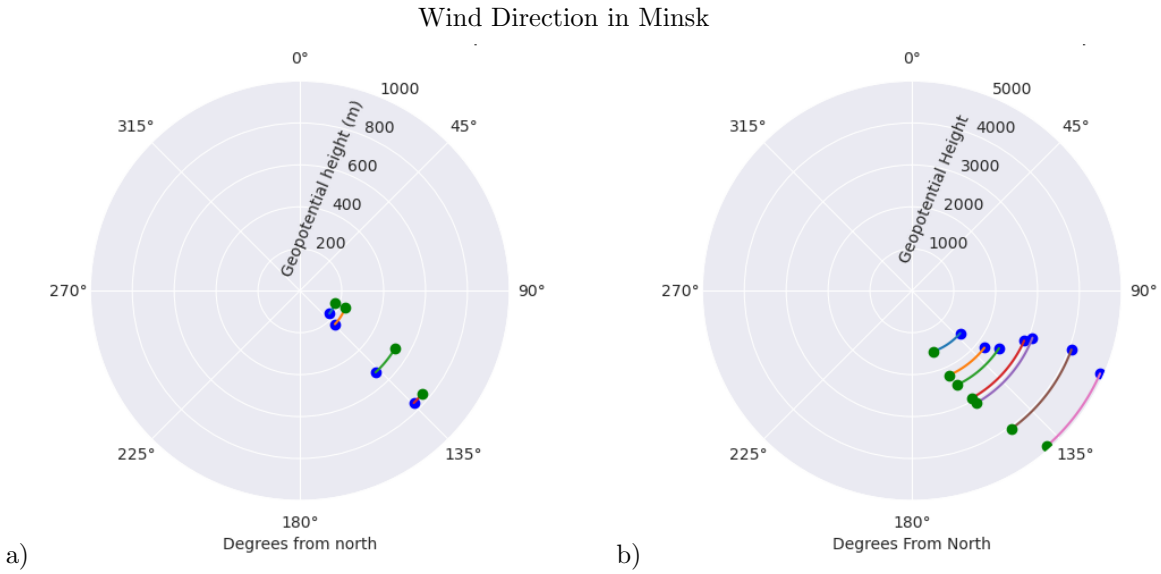

a) b)

Figure 10: Wind direction in Minsk at 26.04.1986 00 UTC predicted by the model in blue, the measurements done by the radiosonde is plotted in green. a) shows the wind directions below 1000 meters and b) shows the wind directions between 1000 and 5000 meters. The line linking the two dots is the error.

B.2 Error in Wind Direction 27.04.1986 00 UTC

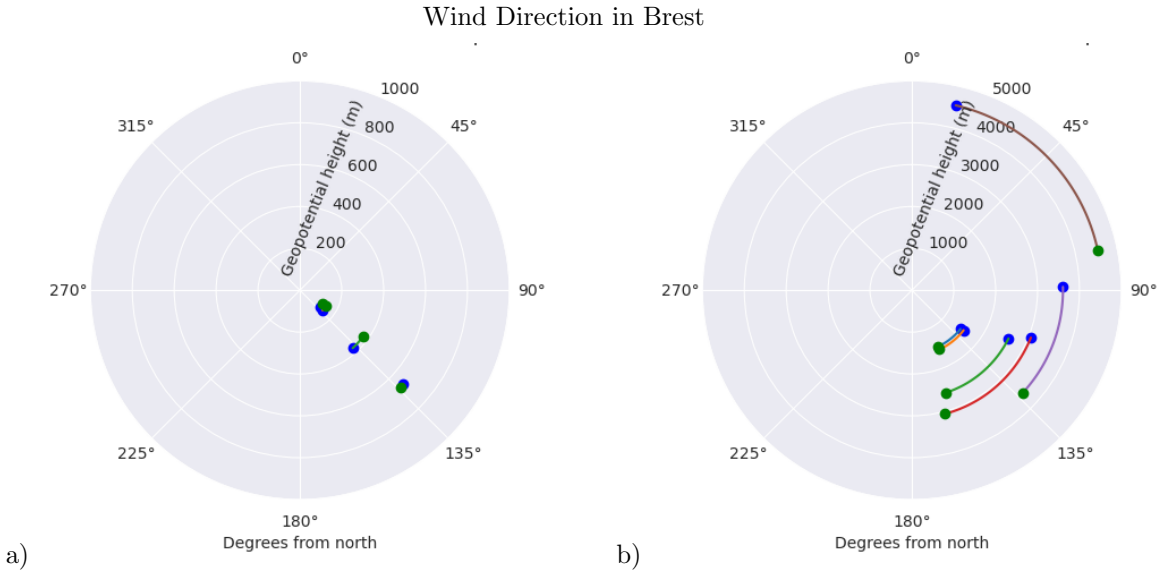

a) b)

Figure 11: Wind direction in Brest at 27.04.1986 00 UTC predicted by the model in blue, the measurements done by the radiosonde is plotted in green. a) shows the wind directions below 1000 meters and b) shows the wind directions between 1000 and 5000 meters. The line linking the two dots is the error.

B.3 Error in Wind Direction 28.04.1986 00 UTC

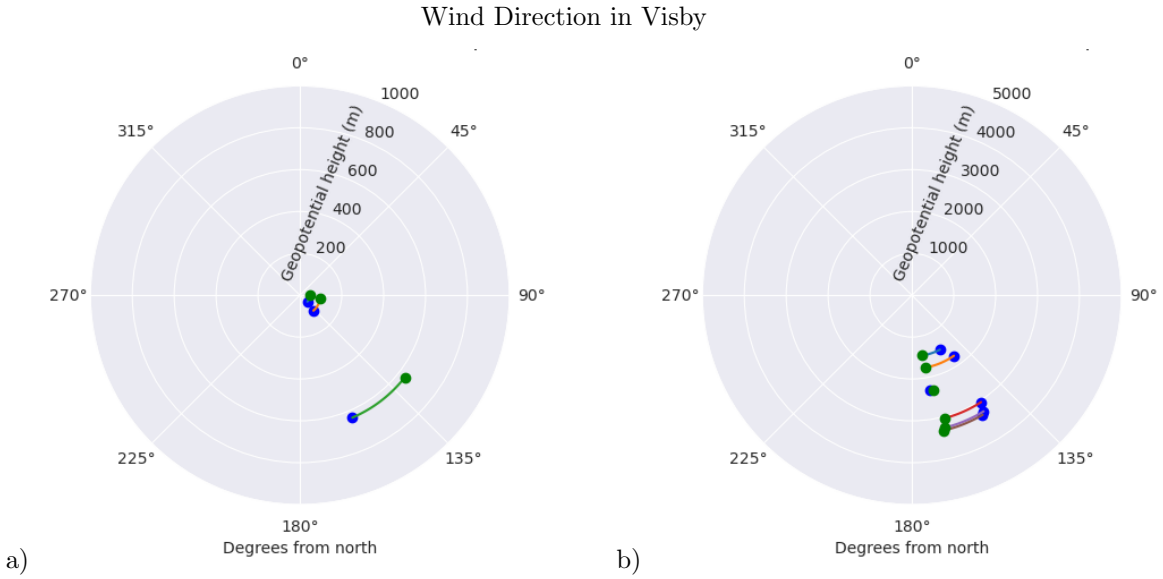

a) b)

Figure 12: Wind direction in Visby at 28.04.1986 00 UTC predicted by the model (blue) and the measurements done by the radiosonde (green). a) shows the wind directions below 1000 meters and b) shows the wind directions between 1000 and 5000 meters. The line linking the two dots is the error.

B.4 Error in Wind Direction 29.04.1986 00 UTC

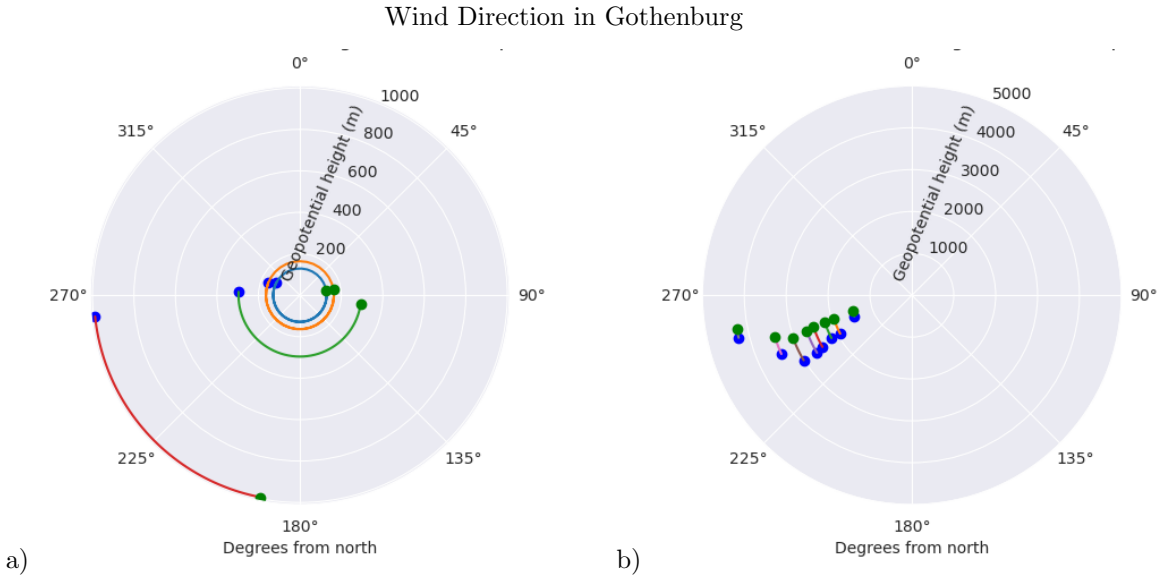

Figure 13: Wind direction in Gothenburg at 29.04.1986 00 UTC predicted by the model (blue) and the measurements done by the radiosonde (green). a) shows the wind directions below 1000 meters and b) shows the wind directions between 1000 and 5000 meters. The line linking the two dots is the error.

Norges miljø- og biovitenskapelige universitet
Noregs miljø- og biovitskapelege universitet
Norwegian University of Life Sciences

Postboks 5003
NO-1432 Ås
Norway